Summer 2010

Chamber studies of the heterogeneous reaction of sulfur dioxide with particulate hematite

Jason Francis Vanlerberghe
University of Iowa

CHAMBER STUDIES OF THE HETEROGENEOUS REACTION OF SULFUR DIOXIDE WITH PARTICULATE HEMATITE

by

Jason Francis Vanlerberghe

A thesis submitted in partial fulfillment
of the requirements for the Master of
Science degree in Chemistry
in the Graduate College of
The University of Iowa

July 2010

Thesis Supervisor: Associate Professor Mark A. Young

Graduate College
The University of Iowa
Iowa City, Iowa

CERTIFICATE OF APPROVAL

_____

MASTER'S THESIS

_____

This is to certify that the Master's thesis of

Jason Francis Vanlerberghe

has been approved by the Examining Committee
for the thesis requirement for the Master of Science
degree in Chemistry at the July 2010 graduation.

Thesis Committee: _____
Mark A. Young, Thesis Supervisor

_____
Vicki H. Grassian

_____
Lei Geng

ACKNOWLEDGMENTS

I would like to thank everyone who helped make this work possible. I am grateful to Dr. Jennifer Schuttlefield, who showed me how to use both the XRD and BET instruments. Drs. Praveen Mogili and Juan Navea also used this environmental chamber for their research, and provided many helpful tips and useful discussion. Although I never actually met her, I am very grateful for Dr. Amy Preszler Prince's enormous amount of work assembling and testing the operation of the chamber so that it would be ready for future graduate students.

I would also like to thank each of the faculty who served as committee members for me at some time, but whose names don't appear on this thesis: Drs. Amnon Kohen, Paul Kleiber, Sarah Larsen, Donald Cannon, and Jan Jensen. I would like to especially thank Dr. Grassian, who allowed me to present at her group's meetings for feedback, and has been to all of my seminars. More big thanks for Dr. Lei Geng, who was very helpful with his advice for graduation and joined my thesis committee on short notice.

Of course, I am most indebted to Dr. Mark Young, who as my advisor, was there for it all. When I started graduate school, I knew I was interested in instrument development, and his lab was the ideal place to get all kinds of experience in the processes of planning, drafting, assembling, and especially troubleshooting that is required for that kind of work. I feel like I've gained a very broad skill set under his tutelage. I really appreciate all the individual attention I received from him, and how he always looked out for my needs as a student. Thanks, Mark!

TABLE OF CONTENTS

LIST OF TABLES

Table

LIST OF FIGURES

Figure

CHAPTER 1
INTRODUCTION

Aerosols, a general term for solid or liquid particles suspended in a gas, are a ubiquitous component of both indoor and outdoor atmospheres. Various sources are responsible for the emission of aerosols with vastly different compositions, ranging from largely inorganic (e.g., sea salt, mineral dust, ice particles, soot from biomass burning) to organic (e.g., terpene emissions from forests) to biogenic (e.g., pollen, spores, viable bacteria). The transport properties of an aerosol are determined by it size (generally ranging from several nm to tens of μm), morphology, and chemical composition [1, 2]. It is a common occurrence that natural or anthropogenic aerosols can have a long lifetime in the atmosphere, up to several weeks. For example, dust storm events from continental Asia can transport dust to the remote regions of the Pacific Ocean, where it can act as a source of essential minerals to marine microorganisms [3-5]. Aerosols may also affect climate change via their optical properties, producing a cooling effect by backscattering solar radiation, or a warming effect by absorbing long wavelength radiation emitted by the planet's surface. Currently, limited knowledge of the optical properties of very heterogeneous natural aerosols over the entire ultraviolet to infrared spectrum makes the global climate impact of aerosols very uncertain [6-8].

Detrimental health effects have been observed to correlate with high mass loadings of particulate matter (PM). The occurrence and severity of respiratory and cardiovascular problems, as well as general mortality, increase significantly as exposure to PM increases, particularly to the finer fractions denoted $PM_{2.5}$ (the subscript indicates maximum aerodynamic diameter of particles in μm) [9, 10]. These effects are expected to

become further aggravated if climate change trends continue [11]. The biochemical mechanisms of aerosol toxicity are numerous, and vary greatly depending on aerosol composition and size [12-14]. Some studies have specifically implicated iron from PM samples as a chief factor in toxicity [15-17]. Donaldson *et al.* measured the extent of damage to supercoiled DNA samples caused by a suspension of urban PM_{10} samples which contained 18% iron (mole fraction, not counting oxygen) [15]. The extent of damage due to the production of hydroxyl radicals was largely reduced by treating the PM_{10} suspension with an iron chelator; similar results were obtained for the supernatant liquid of centrifuged PM_{10}, suggesting soluble iron plays a role in aerosol toxicity. The environment within human lung epithelial cells mobilizes iron from urban PM_{10} samples, creating a pathway for oxidative damage by formation of reactive oxygen species (ROS) [17]. Heterogeneous reactions that may increase the solubility of iron in respirable PM are thus of interest from a health standpoint.

During transport through the troposphere, aerosol plumes provide a large surface area for heterogeneous reactions with atmospheric gases of natural or anthropogenic origin. A major paradigm shift in atmospheric research occurred as scientists realized that heterogeneous reactions in the atmosphere could have a massive effect on the balance of trace gases, in addition to the homogeneous gas phase reactions that were more thoroughly studied. One of the classic examples of the impact of heterogeneous atmospheric reactions is the activation of the chlorine reservoir species $ClONO_2$ on solid particles in polar stratospheric clouds (PSCs) [1].

$$ClONO_2(g) + HCl(s) \rightarrow Cl_2(g) + HNO_3(s) \qquad 1.1$$

$$ClONO_2(g) + H_2O(s) \rightarrow HOCl(g) + HNO_3(s) \qquad 1.2$$

Both Cl_2 and HOCl can easily photolyse, producing chlorine radicals which can then catalytically destroy ozone, thus depleting the Antarctic ozone level beyond what would occur from homogeneous reactions alone. Due to the large number of variables in the atmosphere that may affect heterogeneous chemistry (particle composition, humidity, the simultaneous presence of several trace gases, photochemistry in the sunlight, temperature, etc.), many laboratory studies use greatly simplified models of very specific gas-solid reactions in order to gain some mechanistic insight into a process that is difficult to obtain from field studies alone. The expanding body of work on the kinetics of both homogeneous and heterogeneous reactions in the atmosphere will lead to improvements in computer modeling studies, yielding greater predictive power for key parameters such as pollutant concentration or climate change impact [18]. New techniques, such as aerosol mass spectrometry, which samples and analyzes individual aerosols in real time, will be valuable tools in gaining a more complete understanding of heterogeneous atmospheric chemistry [19-23].

The oxidation of gaseous sulfur species in the atmosphere is a key part of the global sulfur budget. Dimethyl sulfide (DMS), which is emitted to the atmosphere by microorganisms, and sulfur dioxide (SO_2), which originates from volcanic activity as well as anthropogenic activity, are major forms of reduced sulfur in the atmosphere. The concentration of SO_2 can reach hundreds of ppb near anthropogenic emission sources [24]. Sulfur dioxide is able to partition into aqueous droplets in concentrations determined by the Henry's Law constant, H, followed by rapid hydrolysis to form H_2SO_3.

As H_2SO_3 is a biprotic weak acid, dissociation follows to an extent determined by K_{a1} and K_{a2} in the reactions below.

$$SO_2(g) + H_2O(l) \xleftrightarrow{H_{SO_2}} H_2SO_3(aq) \quad 1.3$$

$$H_2SO_3(aq) \xleftrightarrow{K_{a1}} H^+(aq) + HSO_3^-(aq) \quad 1.4$$

$$HSO_3^-(aq) \xleftrightarrow{K_{a2}} H^+(aq) + SO_3^{2-}(aq) \quad 1.5$$

It is well established that oxidation by dissolved hydrogen peroxide or ozone in aqueous droplets is a major contributor to S(IV) conversion in the atmosphere [1, 25-27].

$$HSO_3^-(aq) + H_2O_2(aq) \rightarrow SO_4^{2-}(aq) + H_2O + H^+(aq) \quad 1.6$$

$$HSO_3^-(aq) + O_3(aq) \rightarrow SO_4^{2-}(aq) + O_2(aq) + H^+(aq) \quad 1.7$$

A number of studies have been conducted to determine the relative importance of other potential oxidants [28, 29], such as transition metal catalysts [30, 31], on sulfate formation in aqueous solution. The relative importance of the aqueous oxidation pathways depend strongly on pH and the concentrations of trace gases and metals.

The role of heterogeneous reactions in the oxidation of atmospheric SO_2 to sulfate has recently received increased attention. Coatings of sulfate formed on mineral dust may alter the optical properties of the aerosol, leading to changes in radiative climate forcing [32, 33]. The uptake of SO_2 by a large variety of atmospherically relevant particle surfaces has been investigated [24, 34-51]. It has been discovered that the coadsorption of SO_2 and an atmospheric oxidant such as O_3 or NO_2 can lead to sulfate formation on a number of particulate surfaces, including NaCl (the major component of aerosolized sea salt) [41], calcium carbonate [40], and authentic samples of Saharan dust [45, 46]. In some cases, sulfate formation was observed with much weaker oxidants, such as O_2 [34,

35]. It has been proposed that acidification of mineral dust aerosols through heterogeneous reactions with SO_2 or HNO_3 gas may significantly affect the solubility of trace minerals, in particular iron, leading to increased growth rates for marine microorganisms [52, 53]. The majority of these uptake experiments however, were performed on dry, bulk powder samples which were deposited as multiple layers on a surface. A number of recent studies have shown dramatic differences in uptake kinetics and extent as the relative humidity (RH) is varied to reflect the ubiquitous presence of water vapor in the troposphere [42, 54-56]. The goal of this thesis is to investigate the kinetics and amount of SO_2 uptake on hematite, which will act as a representative mineral dust aerosol. The environmental reaction chamber used here will allow the variation of water vapor pressure to examine the effect of RH on these parameters. The role of a common atmospheric oxidant, ozone, in the uptake process will also be investigated. The results will be presented with emphasis on the role of hematite in mineral dust aerosols as a sink of SO_2, and the possible acidification of hematite particles through heterogeneous reaction pathways.

Notes

1. Brimblecombe, P., *Air composition and chemistry*. 2nd ed.; Cambridge University Press: Cambridge, 1996.

2. Gaffney Jeffrey, S.; Marley Nancy, A., The Importance of the Chemical and Physical Properties of Aerosols in Determining Their Transport and Residence Times in the Troposphere. In *Urban Aerosols and Their Impacts*, American Chemical Society: Washington, DC, 2005; pp 286-299.

3. Duce, R. A.; Tindale, N. W., Atmospheric Transport of Iron and its Deposition in the Ocean. *Limnology and Oceanography* **1991,** *36* (8), 1715-1726.

4. Fan, S.-M.; Moxim, W. J.; Levy II, H., Aeolian input of bioavailable iron to the ocean. *Geophysical Research Letters* **2006,** *33* (L07602), doi:10.1029/2005GL024852

5. Prospero, J. M.; Uematsu, M.; Savoie, D. L., Mineral aerosol transport to the Pacific Ocean. In *Chemical Oceanography*, Riley, J. P., Ed. Academic Press: New York, 1989; Vol. 10, pp 187 - 218.

6. Mogili, P. K.; Yang, K. H.; Young, M. A.; Kleiber, P. D.; Grassian, V. H., Environmental aerosol chamber studies of extinction spectra of mineral dust aerosol components: Broadband IR-UV extinction spectra. *J. Geophys. Res.* **2007,** *112*, D21204, doi:10.1029/2007JD008890.

7. Mogili, P. K.; Yang, K. H.; Young, M. A.; Kleiber, P. D.; Grassian, V. H., Extinction spectra of mineral dust aerosol components in an environmental aerosol chamber: IR resonance studies. *Atmospheric Environment* **2008,** *42* (8), 1752-1761.

8. Forster, P.; Ramaswarmy, V.; Artaxo, P.; Berntsen, T.; Betts, R.; Fahey, D. W.; Haywood, J.; Lean, J.; Lowe, D. C.; Myrhe, G.; Nganga, J.; Prinn, R.; Raga, G.; Schulz, M.; Van Dorland, R., Changes in Atmospheric Constituents and in Radiative Forcing. In *Climate Change 2007: The Physical Science Basis. Contribution of Working Group I to the Fourth Assessment Report of the Intergovernmental Panel on Climate Change*, Solomon, S.; Qin, D.; Manning, M.; Chen, Z.; Marquis, M.; Averyt, K. B.; Tignor, M.; Miller, H. L., Eds. Cambridge University Press, Cambridge, United Kingdom and New York, NY, USA: 2007.

9. Curtis, L.; Rea, W.; Smith-Willis, P.; Fenyves, E.; Pan, Y., Adverse health effects of outdoor air pollutants. *Environment International* **2006,** *32*, 815-830.

10. Nel, A., ATMOSPHERE: Enhanced: Air Pollution-Related Illness: Effects of Particles. *Science* **2005,** *308* (5723), 804-806.

11. Shea, K. M.; Truckner, R. T.; Weber, R. W.; Peden, D. B., Climate change and allergic disease. *Journal of Allergy and Clinical Immunology* **2008,** *122* (3), 443-453.

12. Bernstein, J. A.; Alexis, N.; Barnes, C.; Bernstein, I. L.; Nel, A.; Peden, D.; Diaz-Sanchez, D.; Tarlo, S. M.; Williams, P. B., Health effects of air pollution. *Journal of Allergy and Clinical Immunology* **2004,** *114* (5), 1116-1123.

13. Poeschl, U., Atmospheric aerosols: Composition, transformation, climate and health effects. *Angew. Chem., Int. Ed.* **2005,** *44* (46), 7520-7540.

14. Ciencewicki, J.; Trivedi, S.; Kleeberger, S. R., Oxidants and the pathogenesis of lung diseases. *Journal of Allergy and Clinical Immunology* **2008,** *122* (3), 456-468.

15. Donaldson, K.; Brown, D. M.; Mitchell, C.; Dineva, M.; Beswick, P. H.; Gilmour, P.; MacNee, W., Free Radical Activity of PM_{10}: Iron-mediated Generation of Hydroxyl Radicals. *Environmental Health Perspectives* **1997,** *105* (Suppl 5), 1285-1289.

16. Gilmour, P. S.; Brown, D. M.; Lindsay, T. G.; Beswick, P. H.; MacNee, W.; Donaldson, K., Adverse health effects of PM10 particles: involvement of iron in generation of hydroxyl radical. *Occupational and Environmental Medicine* **1996,** *53* (12), 817-822.

17. Smith, K. R.; Aust, A. E., Mobilization of Iron from Urban Particulates Leads to Generation of Reaction Oxygen Species *in Vitro* and Induction of Ferritin Synthesis in Human Lung Epithelial Cells. *Chemical Research in Toxicology* **1997,** *10* (7), 828-834.

18. Cox, R. A., Chemical Kinetics and Atmospheric Chemistry: Role of Data Evaluation. *Chemical Reviews* **2003,** *103* (12), 4533-4548.

19. Nash, D. G.; Baer, T.; Johnston, M. V., Aerosol mass spectrometry: An introductory review. *International Journal of Mass Spectrometry* **2006,** *258* (1-3), 2-12.

20. Noble, C. A.; Prather, K. A., Real-time single particle mass spectrometry: A historical review of a quarter century of the chemical analysis of aerosols. *Mass Spectrometry Reviews* **2000,** *19* (4), 248-274.

21. Suess, D. T.; Prather, K. A., Mass Spectrometry of Aerosols. *Chemical Reviews* **1999,** *99* (10), 3007-3035.

22. Sullivan, R. C.; Prather, K. A., Recent Advances in Our Understanding of Atmospheric Chemistry and Climate Made Possible by On-Line Aerosol Analysis Instrumentation. *Analytical Chemistry* **2005,** *77* (12), 3861-3886.

23. Sipin, M. F.; Guazzotti, S. A.; Prather, K. A., Recent Advances and Some Remaining Challenges in Analytical Chemistry of the Atmosphere. *Analytical Chemistry* **2003,** *75* (12), 2929-2940.

24. Adams, J. W.; Rodriguez, D.; Cox, R. A., The uptake of SO_2 on Saharan dust: a flow tube study. *Atmospheric Chemistry and Physics* **2005,** *5* (10), 2679-2689.

25. Ravishankara, A. R., Heterogeneous and Multiphase Chemistry in the Troposphere. *Science* **1997,** *276* (5315), 1058-1065.

26. Maahs, H., Kinetics and Mechanism of the Oxidation of S(IV) by Ozone in Aqueous Solution with Particular Reference to SO_2 Conversion in Nonurban Tropospheric Clouds. *Journal of Geophysical Research* **1983,** *88* (C15), 10721 - 10732.

27. Caffrey, P.; Hoppel, W.; Frick, G.; Pasternack, L.; Fitzgerald, J.; Hegg, D.; Gao, S.; Leaitch, R.; Shantz, N.; Albrechcinski, T.; Ambrusko, J., In-cloud oxidation of SO_2 by O_3 and H_2O_2: Cloud chamber measurements and modeling of particle growth. *J. Geophys. Res.* **2001,** *106* (D21), 27587-27601.

28. Lind, J.; Lazrus, A.; Kok, G., Aqueous Phase Oxidation of Sulfur(IV) by Hydrogen Peroxide, Methylhydroperoxide, and Peroxyacetic Acid. *Journal of Geophysical Research* **1995,** *92* (D4), 4171-4177.

29. Connick, R. E.; Zhang, Y.-X.; Lee, S.; Adamic, R.; Chieng, P., Kinetics and Mechanism of the Oxidation of HSO_3- by O_2. 1. The Uncatalyzed Reaction. *Inorganic Chemistry* **1995,** *34* (18), 4543-4553.

30. Connick, R. E.; Zhang, Y.-X., Kinetics and Mechanism of the Oxidation of HSO_3^- by O_2. 2. The Manganese(II)-Catalyzed Reaction. *Inorganic Chemistry* **1996,** *35* (16), 4613-4621.

31. Sedlak, D. L.; Hoigne, J., Oxidation of S(IV) in Atmospheric Water by Photooxidants and Iron in the Presence of Copper. *Environmental Science & Technology* **1994,** *28* (11), 1898-1906.

32. Bauer, S. E.; Koch, D., Impact of heterogeneous sulfate formation at mineral dust surfaces on aerosol loads and radiative forcing in the Goddard Institute for Space Studies general circulation model. *J. Geophys. Res.* **2005,** *110*, D17202, doi:10.1029/2005JD005870.

33. Bauer, S. E.; Mishchenko, M. I.; Lacis, A. A.; Zhang, S.; Perlwitz, J.; Metzger, S. M., Do sulfate and nitrate coatings on mineral dust have important effects on radiative properties and climate modeling? *J. Geophys. Res.* **2007,** *112*, D06307, doi:10.1029/2005JD006977.

34. Baltrusaitis, J.; Cwiertny, D. M.; Grassian, V. H., Adsorption of sulfur dioxide on hematite and goethite particle surfaces. *Physical Chemistry Chemical Physics* **2007,** *9* (41), 5542-5554.

35. Fu, H.; Wang, X.; Wu, H.; Yin, Y.; Chen, J., Heterogeneous Uptake and Oxidation of SO_2 on Iron Oxides. *Journal of Physical Chemistry C* **2007,** *111* (16), 6077-6085.

36. Fu, H.; Xu, T.; Yang, S.; Zhang, S.; Chen, J., Photoinduced Formation of Fe(III)-Sulfato Complexes on the Surface of α-Fe2O3 and Their Photochemical Performance. *The Journal of Physical Chemistry C* **2009,** *113* (26), 11316-11322.

37. Goodman, A. L.; Li, P.; Usher, C. R.; Grassian, V. H., Heterogeneous Uptake of Sulfur Dioxide On Aluminum and Magnesium Oxide Particles. *The Journal of Physical Chemistry A* **2001,** *105* (25), 6109-6120.

38. Judeikis, H. S.; Stewart, T. B.; Wren, A. G., Laboratory Studies of Heterogeneous Reactions of SO_2. *Atmospheric Environment* **1978,** *12*, 1663-1641.

39. Kim, K. H.; Choi, J. S., Kinetics and Mechanism of the Oxidation of Sulfur Dioxide on α-Fe_2O_3. *Journal of Physical Chemistry* **1981,** *85* (17), 2447-2450.

40. Li, L.; Chen, Z. M.; Zhang, Y. H.; Zhu, T.; Li, J. L.; Ding, J., Kinetics and mechanism of heterogeneous oxidation of sulfur dioxide by ozone on surface of calcium carbonate. *Atmos. Chem. Phys.* **2006,** *6* (9), 2453-2464.

41. Li, L.; Chen, Z. M.; Zhang, Y. H.; Zhu, T.; Li, S.; Li, H. J.; Zhu, L. H.; Xu, B. Y., Heterogeneous oxidation of sulfur dioxide by ozone on the surface of sodium chloride and its mixtures with other components. *J. Geophys. Res.* **2007,** *112,* D18301, doi:10.1029/2006JD008207.

42. Preszler Prince, A.; Kleiber, P.; Grassian, V. H.; Young, M. A., Heterogeneous interactions of calcite aerosol with sulfur dioxide and sulfur dioxide-nitric acid mixtures. *Physical Chemistry Chemical Physics* **2007,** *9*, 3432-3439.

43. Seisel, S.; Keil, T.; Lian, Y.; Zellner, R., Kinetics of the uptake of SO_2 on mineral oxides: Improved initial uptake coefficients at 298 K from pulsed Knudsen cell experiments. *International Journal of Chemical Kinetics* **2006,** *38* (4), 242-249.

44. Toledano, D. S.; Henrich, V. E., Kinetics of SO_2 Adsorption on Photoexcited α-Fe_2O_3. *Journal of Physical Chemistry B* **2001,** *105* (18), 3872-3877.

45. Ullerstam, M.; Johnson, M. S.; Vogt, R.; Ljungstrom, E., DRIFTS and Knudsen cell study of the heterogeneous reactivity of SO_2 and NO_2 on mineral dust. *Atmospheric Chemistry and Physics* **2003,** *3* (6), 2043-2051.

46. Ullerstam, M.; Vogt, R.; Langer, S.; Ljungstrom, E., The kinetics and mechanism of SO_2 oxidation by O_3 on mineral dust. *Physical Chemistry Chemical Physics* **2002,** *4* (19), 4694-4699.

47. Usher, C. R.; Al-Hosney, H.; Carlos-Cuellar, S.; Grassian, V. H., A laboratory study of the heterogeneous uptake and oxidation of sulfur dioxide on mineral dust particles. *Journal of Geophysical Research* **2002,** *107*, 4713, doi:10.1029/2002JD002051.

48. Usher, C. R.; Michel, A. E.; Grassian, V. H., Reaction on Mineral Dust. *Chemical Reviews* **2003,** *103* (12), 4882-4939.

49. Waqif, M.; Saad, A. M.; Bensitel, M.; Bachelier, J.; Saur, O.; Lavalley, J.-C., Comparative Study of SO_2 Adsorption on Metal Oxides. *Journal of the Chemical Society, Faraday Transactions* **1992,** *88* (19), 2931-2936.

50. Zhang, X.; Zhuang, G.; Chen, J.; Wang, Y.; Wang, X.; An, Z.; Zhang, P., Heterogeneous Reactions of Sulfur Dioxide on Typical Mineral Particles. *Journal of Physical Chemistry B* **2006,** *110* (25), 12588-12596.

51. Gebel, M. E.; Finlayson; Pitts, B. J.; Ganske, J. A., The uptake of SO2 on synthetic sea salt and some of its components. *Geophys. Res. Lett.* **2000,** *27* (6), 887-890.

52. Meskhidze, N.; Chameides, W. L.; Nenes, A., Dust and pollution: A recipe for enhanced ocean fertilization? *J. Geophys. Res.* **2005,** *110*, D03301, doi:10.1029/2004JD005082.

.

53. Meskhidze, N.; Chameides, W. L.; Nenes, A.; Chen, G., Iron mobilization in mineral dust: Can anthropogenic SO_2 emissions affect ocean productivity? *Geophys. Res. Lett.* **2003,** *30*, 2085, doi:10.1029/2003GL018035.

54. Mogili, P. K.; Kleiber, P. D.; Young, M. A.; Grassian, V. H., Heterogeneous Uptake of Ozone on Reactive Components of Mineral Dust Aerosol: An Environmental Aerosol Reaction Chamber Study. *Journal of Physical Chemistry A* **2006,** *110* (51), 13799-13807.

55. Mogili, P. K.; Kleiber, P. D.; Young, M. A.; Grassian, V. H., N_2O_5 hydrolysis on the components of mineral dust and sea salt aerosol: Comparison study in an environmental aerosol reaction chamber. *Atmospheric Environment* **2006,** *40*, 7401-7408.

56. Preszler Prince, A.; Wade, J. L.; Grassian, V. H.; Kleiber, P. D.; Young, M. A., Heterogeneous reactions of soot aerosols with nitrogen dioxide and nitric acid: atmospheric chamber and Knudsen cell studies. *Atmospheric Environment* **2002,** *36*, 5729-5740.

CHAPTER 2
EXPERIMENTAL APPARATUS AND PROTOCOL

2.1 Experimental Design

2.1.1 Environmental Reaction Chamber

An environmental reaction chamber was used to study the heterogeneous uptake of trace gases on particulate surfaces. The chamber was designed to operate at atmospherically relevant levels of total pressure, temperature, and relative humidity, and to suspend the solid sample as an aerosol in order to mimic actual environmental conditions. This chamber has been described previously in several studies [1-7], and is shown schematically in Figure 2.1. The chamber is an 83 cm high, 51 cm diameter cylinder constructed of stainless steel, with a chemically inert, 3 mm thick fluorinated ethylene-propylene (FEP) Teflon coating on the inner surface. The mating flanges on the top and bottom of the chamber are made of aluminum, which has also been coated with FEP Teflon on the interior surface to minimize reactions with reagent gases. The chamber is suspended above the floor by a steel frame, allowing the interior to be accessed from below by removing the bottom flange. Six pairs of side arms, arranged in a pattern of three rows consisting of two perpendicular pairs each, provide the interface for the necessary pressure transducers, vacuum connections, spectroscopic probes, and sample introduction. The mating flanges for the side arms are also Teflon coated to reduce unwanted side reactions.

A set of three thermocouple wires are taped near the top, center, and bottom outer walls of the chamber to monitor the temperature. While the environmental chamber has no direct temperature control scheme, it operates in a climate controlled laboratory, and

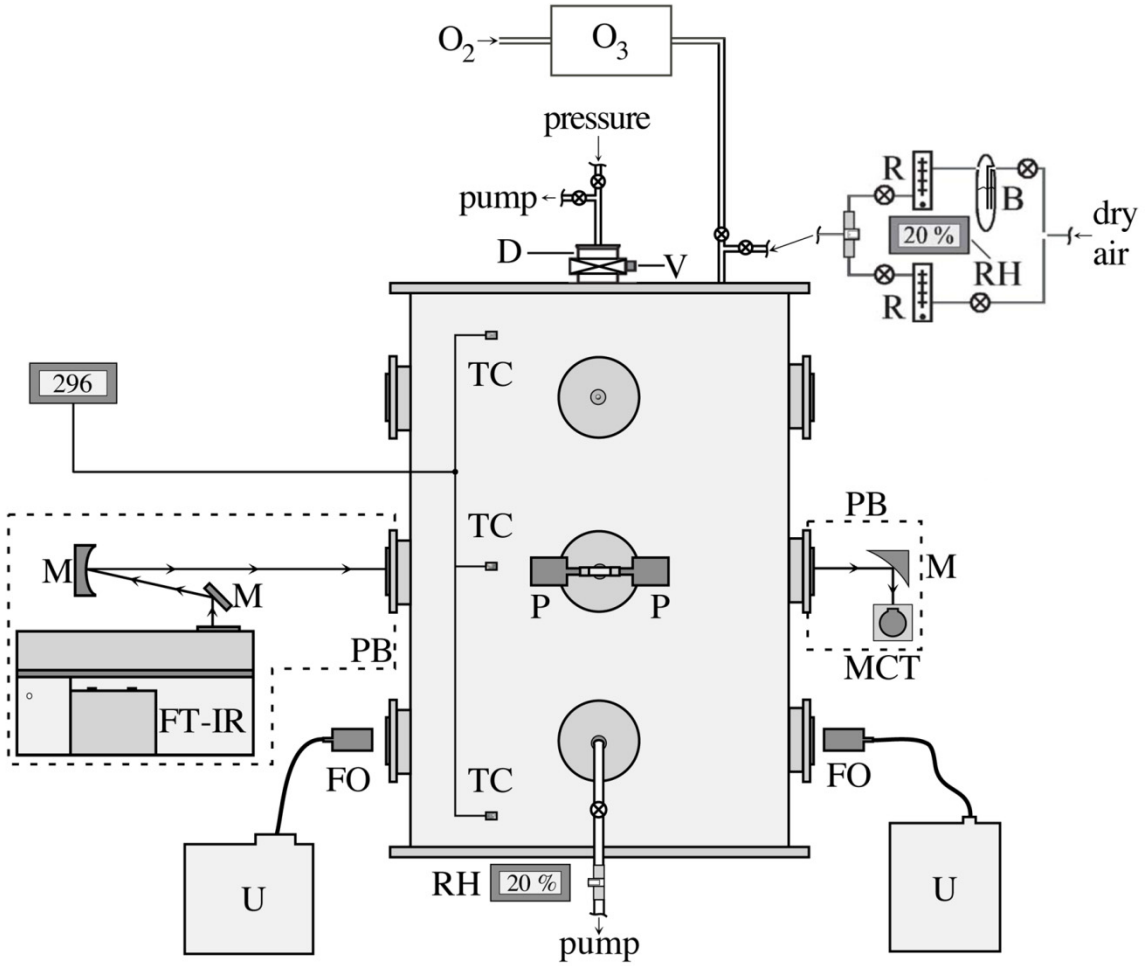

Figure 2.1. Schematic diagram of the environmental reaction chamber. Key components include the dust sample in an isolated antechamber (D), antechamber valve (V), electrical discharge ozone generator (O_3), rotameters (R), water bubbler (B), relative humidity sensors (RH), thermocouple sensors (TC), pressure transducers (P), FTIR spectrometer (FTIR), gold plated mirrors (M), mid-band mercury-cadmium-telluride IR detector (MCT), purge boxes enclosing external IR beam path (PB), fiber optic collimators (FO), and UV/Vis spectrometer (U). There is only one UV/Vis spectrometer in use, represented twice in this diagram to denote its use as both a light source and detector.

the temperature is normally constant to within ± 1 ºC during the course of an experiment. Two capacitance manometers (MKS, models 626A11TBE and 626A13TBE) are used to monitor the pressure inside the chamber. As absolute pressure transducers, the pressure measurement does not depend on the identity of the gasses used. One manometer has a range of 0.000 to 10.000 Torr, which is useful for adding precise amounts of trace gases, and creating corresponding calibration curves in conjunction with the spectroscopic probes. The other manometer has a 0.0 – 1000.0 Torr range, which is required for filling the chamber to atmospherically relevant pressures. A mechanical pump (Edwards 12), protected from harsh reactive gases with a molecular sieve trap, can be used to evacuate the chamber to a pressure of 20 – 30 mTorr.

2.1.2 Spectroscopic Analysis

A Fourier transform infrared spectrometer (FTIR, Mattson, Infinity 60 AR) was used to monitor the concentrations of reactive species within the chamber. The instrument is operated in an external mode, allowing the IR beam to be directed external to the spectrometer and pass through the chamber. The beam is directed from the instrument towards the chamber by a pair of gold-coated mirrors with individual alignment control. The beam is coupled in and out of the chamber with a pair of 2" diameter germanium windows (Janos Technology, A1305W658), which are mounted in a parallel set of side arm flanges. Within the 59 cm of active pathlength inside the chamber, the IR beam has a diameter of approximately 2 cm. Upon exiting the chamber, the IR beam is focused by a gold plated, parabolic mirror onto the 1 mm^2 detection element of the external, liquid nitrogen cooled mercury-cadmium-telluride (MCT) detector. With the exception of its path through the interior of the chamber, the entire IR beam path is

enclosed in continuously purged clear polycarbonate boxes, to avoid unwanted interference from infrared absorbers in laboratory air. A dedicated flow of 30 scfh from a Whatman purge gas generator (model 75-62) was used to purge the boxes. The FTIR instrument was typically operated at 8 cm^{-1} resolution, 256 scans per spectrum, which provided adequate spectral resolution and a reasonably fast time resolution of 52 seconds. FTIR spectra were acquired over the range of 650 – 5000 cm^{-1}.

A UV/Visible spectrometer (Ocean Optics, SD2000) could also be used in conjunction with the FTIR probe. The instrument's tungsten/deuterium light sources were coupled through the chamber with fiber optic collimators mounted on the side arms perpendicular to the IR probe but on the same horizontal plane. Two inch diameter quartz windows transmitted the UV/Vis light through the chamber. The instrument used a multi-element array detector that was active in the 220 – 880 nm range. In the studies reported in this thesis, the UV/Vis probe was used primarily to monitor approximate trace gas concentrations during their introduction to the chamber by using settings that provided nearly real time (every 5 ms) spectral updates.

2.1.3 Aerosol Sample Introduction

Prior to the experiment, the dust sample is packed into a cylindrical cartridge and remains isolated in the sample antechamber that is separated from the main chamber by a slide valve. A needle valve allows the antechamber to be evacuated with a mechanical pump (Edwards 8); initially, the needle valve is opened a minimal amount so that the powder is not disturbed by the initial high flow rate of air from the antechamber towards the pump. Once the pressure is sufficiently reduced, the valve could be fully opened and the dust sample held under vacuum for a determined period to remove residual water. To

aerosolize the powder sample within the chamber, the needle valve is shut, and the slide valve to the chamber is opened. The dust delivery system is an “L”-shaped stainless steel tube with the dust cartridge on one end and a partial impactor system[1] at the other end; the tube can be slid through an Ultra-Torr (Cajon) fitting such that the impactor extends into the volume of the main chamber. A solenoid valve connected to the sample cartridge introduces a one second burst of an inert gas from a cylinder source (nitrogen or argon) at 100 psi, which forces the dust sample out of the cartridge, through the tube, and into the chamber. Small particles follow the gas stream closely, and bypass the impactor system, but larger particles with more inertia strike the impactor and become deagglomerated. The burst of gas suspends the dust sample in the chamber as an aerosol, so that the isolated, suspended particles may react with the desired trace gases. The resulting turbulence also mixes the chamber contents on a time scale of less than one minute [1]. Laser diode light scattering was previously used to confirm that aerosol particles remain suspended in the chamber during the span of a typical 8 – 10 hour experiment [1].

Some portion of the dust sample was not aerosolized during the process and remained in the antechamber. After disassembly of the antechamber, the residual dust sample was weighed. For the nominally 2.8 g dust loadings used throughout this thesis, it was found that 0.21 ± 0.13 g typically remained in the chamber (n = 17). A modified procedure was also used, in which prior to introduction, the evacuated antechamber was slowly pressurized to atmospheric pressure with dry buffer gas through the needle valve. It was thought that matching the pressure in the antechamber to that of the main chamber in this way prior to opening the slide valve may reduce dust losses, but no difference was observed (typical losses of (0.20 ± 0.09 g, n = 5).

2.1.4 Gas introduction manifold

A glass manifold was used to deliver both trace gases and unreactive buffer gases to the chamber. The manifold has a number of Teflon valves (Swagelok) for connecting gas cylinders, sample bulbs, or vacuum lines, and a vent to the laboratory exhaust system. A capacitance manometer (MKS, 121A-12204) monitors the pressure within the manifold over the range of 0.0 – 1000.0 Torr. The manifold is evacuated to a minimal pressure by a molecular sieve trapped, Edwards 8 mechanical pump prior to gas introduction.

The manifold also has a connection to a variable humidity flow system, which provides the buffer gas to the chamber. The dry, CO_2 and organic free air flow from the purge gas generator is split through two routes, one "dry" and one "humid", each controlled by a separate rotameter. If humidified air is desired, the "humid" flow is directed through a 1.4 L, 50 cm long glass bubbler which is about half-filled with 6 mm diameter glass beads. The flow bubbles through high purity water (Fischer Chemical, Optima) in the bubbler and becomes saturated with water vapor. The "dry" and "humid" flows are recombined and directed into the chamber; varying the relative flow rates allows any desired relative humidity (RH) in the range of 0 - 88% to be achieved. In nominally dry experiments, water vapor was below the detection limit of ≈ 10 mTorr, indicating RH << 1% at ambient temperature. An in-situ RH sensor (HyCal Sensing Products, HIH-3602-L-CP), glued into an arm of a T-shaped Swagelok fitting within the recombined flow path, allows the RH to be estimated as the chamber is filled, although the RH in the chamber is quantified more precisely by a Beer's Law calibration of IR

integrated absorptions. The humidified flow was directed through a vent to laboratory exhaust until the reading on the RH sensor stabilized, before introduction to the chamber.

2.1.5 Reagent Gasses and Powder Samples

A hematite (α-Fe_2O_3) powder was used as the aerosol sample in all experiments. Although the manufacturer (Sigma-Aldrich) only specified the sample as Fe(III) Oxide, x-ray diffraction (XRD) was used to confirm that the sample consisted entirely of hematite, based on comparison to library XRD spectra. No XRD signals due to other common Fe(III) oxides (such as goethite, FeOOH), were detected. The specific surface area of the hematite sample was measured using a Braun-Emmett-Teller apparatus (BET, Quantachrome, Nova 1200 Multipoint). This instrument measured adsorption isotherms of nitrogen gas on the sample to determine the BET surface area, S_{BET}, of 5.06 ± 0.02 m^2 g^{-1}, with the reported uncertainty based on the standard deviation of triplicate measurements. The residual water content of the sample, due to handling in the laboratory at ambient RH levels, was also estimated by weighing the powder before and after heating overnight in an oven at 112 ºC. It was found that 27 mg H_2O g^{-1} α-Fe_2O_3 could be driven off by the heating process, as measured immediately after removal of the sample from the oven. This water was largely recovered by the hematite upon 10 minutes of re-exposure to the ambient atmosphere.

Laboratory air, passed through the purge gas generator to remove water, CO_2, and trace organics, provided the buffer gas in the chamber with typical tropospheric proportions of N_2 and O_2. A cylinder of Argon (99.9997% purity) was used to pressurize the sample antechamber for aerosol introduction. Sulfur dioxide (SO_2, American Air Gas) was dispensed in the gas handling manifold from a lecture bottle with regulator.

Ozone was generated *in situ* using an electrical arc discharge ozone generator (OREC, Model O3V5-O). Oxygen from a cylinder (Air Products, USP grade) was sent to the input of the ozone generator at a pressure of 10 psi. The rotameter on the ozone generator was set to 10 – 11 (arbitrary units), and the current was set at 2 amperes. The output of the generator was still largely oxygen, along with several thousand ppm of ozone. The output was directed to the laboratory exhaust for about one minute to allow the flow to equilibrate, and then into the environmental reaction chamber. Typically, 10 – 50 Torr of the O_2/O_3 mixture was added to the chamber to achieve ozone concentrations of 10 – 100 ppm. However, it was difficult to reproducibly add a given amount of ozone based solely on measuring the pressure increase in the chamber as the O_2/O_3 mixture was added; it was necessary to use FTIR or UV-Vis spectroscopy to achieve the desired O_3 pressure via a spectroscopic calibration.

2.1.6 Experimental Protocol

The dust sample was weighed on an analytical balance and placed in the sample cartridge assembly, which was sealed and evacuated for at least 2 hours in order to remove adsorbed water. The chamber was evacuated for at least one hour, until a minimal pressure of 20 – 40 mTorr was reached. The MCT detector was filled with liquid nitrogen, and a Winfirst software macro was used to begin continuous collection of FTIR single-beam spectra of the evacuated chamber (every 52 seconds at the setting used). Consecutive spectra were ratioed to one another to obtain absorbance spectra; operation was considered satisfactory if these absorbance spectra exhibited a flat baseline centered at zero absorbance units to within ± 0.0005, and an RMS noise of $1 – 4 \times 10^{-4}$ absorbance units over the 1300 – 1400 cm^{-1} region.

Sulfur dioxide was introduced into the chamber first. To obtain the relatively low pressures used, the regulator on the SO_2 cylinder was set to 1 – 2 psig, and the regulator's valve opened slightly to fill the small volume (<10 mL) between the cylinder and the Teflon valve. The Teflon valve was then opened, allowing the gas to expand into the rest of the gas manifold. The valve to the chamber was then opened, and the desired pressure of SO_2 was introduced by monitoring the 0.000 to 10.000 Torr capacitance manometer. The gas manifold was then flushed for 10 minutes with dry purge air (to minimize the SO_2 which would potentially reach the pump), then evacuated to minimal pressure. Ozone was then added if desired, by the method mentioned above in 2.1.5. The gas manifold was flushed and evacuated again. The chamber was then filled to 760 Torr with the buffer gas, which was either dry or humidified air.

FTIR spectra of the chamber containing the buffer gasses were continuously acquired every 52 seconds, for at least 90 minutes, in order to quantify the background loss rates. The hematite sample was then introduced by opening the slide valve between the chamber and antechamber, sliding the dust delivery tube into the chamber, and triggering the burst of argon that force the powders through the impactor and disperses it as an aerosol. The addition of argon increased the pressure within the chamber to ≈770 Torr, which did not significantly broaden the IR absorbance peaks used for gas quantification. The delivery tube was then withdrawn and the slide valve closed. The delivery system and sample cartridge were then disassembled, and the residual powder was weighed to correct for the reactive dust surface area introduced into the chamber. The residual powder was exposed to the chamber atmosphere for no more than the 20 seconds required for the aerosol introduction. The software macro continues to acquire

FTIR spectra every 52 seconds for the duration of the experiment, which is up to 10 hours.

Following the experiment, the chamber is flushed for at least one hour with dry buffer gas in order to remove residual reactive gasses. The chamber is then evacuated to the minimum base pressure, and vented to the laboratory atmosphere. The germanium and quartz windows are removed and cleaned with lens paper and spectroscopic grade methanol; the window orientation is noted to ensure consistent replacement. The bottom flange is removed from the chamber for cleaning with Kimwipe tissues and Optima grade water. With the flange removed, the chamber can be accessed from below for interior cleaning with damp tissues.

2.2 Data Analysis

2.2.1 Pressure Determinations by FTIR

Following the experiment, the series of single-beam spectra are converted to absorbance spectra by taking the ratio with respect to a spectrum of the evacuated chamber. The pressure of each IR-active gas in the chamber is determined either through integration of the absorbance band used for quantification, or simply the net absorbance relative to a baseline. The baseline slope due to light scattering by aerosols in the IR beam is corrected for in each case.

Water vapor, SO_2, and CO_2 (present in trace amounts as a contaminant) are each determined by previously acquired Beer's Law calibrations[1]. Water vapor is quantified via integration of the peaks in the 3788.5 – 3966.8 cm^{-1} range. P_{SO2} is determined by integration from 1301 – 1407 cm^{-1}, and P_{CO2} by integration from 2219 – 2421 cm^{-1}. In humid experiments, broad, intense absorptions from the water bending mode interfere

with the SO_2 peak. For the purpose of subtracting water contributions, a series of background water vapor spectra were obtained by filling the chamber with very humid air (≈80% RH). FTIR spectra were acquired continuously as the chamber was flushed with a low flow rate of dry buffer gas with the vent to the laboratory exhaust system partially open. The flow rate was such that the total pressure in the chamber remained consistent at 760 Torr. In this way, a series of water vapor spectra representing 0% < RH < 80% were obtained for use in spectral subtraction. Ozone is quantified by the net absorbance at 1054 cm^{-1}, based on the literature absorptivity of 3.74 x 10^{-4} ppm^{-1} m^{-1} at this wavenumber with 1 atm total pressure [2, 8].

2.2.2 Kinetic Analysis

The uptake processes studied here were analyzed based on a simple model of irreversible adsorption/reaction to a particle surface as in Equation 2.1,

$$R + S \xrightarrow{k} P \qquad 2.1$$

where R denotes a reagent gas, S is a reactive surface site, and P is a product or chemisorbed species. The additional simplification of assuming pseudo-first order kinetics can be used if the number of surface sites is high relative to the number of gaseous molecules. The Fuchs-Sutugin approach is used to derive an expression for k, based on the mass concentration ($[c_{mass}]$, g m^{-3}) of an aerosol with a specific surface area S (m^2 g^{-1}), as is shown in Equation 2.2 [1, 9]. k also depends on the mean velocity of the reactive gas, $\bar{c}$ (m s^{-1}).

$$k = \frac{\gamma(\bar{c}/4)[c_{mass}]S}{1 + \gamma\left(\frac{0.750 + 0.283K_n)}{K_n(K_n + 1)}\right)} \quad 2.2$$

The uptake coefficient, γ, is the ratio of gas-surface collisions that lead to uptake (i.e., which form *P*) to the total number of gas-surface collisions, which can be calculated from the kinetic theory of gasses. The Knudsen number, K_n, is the dimensionless ratio of the mean free path of the reactive gas molecule (λ) to the characteristic radius of the particles, R_p.

$$K_n = \frac{\lambda}{R_p} \quad 2.3$$

The mean free path is given by Equation 2.4,

$$\lambda = \frac{3D}{\bar{c}} \quad 2.4$$

where D is the diffusion coefficient of the reagent gas ($cm^2\ s^{-1}$), which is also dependent on the buffer gas.

The behavior of Equation 2.2 can be examined for some limiting cases. The first case is the "continuum" regime, where the particle is much larger than λ, and the high frequency of collisions makes the surrounding gas resemble a continuous fluid. If $K_n << 1$, as in the case of larger particles of several μm in diameter, Equation 2.2 simplifies to:

$$k = \frac{\gamma(\bar{c}/4)[c_{mass}]S}{1 + \frac{3\gamma}{4K_n}} \quad 2.5$$

If however, $K_n >> 1$, and the particles motion is similar to that of a gas molecule, Equation 2.2 rearranges to the form of Equation 2.6.

$$k = \frac{\gamma(\bar{c}/4)[c_{mass}]S}{1 + \frac{0.283\gamma}{K_n}} \quad 2.6$$

In our experiments, where particles with smaller radii will have the highest number density, the kinetics are expected to resemble the limiting case of Equation 2.6.

It can be seen from Equation 2.3 that if the particle radius is much smaller than the mean free path, the Knudsen number will be very large. By using a value of 0.1238 $cm^2\ s^{-1}$ for the diffusion coefficient of SO_2 in air[1], a mean free path of ≈1.2 x 10^{-7} m can be calculated. Thus, for particles between 1 - 100 nm, K_n will range from 1.2 – 120. As it makes no physical sense for γ, a ratio of reactive collisions to total number of collisions, to be greater than 1, it is evident that $\gamma << K_n$ throughout our experiments. This will make the fractional term in the denominator of Equation 2.6 to be negligibly small, leading to the simplified Equation 2.7.

$$k = \gamma(\bar{c}/4)[c_{mass}]S \quad 2.7$$

We can use data fitting of the experimental decay in trace gas pressures to determine the characteristic time constant, τ, for this process. Using the reciprocal relation between k and τ, the uptake coefficient can be written as:

$$\gamma = \frac{4}{\bar{c}\tau[c_{mass}]S_{BET}} \quad 2.8$$

Here, S has been given a subscript to specify that throughout this report, the specific BET surface area will be used to calculate γ. Equation 2.8 is used to calculate γ throughout this report, as this model was found to adequately describe the kinetics of several gas-particle systems utilizing this chamber [2, 6, 7, 10].

Notes

1. Preszler Prince, A. M. Investigations Into The Heterogeneous Atmospheric Interactions of Isolated Metal Oxide, Carbonate, and Soot Aerosols. University of Iowa, Iowa City, **2003**.

2. Mogili, P. K.; Kleiber, P. D.; Young, M. A.; Grassian, V. H., Heterogeneous Uptake of Ozone on Reactive Components of Mineral Dust Aerosol: An Environmental Aerosol Reaction Chamber Study. *Journal of Physical Chemistry A* **2006,** *110* (51), 13799-13807.

3. Mogili, P. K.; Yang, K. H.; Young, M. A.; Kleiber, P. D.; Grassian, V. H., Environmental aerosol chamber studies of extinction spectra of mineral dust aerosol components: Broadband IR-UV extinction spectra. *J. Geophys. Res.* **2007,** *112*, D21204, doi:10.1029/2007JD008890.

4. Mogili, P. K.; Yang, K. H.; Young, M. A.; Kleiber, P. D.; Grassian, V. H., Extinction spectra of mineral dust aerosol components in an environmental aerosol chamber: IR resonance studies. *Atmospheric Environment* **2008,** *42* (8), 1752-1761.

5. Navea, J. G.; Xu, S.; Stanier, C. O.; Young, M. A.; Grassian, V. H., Effect of Ozone and Relative Humidity on the Heterogeneous Uptake of Octamethylcyclotetrasiloxane and Decamethylcyclopentasiloxane on Model Mineral Dust Aerosol Components. *The Journal of Physical Chemistry A* **2009,** *113* (25), 7030-7038.

6. Preszler Prince, A.; Kleiber, P.; Grassian, V. H.; Young, M. A., Heterogeneous interactions of calcite aerosol with sulfur dioxide and sulfur dioxide-nitric acid mixtures. *Physical Chemistry Chemical Physics* **2007,** *9*, 3432-3439.

7. Preszler Prince, A.; Wade, J. L.; Grassian, V. H.; Kleiber, P. D.; Young, M. A., Heterogeneous reactions of soot aerosols with nitrogen dioxide and nitric acid: atmospheric chamber and Knudsen cell studies. *Atmospheric Environment* **2002,** *36*, 5729-5740.

8. Orphal, J., A critical review of the absorption cross-sections of O3 and NO2 in the ultraviolet and visible. *Journal of Photochemistry and Photobiology A: Chemistry* **2003,** *157* (2-3), 185-209.

9. Lovejoy, E. R.; Hanson, D. R., Measurement of the Kinetics of Reactive Uptake by Submicron Sulfuric Acid Particles. *The Journal of Physical Chemistry* **1995,** *99* (7), 2080-2087.

10. Mogili, P. K.; Kleiber, P. D.; Young, M. A.; Grassian, V. H., N_2O_5 hydrolysis on the components of mineral dust and sea salt aerosol: Comparison study in an environmental aerosol reaction chamber. *Atmospheric Environment* **2006,** *40*, 7401-7408.

CHAPTER 3
THE HETEROGENEOUS REACTION OF SULFUR DIOXIDE ON HEMATITE UNDER SIMULATED ATMOSPHERIC CONDITIONS

3.1 Abstract

The uptake of sulfur dioxide (SO_2) on hematite (α-Fe_2O_3) was investigated using an environmental reaction chamber. Fourier Transform Infrared (FTIR) spectroscopy was used to determine the kinetics and total amount of SO_2 uptake on aerosolized hematite. Under dry conditions, the hematite surface became saturated at a coverage of $1.8 \pm 0.1 \times 10^{14}$ cm^{-2} with an uptake coefficient of $\gamma_{SO2} > 2.6 \times 10^{-6}$, a lower limit determined by the finite time resolution of the technique. The presence of water vapor corresponding to 10 - 81% relative humidity increased the amount of SO_2 uptake by a factor of 1.3 - 1.7, while also reducing γ_{SO2} to $3.0 - 8.9 \times 10^{-8}$. No significant difference was observed in the SO_2 uptake capacity of hematite when the partial pressure of oxygen in the chamber was reduced from atmospheric levels to $\leq$ 6 mTorr.

3.2 Introduction

It is estimated that 800 - 1700 Mt yr^{-1} of mineral dust are entrained into the atmosphere as aerosols globally via natural wind action, predominantly in arid regions; expanded human activity such as agricultural practices and deforestation may be increasing this amount further [1]. Although there is, of course, variation between emission sources, the composition of the suspended mineral dust largely parallels that of crustal material, with SiO_2 accounting for over 60% of the total aerosol mass [2]. The iron content in mineral dust aerosol is reported to be between 3-7% by mass, with higher values near anthropogenic sources [2-4]. The speciation of the iron in aerosol samples

typically contains mixtures of goethite, hematite (α-Fe_2O_3), magnetite, and Fe(II or III) incorporated into a silicate framework. Highly colored oxides such as hematite absorb and scatter significant amounts of visible and UV radiation, which can lead to a climate forcing effect in mineral aerosols [5].

Iron oxide aerosol also plays a critical role in biogeochemical cycles in the environment. Aerosolized mineral dust is a major source of iron for remote areas of the oceans [6, 7]. The speciation and solubility of the iron largely determines its bioavailability. Many marine microbes produce siderophores, specialized iron binding ligands, in order to utilize the marginally soluble iron in Fe(III) oxides [8, 9]. The degree of iron dissolution in seawater has also been correlated with the dissolved organic carbon (DOC) content [10]. In general, however, microbes can grow at much faster rates when directly provided with dissolved iron rather than colloids of iron oxides [11]. Phytoplankton blooms act as a natural source of isoprene, which can then be oxidized into secondary organic aerosols (SOA); the light scattering properties of the SOA may then cause negative climate forcing via scattering of incoming solar radiation [12]. Explosive growth of phytoplankton colonies may also affect the rate of CO_2 fixation by marine biota to a degree that would contribute to climate change [13, 14]. The growth rate of phytoplankton is often limited by the availability of nutrients, including iron [15]. Heterogeneous reactions that increase the solubility of iron in mineral aerosols could thus indirectly affect climate by stimulating blooms in ocean phytoplankton colonies. A wide range of solubility has been reported for the iron fraction of aerosols, as a result of both differing aerosol sources and analytical method. The iron solubility is commonly reported as a mass percentage as in Equation 3.1.

$$\% \text{ sol} = 100[Fe_{sol}]/[Fe_{tot}] \quad 3.1$$

The sample is divided into aliquots for determination of the soluble and total iron contents. A strong acid leach will completely dissolve the aerosol, and various analytical methods can be used to determine the total iron concentration in the resulting solution, $[Fe_{tot}]$. Methods for determining the soluble iron content $[Fe_{sol}]$ vary, but in general involve allowing an aerosol sample to dissolve in a buffer solution, removal of the remaining solid particles by filtration or centrifugation, and analysis of the iron content in the supernatant liquid. There are also methods to determine the speciation of aerosolized iron as Fe(II) or Fe(III), which is crucial for understanding the red-ox behavior and solubility of the sample [16]. Numerous reports suggest the solubility of iron in natural aerosols is in the range 0.04 - 7.9% [17-22], with a few studies reporting much higher values, over 50% [23]. It should be noted that many of these studies used acidic leaches to determine iron solubility, and that solubility may actually be orders of magnitude lower in weakly basic seawater [10]. Iron incorporated into aluminosilicate clays is generally much more soluble than iron oxides such as goethite or hematite [24]. Anthropogenic aerosol sources also contain more soluble iron than mineral sources [21]. There is also debate about whether observed increases in particle solubility with atmospheric lifetime are simply the result of a physical phenomenon. As a dust plume travels through the atmosphere, larger particles are lost due to gravitational settling, leaving behind submicron particles which are more soluble due to a higher surface area-to-volume ratio [25, 26].

Acidification of mineral aerosols by anthropogenically produced pollutants such as SO_2 or HNO_3 could lead to increased solubility of the iron oxide components.

Meskhidze et al. used hematite as a model iron-containing mineral aerosol to illustrate this concept [20]. Based on literature values for pH-dependant rates of dissolution, representative values of the specific surface area of mineral aerosols, and typical atmospheric lifetimes, they deduce that pH < 2 would be required to produce an iron solubility of 1 - 2%. The threshold of 1 - 2% was chosen as a reasonable range based on numerous reports (ex., [17-20]); it should be noted that a significantly higher pH could produce the lowest reported percentages of solubility. These authors further present a case study in which a plume of aerosols was observed in an area of high SO_2 and HNO_3 mixing ratios that suggest the aerosol pH was indeed 2 or less [20]. This mechanism of acidification can be greatly suppressed if the aerosols are heterogeneous in composition and contain alkaline components such as $CaCO_3$, which can act as a buffer in the deliquesced aerosols [13]. If the buffering capacity of the aerosol is high, or if there are no nearby anthropogenic sources of SO_2, the amount of dissolved Fe resulting from atmospheric deposition may be insufficient to enhance phytoplankton growth.

Several studies have investigated the reaction of SO_2 with various mineral dust substrates. The combustion of sulfur-containing fossil fuels can lead to SO_2 mixing ratios on the order of hundreds of ppb near urban areas [27, 28]. By incorporating kinetic parameters obtained with a flow tube reactor into a simple box model, Adams et al. determined that Saharan mineral dust may contribute significantly to removal of gas-phase SO_2 at mixing ratios below 250 ppt [27]. Diffuse reflectance infrared Fourier transform spectroscopy (DRIFTS) was used to study the oxidation of SO_2 by ozone on mineral dust (collected near Cape Verde) [29]. The results indicate that surface hydroxyl groups are consumed as SO_2 uptake proceeds. Determination of the potential atmospheric

relevance of a reaction depends greatly on whether the uptake coefficient is defined in terms of the geometric or BET (Brunauer-Emmett-Teller) surface area of the suspended particles. The BET surface area is typically determined from the uptake of inert N_2 and includes surface area within pores. Thus, the BET area represents the maximum area that could participate in heterogeneous chemistry; however, different sites may have different reactivity or be inaccessible to bulkier gaseous molecules. While these studies are useful for establishing the importance of mineral dust in atmospheric reactions with SO_2, the field-collected aerosols have a heterogeneous composition, and therefore it is not clear specifically which chemical species play important roles. It is sometimes possible to infer the reactivity of an externally mixed aerosol sample by taking a weighted average of the reactivity of its major components [30]. Heterogeneous, internally mixed particles may have certain minerals concentrated near the surface which will dominate the overall particle reactivity.

Gaseous SO_2 can partition into liquid water aerosols, or into adsorbed water layers on a particle surface, after which it may dissociate into sulfite or bisulfate as described by the following equilibria [31]:

$$SO_2(g) + H_2O(l) \overset{H}{\longleftrightarrow} H_2SO_3(aq) \qquad 3.2$$

$$H_2SO_3(aq) \overset{K_{a1}}{\longleftrightarrow} H^+ + HSO_3^- \qquad 3.3$$

$$HSO_3^- \overset{K_{a2}}{\longleftrightarrow} H^+ + SO_3^{2-} \qquad 3.4$$

The pH dependence of the equilibria shown in Equations 3.3 and 3.4 leads to a pH dependent SO_2 solubility, and the total amount of dissolved S(IV) species can be described by the effective Henry's Law constant H^*.

$$H^* = H_{SO2}\left(1 + \frac{K_{a1}}{[H^+]} + \frac{K_{a1}K_{a2}}{[H^+]^2}\right) \quad 3.5$$

Here, H_{SO2} is the Henry's Law constant for SO_2, and K_{a1} and K_{a2} are the equilibrium constants for the equilibria in Equations 3.3 and 3.4, respectively (H_{SO2} = 5.42 mol L^{-1} atm^{-1}, K_{a1} = 7 x 10^{-2} mol L^{-1}, K_{a2} = 10^{-7}, at 15 ^oC) [32]. From Equation 3.5 it can be seen that effective solubility is inversely dependent on $[H^+]$ concentration.

Hematite (α-Fe_2O_3) was chosen as a proxy for iron-containing dust aerosols, based on previous reports that it is the most active iron oxide towards SO_2 [33]. Knudsen cell experiments indicate that the initial uptake coefficient for SO_2 on γ-Fe_2O_3 is of the same magnitude as Saharan dust, suggesting iron oxides may play an important role in determining the reactivity of airborne dusts [34]. Catalytic oxidation of SO_2 to sulfite on α-Fe_2O_3 has been observed in the presence of oxygen; the authors proposed that SO_2 adsorbs onto a lattice oxygen on the α-Fe_2O_3 surface and subsequently reacts with oxygen which has dissociatively adsorbed on a nearby oxygen vacancy site [35]. Hematite was also found to be more reactive towards SO_2 (after normalization for BET surface area) than the more atmospherically abundant oxides Al_2O_3 and SiO_2 by factors of 5 and 25, respectively [36]. While some studies have investigated the effect of water and oxygen on the speciation of products from the heterogeneous reaction of SO_2 with hematite [33, 37], the kinetics and extent of SO_2 uptake have not been systematically studied as a function of relative humidity.

Other researchers have noted that due to a wide range of reported uptake coefficients and mechanisms, it is difficult to determine the contribution of sulfate formation via heterogeneous reactions on mineral dust to global radiative forcing [38]. Laboratory methods that determine rates and amounts of SO_2 uptake onto dry mineral

dusts often neglect the possibly large effect that water vapor, a ubiquitous component of the troposphere, may have on measured values. The goal of this study is to determine the effects of water vapor on the uptake of SO_2 on hematite aerosol. The hematite is suspended in an environmental reaction chamber, where the heterogeneous uptake of SO_2 can be studied under atmospherically relevant conditions of temperature, relative humidity (RH), and partial pressure of oxygen via FTIR spectroscopy. Isolated particle conditions also mitigate the complications of bulk, powdered samples, such as diffusion and surface area ambiguities. Mogili et al. recently used the same instrument to determine that the uptake of ozone on mineral dust is strongly dependant on RH, with up to 50-fold reduction in uptake rates at 58% RH [39]. The observation of a strong RH dependence on SO_2 uptake would necessitate a reevaluation of the importance of this reaction in the atmosphere.

3.3 Experimental

The environmental reaction chamber has been described previously in Chapter 2 and in prior publications [39-41]. A brief description of the method follows. The IR beam from a Mattson Infinity 60 AR FTIR spectrometer is directed into the chamber using a pair of gold-plated mirrors. Germanium windows were chosen for coupling the beam into the chamber, as the high humidity conditions used in some experiments would quickly degrade salt windows. The beam is focused with a gold-plated parabolic mirror onto an external, liquid nitrogen cooled mercury cadmium telluride (MCT) detector. The IR beam samples a 59 cm pathlength inside the chamber, while the rest of the beam is enclosed in boxes purged by a Whatman purge gas generator (Model 75-62) which removes water, CO_2, and organics from a laboratory compressed air source. With the exception of the

germanium and several quartz windows (for other spectroscopic probes), all inner surfaces of the chamber are Teflon coated to reduce side reactions of gasses with the chamber walls. The chamber is not directly temperature controlled, but operates at room temperature in a climate controlled environment, and is consistent to ±1 ^{o}C throughout the course of an experiment.

Prior to an experiment, a trapped mechanical pump is used to evacuate the chamber to a base pressure of 20-30 mTorr. A gas handling manifold (which is evacuated whenever not delivering gasses) is used to add the desired pressure of sulfur dioxide to the chamber. A 0 - 10 Torr capacitance manometer inside the chamber was used to create a Beer's Law calibration for SO_2; a similar calibration was performed for water and CO_2. The chamber is filled to about 760 Torr with purge air; for humidity studies the flow of purge air can be split through a bubbler containing Optima grade water until the desired nominal humidity is reached as determined by a relative humidity (RH) sensor in the recombined flow path. Single beam FTIR spectra (256 scans at 8 cm^{-1} resolution, leading to a time resolution of 51 seconds) of the chamber contents are acquired continuously for at least one hour to determine the rate of loss of reagent gasses due to interaction with each other or the chamber walls. The same FTIR data is used to quantitatively determine the amount of water in the chamber which, combined with the chamber temperature, yields the experimental RH conditions. Single beam data is converted to absorbance using a background spectrum of the evacuated chamber.

A sample of hematite (α-Fe_2O_3) powder with a total BET surface area of 13 - 14 m^2 is placed in an L-shaped stainless steel tube capped with a dust impactor at one end. The tube assembly is isolated from the main reaction chamber by a slide valve. After

evacuation for at least three hours to remove residual water, the slide valve is opened to allow the tube assembly to be slid into the main chamber. A 100 psi burst of Argon gas, actuated by a solenoid valve, forces the powder through the dust impactor assembly for deagglomeration and dispersal into the main chamber. The addition of argon upon aerosol introduction raises the total pressure in the chamber to approximately 770 Torr, which does not significantly broaden any peaks from their shapes at 760 Torr. Following injection and closing of the slide valve, the tube and impactor are disassembled and residual powder sample is collected and weighed. The total BET surface area used in kinetic and uptake calculations accounts for any loss of powder in the tubing, which is normally 3 - 5% but occasionally in excess of 10%. FTIR spectra are collected continuously for 8 - 12 hours to monitor the concentrations of gas phase species in the chamber.

3.4 Results

3.4.1 FTIR Spectral Results

Figure 3.1 displays representative time resolved FTIR results for an experiment in which hematite aerosol is exposed to 40.5 mTorr of SO_2 under the driest possible conditions in our experiment (RH<<1%). The asymmetric stretch of SO_2 is responsible for the band seen at 1365 cm^{-1}. Water vapor, which is present in trace amounts as a contaminant in the dry experiments, has a broad series of absorption bands over the 1300 - 2100 cm^{-1} region, which causes significant spectral interference with the SO_2 peak at the low P_{SO2} used in these experiments. Water absorptions are removed from the FTIR spectra in Figure 3.1 by subtracting a suitable background. A peak is also seen at 2349

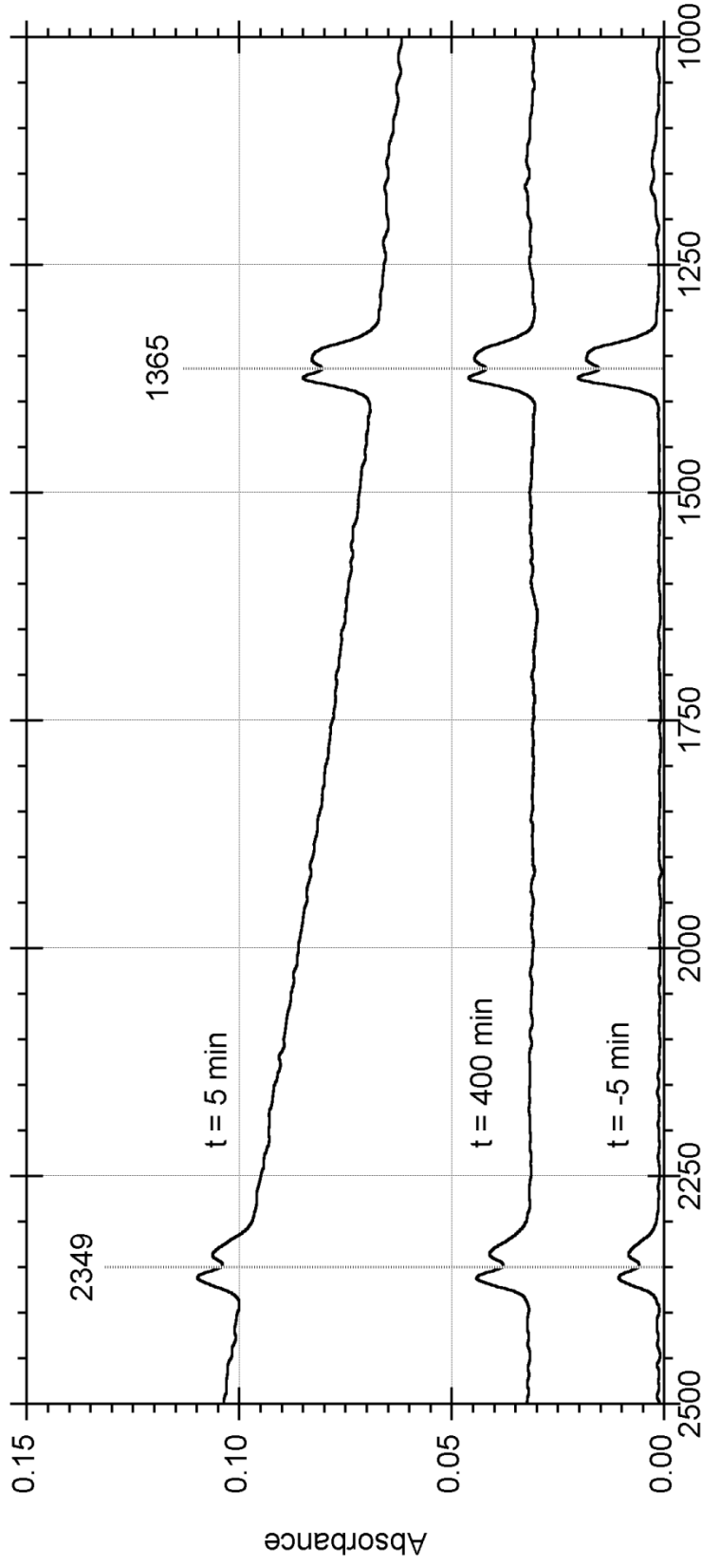

Figure 3.1. Representative FTIR spectra during an experiment performed under driest possible conditions (RH << 1%). Hematite aerosol is injected into the chamber containing 40.5 mTorr of SO_2 and 760 Torr of dry buffer gas at time t = 0 minutes, causing an increase in baseline slope towards higher wavenumbers due to Mie scattering. Following injection, gravitational settling removes aerosols from the active IR pathlength, causing the baseline slope to return to its initial value. The 1301 - 1407 cm^{-1} peak is due to the asymmetric stretch of SO_2; the 2280 - 2400 cm^{-1} peak is due to trace CO_2 in the chamber. Water absorptions have been subtracted, and spectra are offset for clarity.

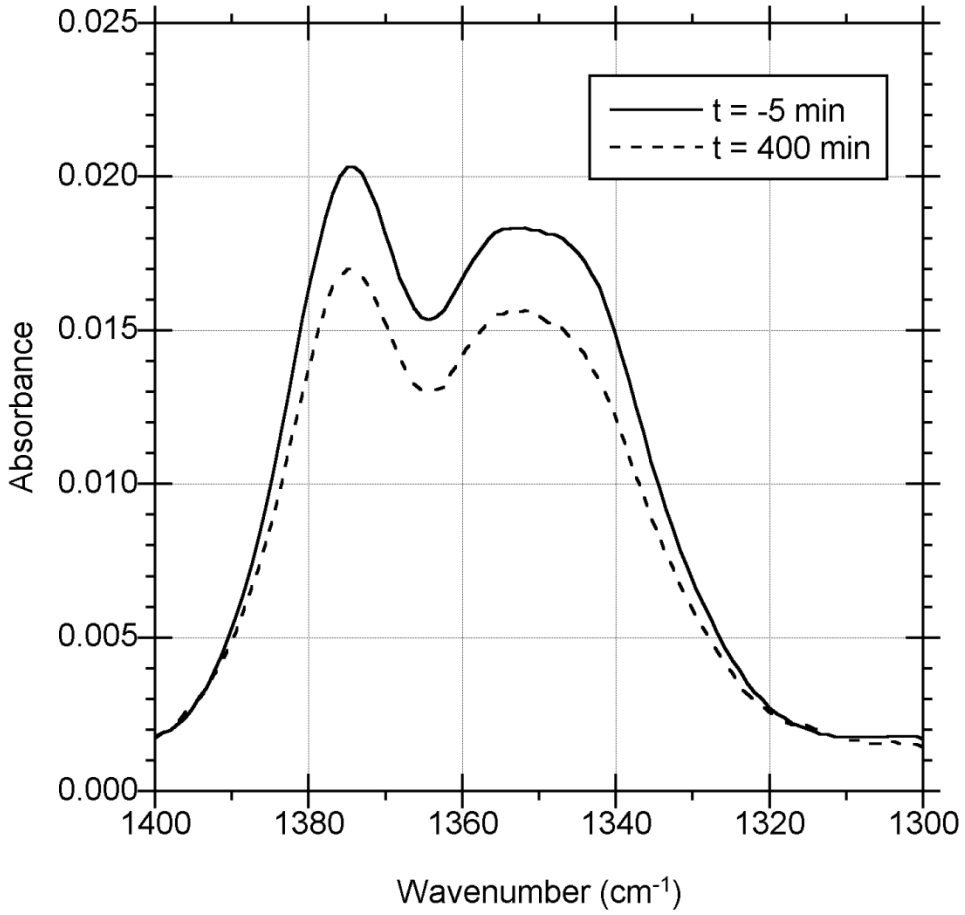

Figure 3.2. Detail of Figure 3.1. The integrated area in the region 1301 - 1407 cm^{-1} is used to quantify P_{SO2}. It can be seen that long after exposure to hematite aerosol (t = 400 minutes, dashed line), the integrated area of the peak is reduced compared to its value before aerosol introduction (t = -5 minutes, solid line).

cm^{-1} due to CO_2 gas. A previously obtained Beer's Law calibration is used to determine that only 5mTorr of CO_2 is present in this case.

Once the hematite is introduced and suspended in the chamber by a high pressure burst of buffer gas, the FTIR spectra immediately display an increased slope in the baseline towards higher wavenumbers, consistent with light scattering by the aerosol particles. The slope gradually decays towards its original value as gravitational settling removes the largest aerosols, which are the most responsible for the observed scattering, from the active IR pathlength. After several hundred minutes of reaction, no significant production of gas-phase products is observed. Qualitatively similar FTIR results were obtained whether the buffer gas in the chamber was argon or dried, CO_2-free air. Figure 3.2 shows a detailed view of the SO_2 peak before and after exposure to aerosol. In this case, about 6 mTorr of uptake occurred as seen by the reduction in peak area in the 1301 - 1407 cm^{-1} region.

When experiments are performed under humid conditions, subtraction of a gas phase H_2O spectrum of similar concentration is required to remove spectral interference and quantify SO_2. Figure 3.3 displays the typical quality of an H_2O subtraction at 43% RH, corresponding to 7.5 Torr of water vapor. Following subtraction, the time resolved FTIR for humid experiments have an identical qualitative pattern to that of the dry experiments (see Figure 3.1), namely the increased light scattering upon aerosol introduction and reduction in the height of the SO_2 peak as uptake occurs. The presence of water vapor during exposure of hematite aerosol to SO_2 does not cause the formation of any gas phase products in the chamber that are detectable by FTIR.

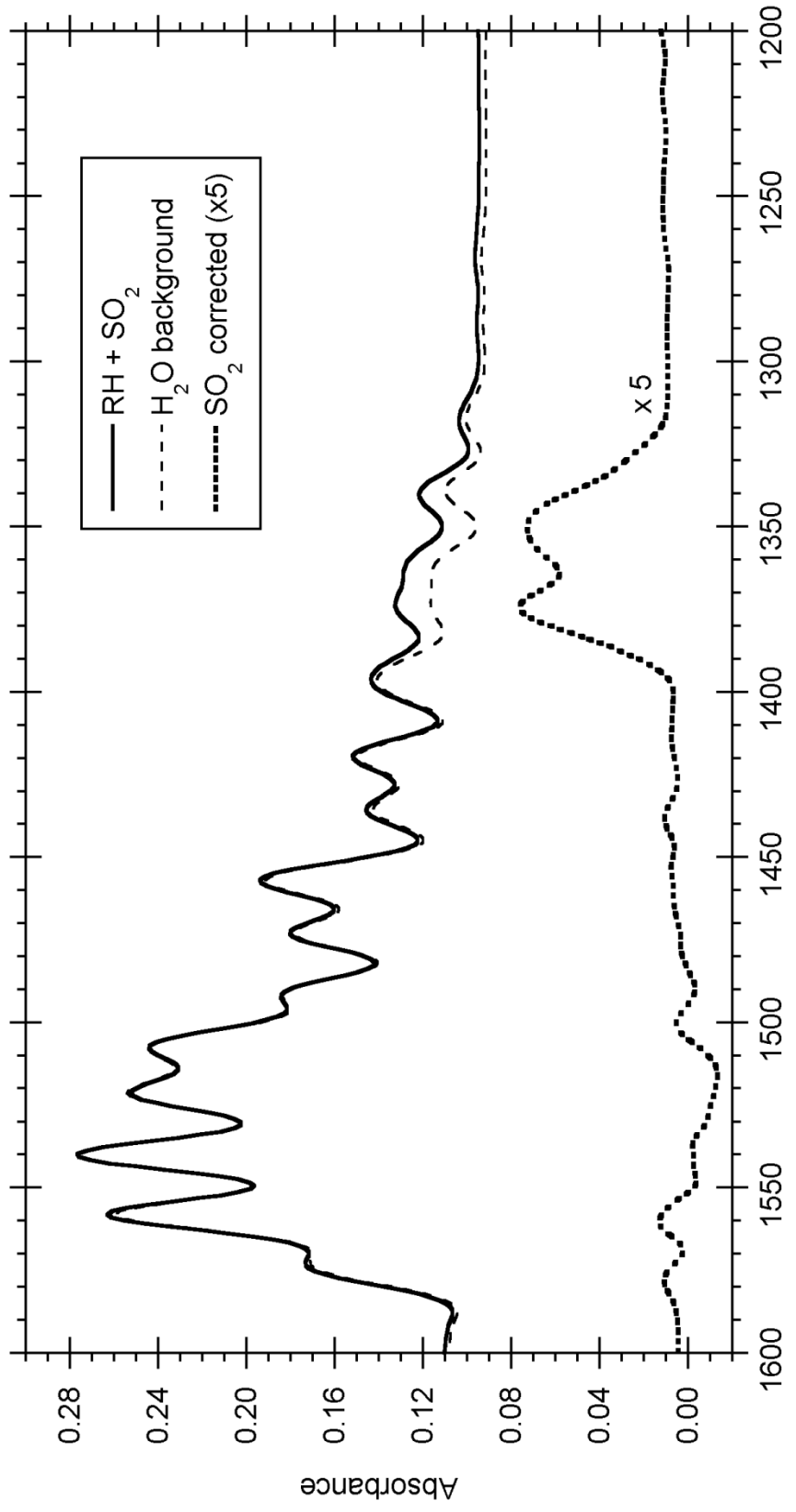

Figure 3.3. Subtraction of interference due to water absorptions for quantification of SO_2. Results are shown for an experiment with initial pSO_2 of 42.2mTorr, RH of 43% at room temperature, prior to introduction of hematite aerosol ($RH+SO_2$, solid line). The subtraction of a spectrum acquired at an RH of 43% (H_2O background, thin dashed line) results in the isolation of the SO_2 asymmetric stretch band (SO_2 corrected (x5), thick dashed line).

3.4.2 Time resolved uptake of SO_2 by hematite aerosol

Using a Beer's Law calibration of the peak area in the 1301 - 1407 cm^{-1} region (corrected for H_2O interference if necessary), the pressure of SO_2 in the chamber can be monitored as a function of time as shown in Figure 3.4. Hematite aerosol with a BET surface area of 14 m^2 was exposed to 40.5 mTorr of SO_2 in the chamber under dry conditions. The integration is adequate to determine P_{SO2} to within ±0.3 - 0.5 mTorr, a precision determined by the variation in consecutive FTIR spectra. Under dry conditions, background loss of SO_2 to the chamber surfaces is minimal as seen by the $t < 0$ minutes data (i.e. time before aerosol introduction). Typical background SO_2 loss rates were less than 3 μTorr min^{-1}. When the hematite aerosol is introduced, at $t = 0$ minutes, P_{SO2} is immediately reduced as uptake and possibly heterogeneous reactions occur with the aerosol. This fast uptake continues for several minutes. Sulfur dioxide uptake then continues at a slower rate until a final value is reached; this slow uptake occurs for approximately 20 minutes and accounts for removal of 1 mTorr of SO_2 in Figure 3.4. The rate of SO_2 loss after 100 minutes is the same as that before aerosol introduction (i.e. the wall loss rate), within experimental error.

Figure 3.5 shows the typical results of an uptake experiment performed under humid conditions, in this case 64% RH. The initial P_{SO2} used was 38.5 mTorr, comparable to that of the dry experiment in Figure 3.4. In humid experiments, the background loss rate of SO_2 from the gas phase is larger than that of dry experiments, typically greater than 10 μTorr min^{-1}, three times larger than the dry wall loss rate. When hematite aerosol is injected into the chamber at $t = 0$ minutes, there is a sharp decrease in P_{SO2} which is faster than the 50 s time resolution of this experiment. This sharp decrease

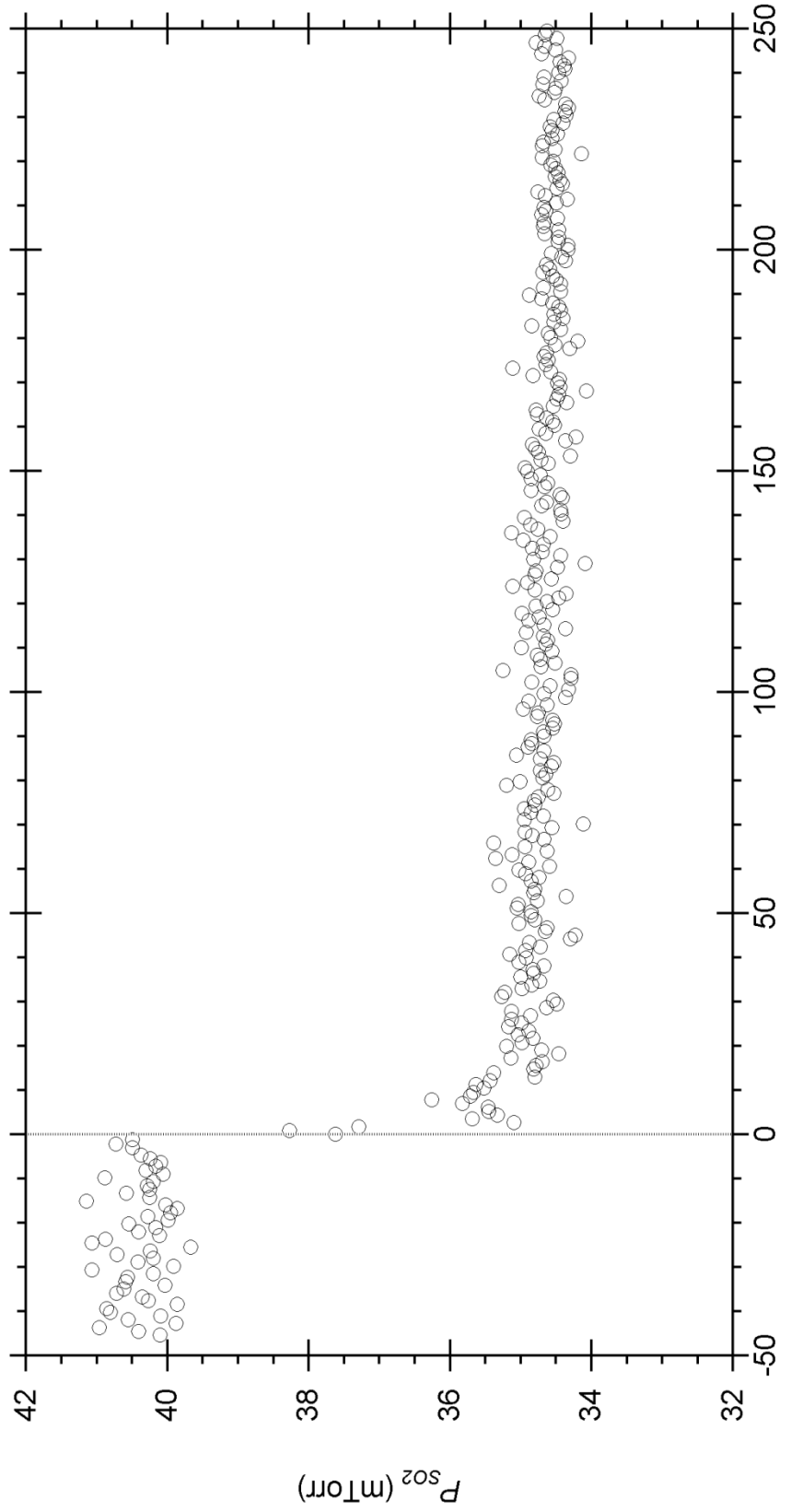

Figure 3.4. Uptake of SO_2 on hematite aerosol under driest possible conditions (RH<<1%). Hematite aerosol with a BET surface area of 14 m^2 was exposed to 40.5 mTorr of SO_2 in the chamber. Aerosol is injected at t = 0 minutes.

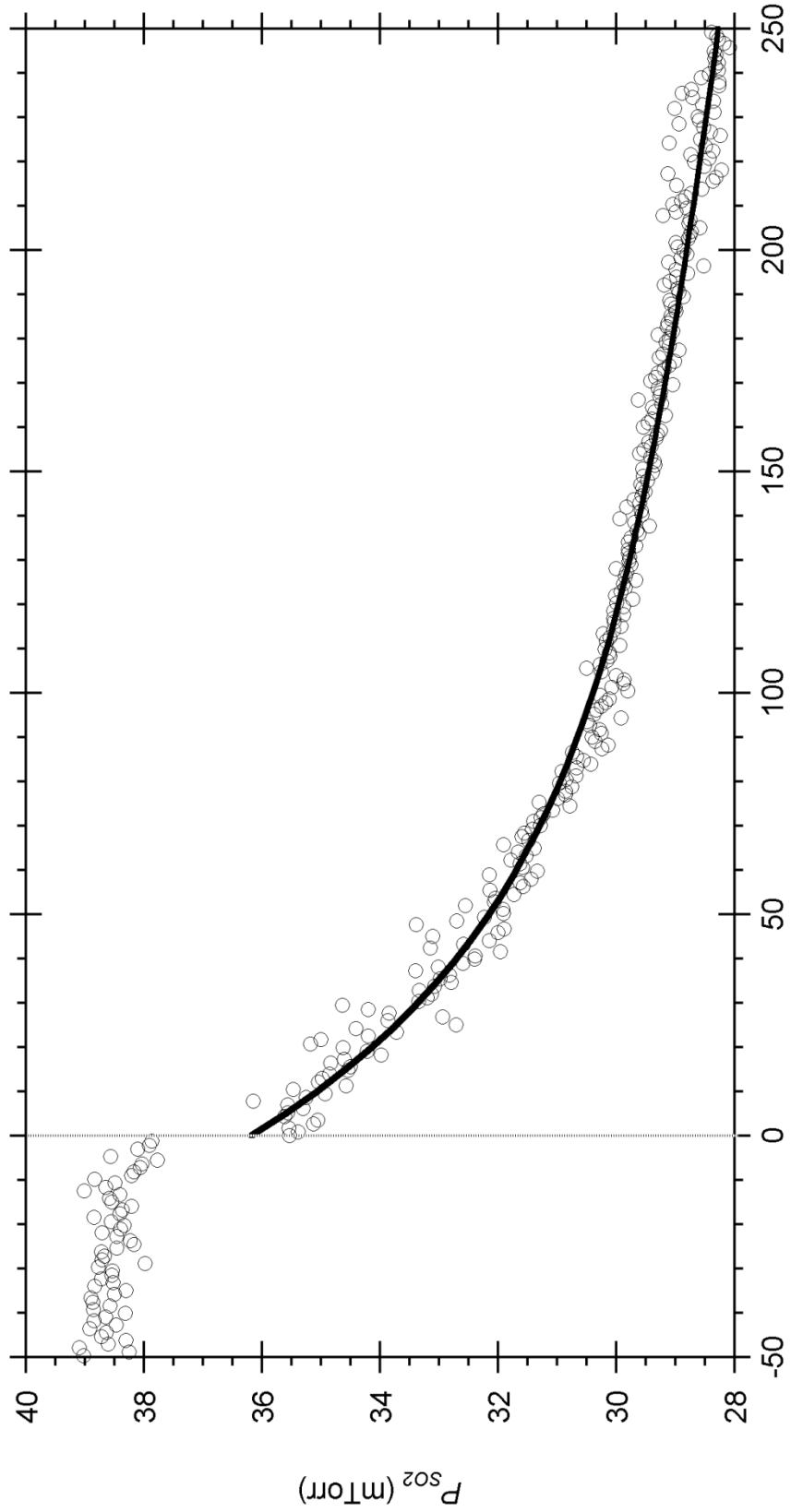

Figure 3.5. Uptake of SO_2 on hematite aerosol under humid conditions. Hematite aerosol with a BET surface area of 12.8 m^2 was exposed to 38.5mTorr of SO_2 in the chamber with a water vapor pressure equivalent to 64% RH. Aerosol is injected at t = 0 minutes. The solid line is a combination exponential - linear fit of the data after exposure to hematite.

is followed by continued uptake at a slower rate. The amount of slow uptake is greater than that in the dry experiment with similar P_{SO2}, and appears to follow an exponential decay. Within 300 minutes, the loss rate of SO_2 approaches that of the background, suggesting no further uptake on hematite is occurring. The total uptake (normalized for surface area as detailed below) in this humid experiment is greater than that under dry conditions, but still only 15% of the total SO_2 in the chamber was consumed. The amount of gas phase water in the chamber remains constant following aerosol injection, and no IR bands corresponding to water adsorbed on hematite aerosol are observed with this experimental method.

3.4.3 Saturation coverage of SO_2 on hematite

In all experiments under dry conditions, the hematite surface appeared to reach saturation with SO_2 well before the end of the experiment. After the fast initial uptake immediately following introduction of the aerosol to the chamber, a new baseline level of P_{SO2} was established. Using the ideal gas law, the decrease in P_{SO2} can be used to determine the number of molecules removed from the gas phase. Knowledge of the total BET surface area available for reaction allows the coverage n_{SO2} (cm^{-2}) of the hematite surface to be calculated as in Equation 3.6.

$$n_{so2} = \frac{(P_i - P_f)VN_A}{RTS_{BET}} \qquad 3.6$$

Here, P_I and P_F are the initial and final pressures of SO_2, V is the chamber volume (151L), T is the temperature (K), R is the ideal gas constant, N_A is Avogadro's number, and S_{BET} is the surface area of aerosol suspended in the chamber (cm^2). The final pressure is determined by a linear fit of the P_{SO2} vs. time data for t > 100 minutes (to ensure that

only background losses and not further uptake are occurring) and determining the intercept at t = 0. Uncertainties in the pressure are conservatively estimated to be up to ±0.5 mTorr by noting the range of measured P_{SO2} values over a 10 minute period prior to aerosol introduction, during which background loss is negligible. By making a reasonable assumption about the density of reactive sites on the hematite surface, the coverage can also be reported in terms of the dimensionless term θ_{SO2} - this relative coverage approaches unity as all surface sites become occupied, but can also be greater than one if multilayer adsorption or catalytic reactions occur.

$$\theta_{SO2} = \frac{n_{SO2}}{n_0} \qquad 3.7$$

Here, n_0 is the number density of surface sites (cm^{-2}). A value of $n_0 = 4.8 \times 10^{14}$ sites cm^{-2} for α-Fe_2O_3 will be used throughout this report based on published literature values [39, 42, 43]. It should be noted that only a fraction of the total sites may actually be reactive towards SO_2; however, the utility of reporting θ_{SO2} in this study is that it provides a convenient way to determine the relative reactive capacity of hematite towards SO_2 under various conditions.

Three repeated measurements of the uptake value for a small given initial P_{SO2} range (33 - 36.7 mTorr) gave a mean value of $n_{SO2} = 1.53 \pm 0.13 \times 10^{14}$ cm^{-2}, or a relative standard deviation of 8.4%. For argon experiments with P_{SO2} of 11 – 12 mTorr, a higher standard deviation of 18.8% in the measured uptake capacity was observed. The propagated error associated with the calculation of uptake capacity is somewhat greater, in the range of ±10 - 20%. The measured uptake capacity for each dry experiment (with either purged air or argon as the buffer gas) is displayed in Figure 3.6. The initial conditions of P_{SO2} do not produce an observable trend in the measured uptake capacity of

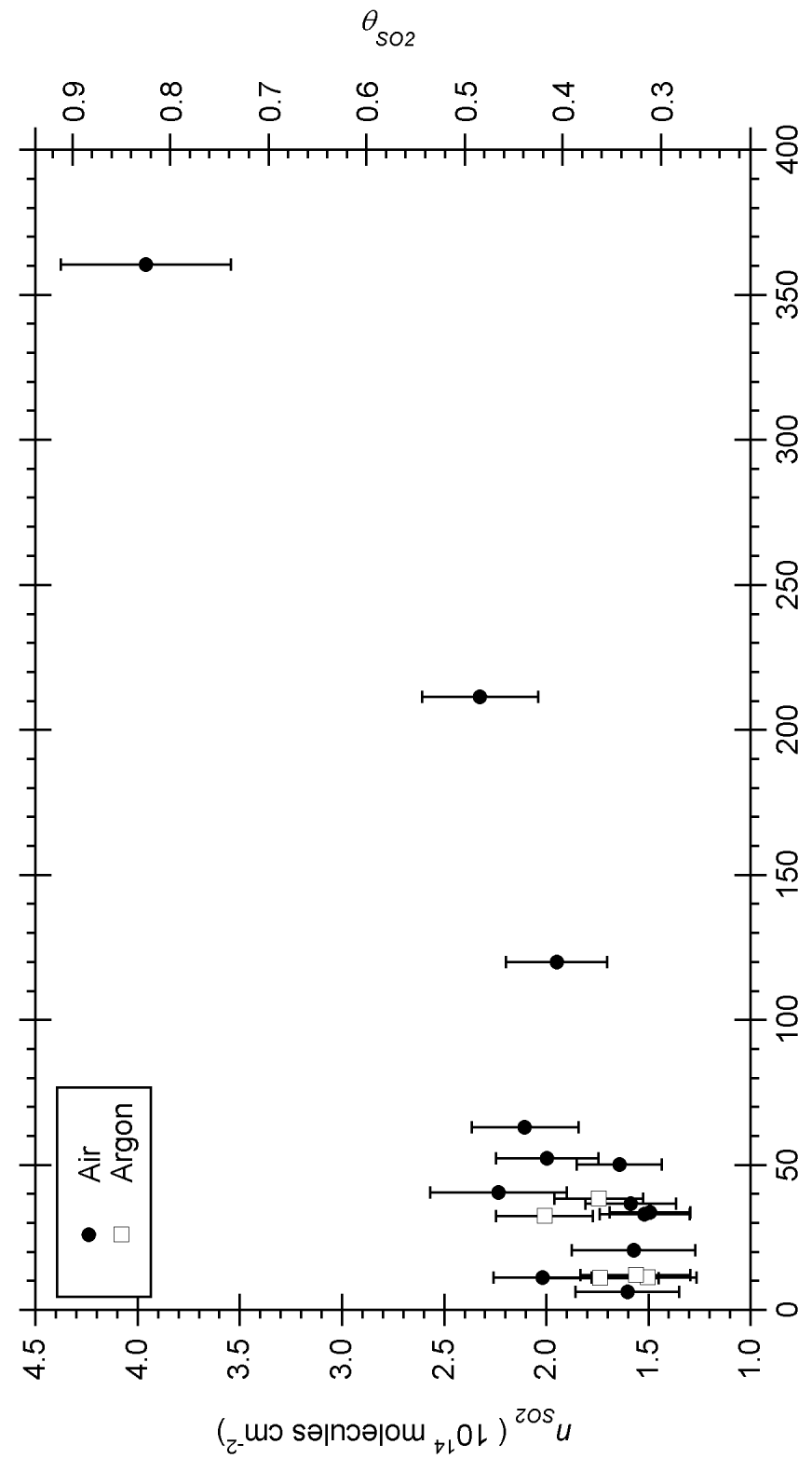

Figure 3.6. SO_2 uptake as a function of initial pressure of SO_2 in the chamber (P_{SO2}) for experiments under driest possible conditions (RH<<1%). SO_2 uptake is reported in terms of coverage (n_{SO2}, left axis) and relative coverage (θ_{SO2}, right axis). The buffer gas in the chamber was either purged, dry air (closed circles) or argon (open squares). Error bars represent propagated error in calculation of uptake, assuming 10% uncertainty in surface area of the dust.

dry hematite for sulfur dioxide, with the exception of the highest P_{SO2} studied (360mTorr), for which the n_{SO2} is roughly doubled. In all cases, θ_{SO2} is less than unity, indicating that not every α-Fe_2O_3 surface site adsorbed a molecule of SO_2. There is no observable dependence on identity of the buffer gas used; the mean uptake capacities measured in air and argon were $1.8 \pm 0.1 \times 10^{14}$ (n = 12, 360mTorr data not included) and $1.7 \pm 0.3 \times 10^{14}$ (n = 5) molecules cm^{-2}, respectively. This implies that the pressure of oxygen, which varies over a thousand-fold between the argon-filled and air-filled chamber experiments, has a negligible effect on the amount of SO_2 uptake on hematite.

As seen in the representative data for a humid experiment shown in Figure 3.5, significant uptake occurs immediately after dust introduction at a rate faster than the time resolution of the FTIR under our conditions; this is followed by additional, slower uptake. In this particular example, about 40% of the total uptake occurred within the first 5 minutes, and the remaining 60% continued on a considerably longer time scale. The uptake within the first 5 minutes following dust injection was determined using Equations 3.6 and 3.7, and is denoted θ_I; it can be compared to the total SO_2 uptake in the experiment (θ_F),. Five minutes was chosen as the time to report θ_I in order to avoid the large variability in uptake that occurs during the first few points after dust injection.

Figure 3.7 shows how both θ_I and θ_F vary with P_{SO2} under dry conditions. A θ_I / θ_F ratio of 1 means that all measurable uptake occurred within 5 minutes of dust introduction. For the 120, 211 (not shown), and 360 (not shown) mTorr experiments, the θ_I / θ_F ratio is close to 1, and there is little or no additional uptake beyond the first 5 minutes. At lower pressures, there is a large variation in the amount of initial uptake, with the fast initial uptake accounting for between 44 and 100% of the total SO_2 uptake.

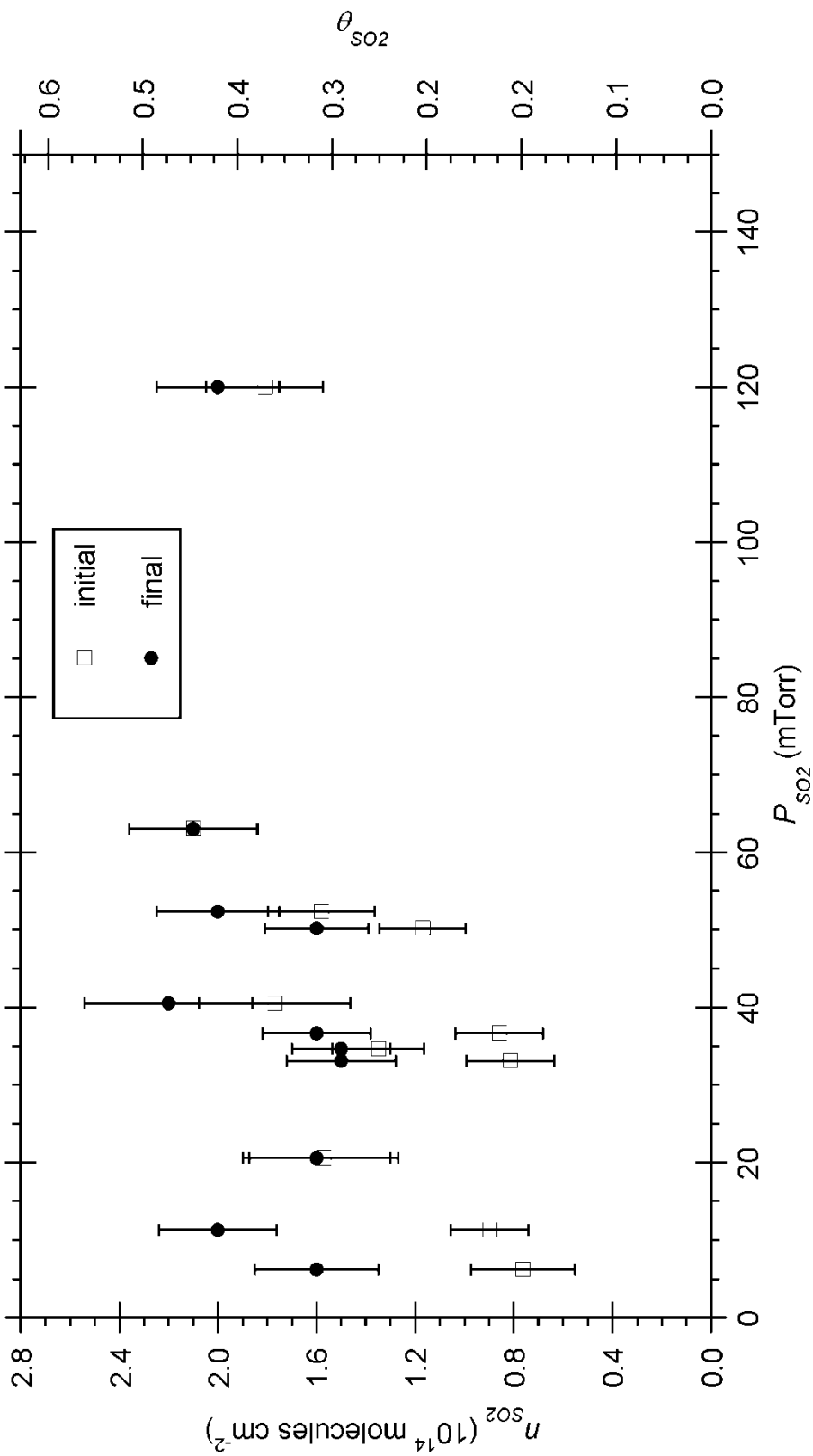

Figure 3.7. Initial and final uptake of SO_2 on hematite aerosol as a function of initial P_{SO2}. Data shown for experiments under the driest possible conditions (RH<<1%). Initial uptake is defined as uptake occurring within five minutes after aerosol injection. SO_2 uptake is reported in terms of coverage (n_{SO2}, left axis) and relative coverage (θ_{SO2}, right axis).

The dependence of hematite's SO_2 uptake capacity on relative humidity was also investigated. Figure 3.8 summarizes the results for experiments in which the RH was varied between 10 - 88%, including the results of several dry experiments (RH < 1%) for comparison. As the dependence of SO_2 uptake capacity on P_{SO2} was found to be negligible for dry experiments, it is reasonable to assume that the RH level is mainly responsible for any observed variation in uptake capacity. However, the effect of P_{SO2} in the presence of water vapor was also investigated by comparing several RH studies with 8.8 ± 3 and 37 ± 5 mTorr initial pressures of SO_2. Comparing 5 pairs of uptake capacities acquired using different P_{SO2} at a given RH, the uptake capacity is significantly ($p > 0.95$) higher, by up to 25%, when the lower initial P_{SO2} is used. Regardless of the P_I used, the effect of water vapor on uptake capacity was consistent; any amount of water vapor in the range 10 - 81% RH led to an increased SO_2 uptake capacity compared to that on dry hematite, by a factor of 1.3 - 1.7. At the highest RH studied, 88%, the uptake was the same as that on dry hematite, within the margin of error.

Figure 3.9 shows how the ratio θ_I / θ_F is affected by the relative humidity. The average value of several θ_I / θ_F measurements obtained at ≤ 1% RH are plotted for direct comparison. It can be seen that for the range 10 - 81% RH, the θ_I / θ_F ratio is lower than that of corresponding dry experiments, with the fast initial uptake accounting for less than 50% of the total uptake. The initial pressure of SO_2 used (either 8.8 ± 2 or 37 ± 5 mTorr) did not have a statistically significant ($p < 0.95$) effect on this ratio. The presence of water vapor reduces the ratio θ_I / θ_F by both decreasing the amount of fast initial uptake (θ_I) moderately, and by increasing the amount of slower uptake by a factor of 2 relative to dry conditions.

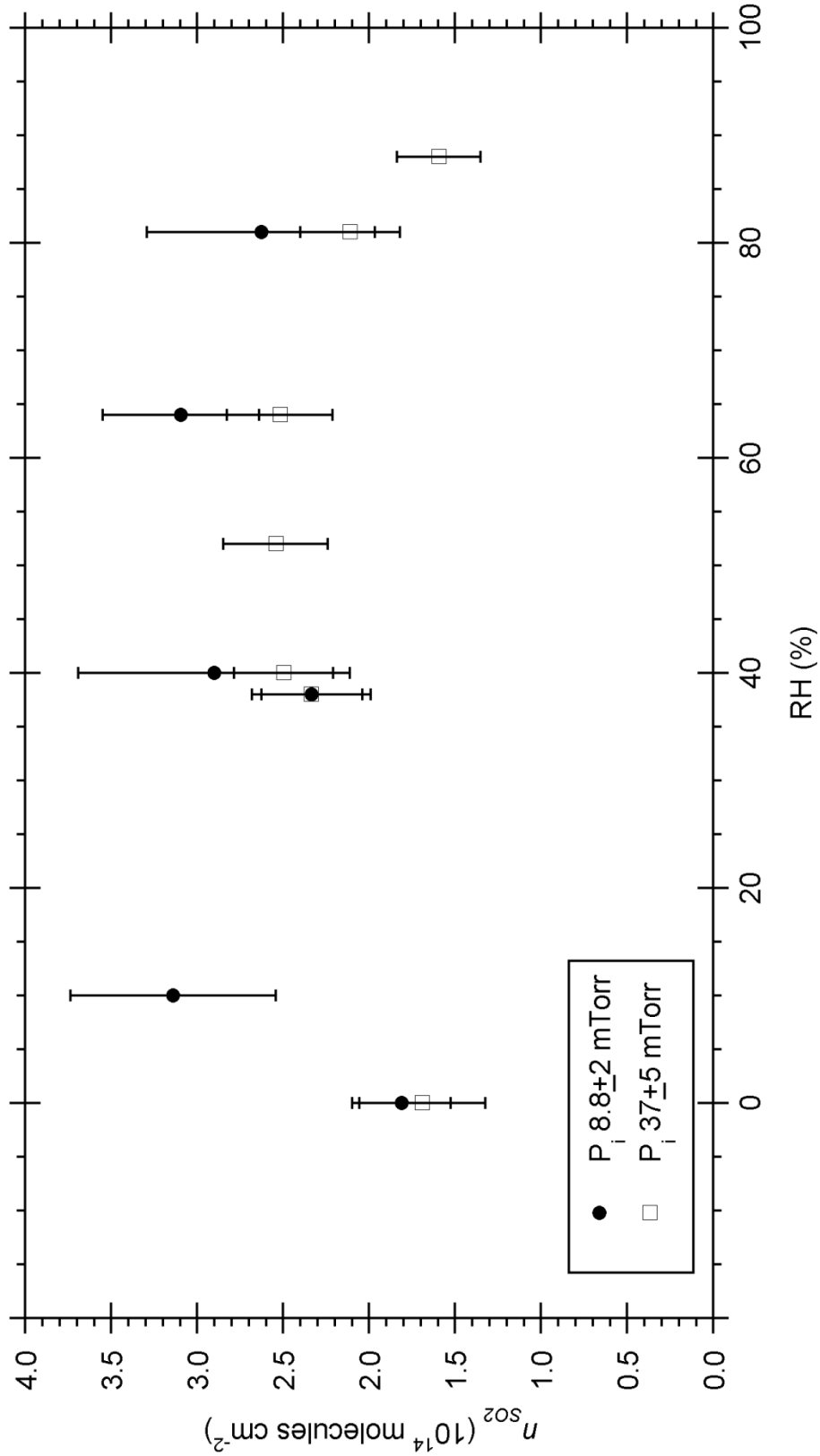

Figure 3.8. SO_2 uptake as a function of relative humidity (RH). Experiments were performed with initial conditions of 8.8 ± 2 (filled circles) or 37 ± 5 (open squares) mTorr of SO_2. The points at RH = 0% represent the average uptake obtained from experiments under the driest possible conditions (RH<<1%).

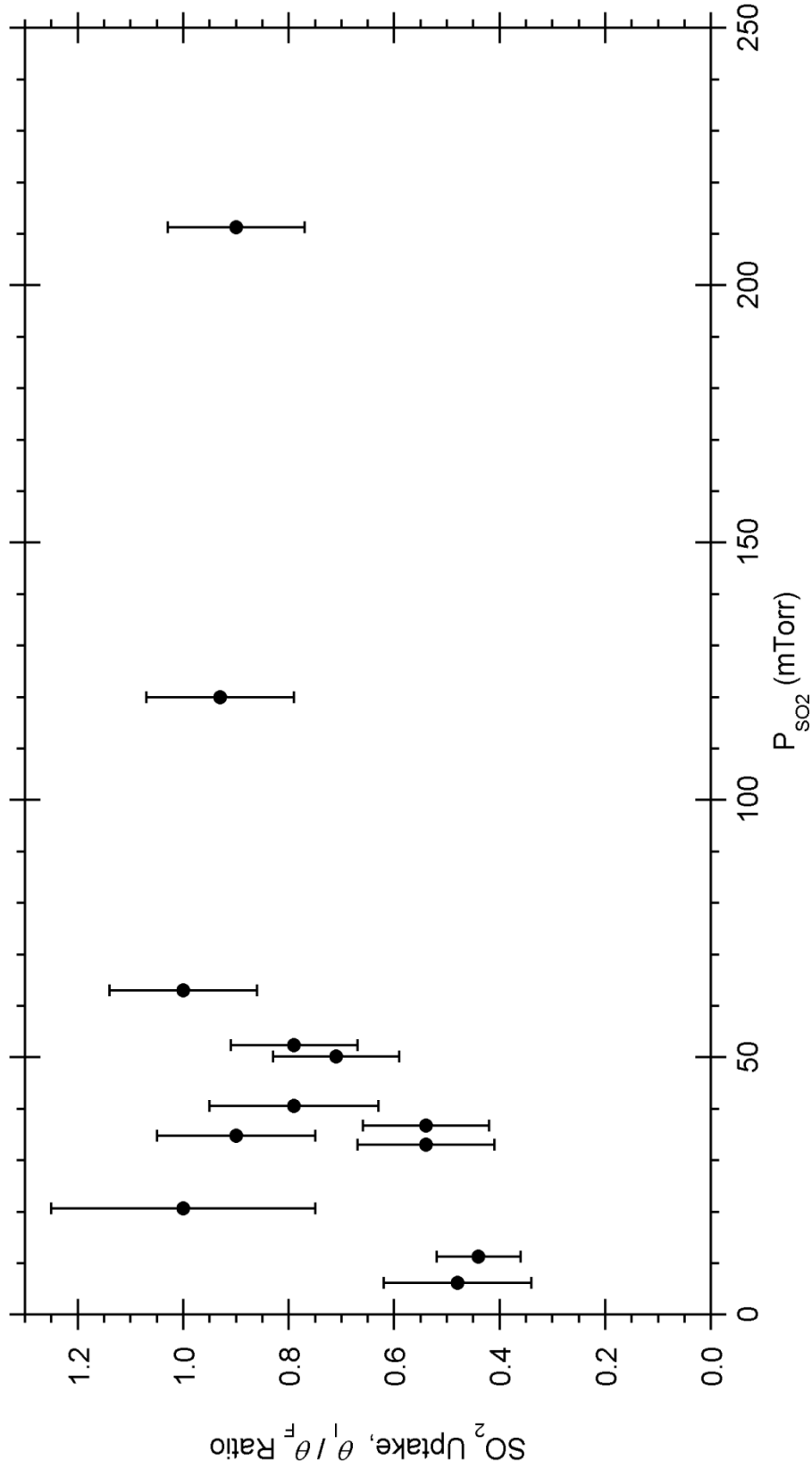

Figure 3.9. Ratio of initial to final SO_2 uptake on hematite aerosol as a function of relative humidity (RH). Initial uptake is defined as the uptake occurring within 5 minutes after aerosol introduction. Experiments were performed with initial conditions of 8.8 ± 2 (filled circles) or 37±5 (open squares) mTorr of SO_2. The points at ≈0% RH represent the average uptake obtained from experiments under the driest possible conditions (RH<<1%).

3.4.4 Kinetics of SO_2 uptake

Water vapor increases the amount of slow SO_2 uptake on hematite enough so that the decay can be seen to follow an exponential trend. The time-resolved P_{SO2} data after dust exposure can be fit by a combination exponential-linear function as shown in Equation 3.8.

$$P_{SO2} = P_F + Ae^{-t/\tau} - Bt \qquad 3.8$$

Here, τ is the characteristic time decay constant, in minutes. A and B are fitting parameters corresponding to the amount of slow uptake and the rate of background SO_2 loss, respectively. Using values of τ from the fit, as well as the mean speed of SO_2 ($\bar{c}$), the BET surface area of the hematite aerosol (S_{BET}), and the aerosol mass concentration (C_{mass}), the SO_2 uptake kinetics can be described by an uptake coefficient, γ_{SO2}, as described in Equation 3.9.

$$\gamma_{SO2} = \frac{4}{\tau S_{BET}[C_{mass}]\bar{c}} \qquad 3.9$$

Using Equation 3.9 with typical mass loadings, temperature, and the experimental time resolution of 52 seconds, it can be estimated that the fast initial uptake corresponds to a $\gamma_{SO2} \geq 2.7\text{x}10^{-6}$. The amount of dust used could be reduced in order to produce a larger, more easily measurable τ for the fast process. However, the hematite samples used had a surface area of only S_{BET} of 5.06 m^2 g^{-1} and a, say, ten-fold reduction in dust loading would be impractical due to the variable dust loss upon injection. Values of γ_{SO2} calculated using the BET surface area, as shown above, should be considered a lower limit to the actual uptake coefficient. Many studies note that uptake coefficients obtained using the geometric surface area (calculating the surface area assuming all particles are

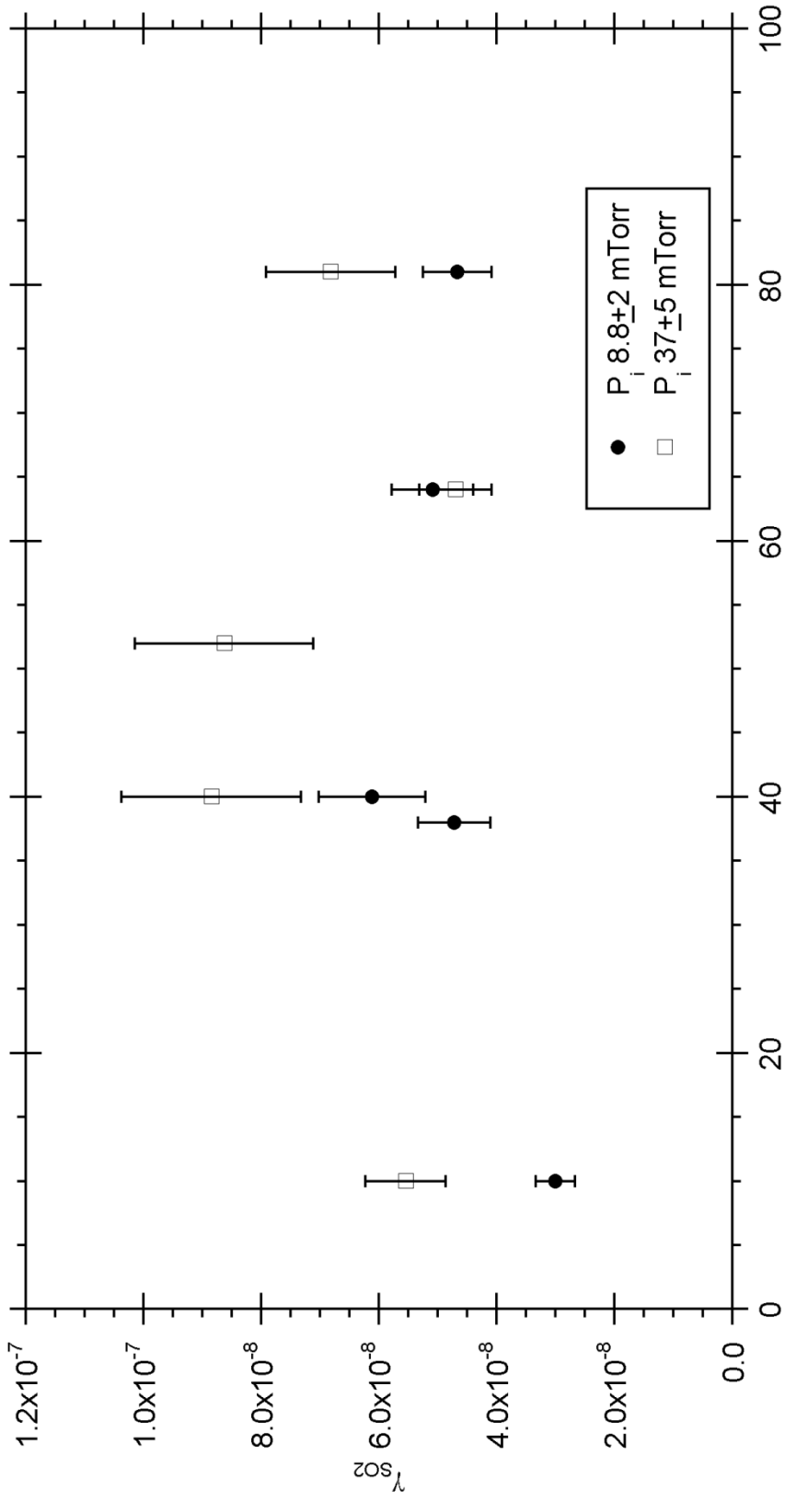

Figure 3.10. γ_{SO2} as a function of relative humidity (RH). Experiments were performed with initial conditions of 8.8 ± 2 (filled circles) or 37 ± 5 (open squares) mTorr of SO_2.

spherical with a known distribution of diameters) are orders of magnitude higher than those using BET surface areas [29, 30, 44]; the difference complicates analysis of the relative importance of heterogeneous reactions compared to other gas phase loss mechanisms.

Figure 3.10 displays γ_{SO2} as a function of relative humidity; again two different initial pressures, 8.8 ± 2 and 37 ± 5 mTorr, are plotted separately to determine whether initial conditions affect the apparent γ_{SO2}. There does not appear to be any clear trend in γ_{SO2} as the RH is varied from 10 - 81%. Therefore, the γ_{SO2} for hematite under humid conditions can be concisely described as the mean of all humid experiments shown, $\gamma_{SO2} = 5.8 \pm 1.3 \times 10^{-8}$. It should, however, be noted that there is large variation in γ_{SO2} over this set of experiments, ranging from $3.0 - 8.9 \times 10^{-8}$. It appears that variations in the aerosolization process may play a large role in the measured kinetic parameters. The hematite sample may require greater pumping times, possibly at elevated temperature, to remove all traces of adsorbed water and truly perform a "dry" experiment. However, if traces of adsorbed water are so difficult to remove, then water will certainly be present on hematite aerosols under typical atmospheric conditions and influence γ_{SO2} accordingly.

3.5 Discussion

3.5.1 Dependence of SO_2 Uptake Capacity on Oxygen

By changing the buffer gas in the chamber from dry, CO_2-free air to argon, the role of oxygen in the uptake capacity of hematite for SO_2 could be investigated. The total SO_2 uptake capacity in an argon-filled chamber, $1.7 \pm 0.3 \times 10^{14}$ cm^{-2}, was not significantly different from experiments with ambient concentrations of oxygen, 1.8 ± 0.1

x 10^{14} cm^{-2}. It is possible oxygen contamination, which is of course undetectable by FTIR, was present in the argon-filled chamber. The argon tank used was specified at 99.9997% purity, so no significant O_2 contamination is expected from the tank itself. One estimate of the oxygen content would be to assume that the minimum pressure achieved in the evacuated chamber, 30 mTorr, contained 21% oxygen, for a maximum of about 6 mTorr O_2. Although this estimated oxygen concentration is five orders of magnitude less than ambient, it may be comparable to the amount of SO_2 used in some of the chamber experiments (i.e., experiments with ≈10 mTorr P_{SO2}).

Baltrusaitis et al. also investigated the effect of oxygen on the adsorption of SO_2 by α-Fe_2O_3 with x-ray photoelectron spectroscopy (XPS) [37]. They found that the amount of sulfur-containing species that adsorb to the surface doubled in the presence of 100 Torr of oxygen and that the ratio of S(VI) to S(IV) species also increased dramatically, to the extent that virtually no S(IV) could be detected. It should be noted that the XPS quantification of the surface sulfur occurred after evacuation, meaning only irreversibly bound species remained; the environmental chamber measures only loss of gaseous SO_2, a significant fraction of which may be reversible in nature. In addition, the XPS studies did not quantify the uptake in terms of the loss of gas phase SO_2 but only monitored product formation. Our data suggests that the total amount of SO_2 uptake from the gas phase is insensitive to the pressure of O_2 present in the chamber. Based on the experiments of Baltrusaitis et al., it may be that the fraction due to reactive, *irreversible* SO_2 uptake does increase with oxygen content (i.e. subsequent oxidation of adsorbed SO_2 due to reaction facilitated by O_2) but that this is a minor pathway for adsorbed SO_2 and reversible uptake accounts for most of the gas phase loss. Alternatively, the small amount

of O_2 contamination in the chamber may be just as effective at increasing the total uptake on hematite as 100 Torr of O_2. Baltrusaitis et al. proposed that dissociatively adsorbed O_2 species lead to SO_2 oxidation. If one O atom is required to oxidize S(IV) to S(VI) then, at the most, the oxygen content in our argon experiments (≈6 mTorr) would be sufficient to oxidize 33 to 100% of the SO_2 lost from the gas phase for the high and low SO_2 pressure experiments, respectively. We do not observe any statistically significant difference between the argon and air results, even for the higher initial pressure experiments. The experimental precision of the chamber apparatus may not be sufficient to detect a change of this magnitude. As mentioned above, it may also be that the dominant pathway is reversible SO_2 uptake and that surface oxidation of the adsorbed sulfur is not limiting the gas phase loss.

Another study utilizing *in situ* FTIR also showed that the extent of reaction of SO_2 with hematite was sensitive to the pressure of O_2, with an order of magnitude increase in product formation when oxygen was increased from 5% to 21% of total (atmospheric) pressure [33]. As in the XPS work, this report examined the oxygen dependence of surface product formation and their only measurement of gas phase SO_2 loss was performed at a fixed, 21%, oxygen pressure. The absence of an observed correlation between pressure of oxygen and loss of gaseous SO_2 in our experiments is not inconsistent with either of these surface sensitive studies. It does suggest, however, that the total SO_2 uptake is not dependent on oxygen pressure and that surface reaction does not limit the gas phase loss. The adsorbed SO_2 molecules, regardless of speciation, likely occupy similar surface sites which can result in saturation of the hematite surface. We are unable to investigate surface speciation, and any possible dependence on oxygen, due to

the lack of sensitivity of the chamber FTIR technique to surface bound species. This may alter the analysis of the importance of this mechanism as a potential pathway for SO_2 oxidation by α-Fe_2O_3. For example, Ullerstam et al. noted that oxidation of SO_2 on mineral surfaces (specifically, by NO_2), was four orders of magnitude slower than uptake from the gas phase [44].

3.5.2 The Effect of Relative Humidity on SO_2 Uptake

The presence of water vapor in the chamber increased the uptake capacity of SO_2 by α-Fe_2O_3 by a factor of 1.3 - 1.7. This is in contrast to the earlier XPS study which reported that in the presence of oxygen, humidity decreased the total amount of irreversibly adsorbed sulfur species on hematite [37]. It was proposed that this effect was due to preferential adsorption of H_2O onto reactive surface sites, blocking the dissociative absorption of O_2 and preventing subsequent oxidation of adsorbed sulfur. The difference between these findings and our results cannot be ascribed to experimental error but, rather, indicate that reversible adsorption is the important uptake pathway and that coadsorbed water facilitates this process. Another possible reason for the conflicting assessments may be due to differences in the experimental measurement protocols. The XPS data was collected after α-Fe_2O_3 was exposed to SO_2, O_2, and H_2O for only 15 minutes. In time resolved XPS uptake experiments performed in the absence of gaseous water, fifteen minutes was found to be a sufficient time for the reaction to saturate, as is the case in our chamber studies. No corresponding experiments were performed with water vapor present. In contrast, the environmental chamber experiments showed that the rate of uptake, as manifested in the measured uptake coefficient, γ_{SO2}, is reduced in the

presence of water vapor, and exposure periods much longer than 15 minutes were required to observe the total SO_2 uptake. It is possible that if the XPS experiments had quantified uptake for longer exposure periods with water, the results might agree with our observation that water increases total SO_2 uptake.

Under dry conditions, the uptake of SO_2 by hematite reaches saturation at n_{SO2} = 1.8 ± 0.1 x 10^{14} molecules cm^{-2}. At least 40%, and in some cases 100%, of the total uptake is via a channel that has an uptake rate greater than the time resolution of the FTIR data collection. Thus, we can only estimate a lower limit to the fast uptake coefficient of $\geq 2 \times 10^{-6}$. Some dry experiments exhibited additional slower uptake which occurred within 30 minutes of injection, but which was generally too noisy or rapid to obtain reliable values of γ_{SO2}. In a few cases, the slow SO_2 uptake accounted for over 50% of the total uptake. As noted in Figure 3.8, n_{SO2} increases in the presence of water vapor due to an increase in the capacity of the slower uptake sites. It is possible that evacuating the hematite sample at room temperature for 3 - 4 hours was not adequate to remove all water that adsorbed onto the powder during storage and sample preparation. The persistent adsorbed water in some of the dry experiments may have been sufficient to increase the capacity of the slower uptake pathway. This difficulty in removing water suggests that laboratory studies which examine reactions of gasses with hematite samples prepared under extreme conditions of heat or ultra high vacuum may not be well representative of those which will occur in the environment, where adsorbed water will persist on α-Fe_2O_3 surfaces.

Fu et al. previously measured γ_{SO2} on dry α-Fe_2O_3 in simulated air (21% O_2 in N_2 at 1 atm total pressure) using in-situ FTIR [33]. Despite using similar pressures of SO_2

(45 ppm), normalizing for BET surface area, and calculating γ_{SO2} based on gas phase SO_2 losses as in this thesis, the reported $\gamma_{SO2} = 5.38 \times 10^{-10}$ is orders of magnitude lower than our measured value of $\gamma_{SO2} \geq 2 \times 10^{-6}$. The large discrepancy here is likely the result of experimental method – Fu et al. allowed the SO_2/air mixture to equilibrate with the dry α-Fe_2O_3 sample for 20 minutes prior to beginning kinetic measurements. Our results (see Figure 3.5) indicate that the surface was already completely saturated during this equilibration period, and the very slow uptake measured by Fu was on an already saturated surface. With the amount of hematite dust currently used in this study, it would take a prohibitively long amount of time to measure an uptake process with γ_{SO2} on the order of 10^{-10}, although use of a sample with a much higher specific surface area could facilitate this measurement.

In all studies with water vapor present, 50% or more of the total uptake occurs slowly enough to measure γ_{SO2}. This indicates that water adsorbed on the surface either slows an existing pathway for SO_2 uptake, or introduces an additional mechanism for SO_2 uptake that does not occur on dry hematite. Water adsorption isotherms indicate that the hematite surface is covered with water equivalent to one monolayer at RH as low as 10%, with steadily increasing coverage of up to ≈4 monolayers at 80% RH [39]. Since at least monolayer water coverage is expected for all conditions of RH investigated here, the observation that γ_{SO2} does not vary over the range 10-80% could be explained as the effect of water blocking active SO_2 uptake sites. It should be noted that the water is not necessarily evenly distributed on the hematite surface in a uniform monolayer but, rather, may preferentially adsorb at certain sites [39]. However, the overall uptake capacity for SO_2 is greater in humid experiments than on dry hematite aerosol. Fu et al. noted that

surface hydroxyl groups appear to play a key role in SO_2 uptake and oxidation on iron oxide surfaces, including hematite [33]. Some surface hydroxyls will be present on dry hematite, but the dissociative adsorption of water vapor could produce more, leading to greater uptake capacity in humid air. The surface of previously hydrated samples of α-Fe_2O_3 may actually be identical to that of goethite (FeOOH), as shown by solubility studies and Mössbauer spectroscopy [45].

The dry hematite surface is limited to adsorption of 0.94 ± 0.05 mg SO_2 g^{-1} Fe_2O_3. This is in good agreement with the value of 0.6 mg SO_2 g^{-1} Fe_2O_3 obtained with a flow tube reactor experiment of Judeikis et al. [46]. This flow tube study also observed an increase in SO_2 uptake capacity in one experiment where water vapor was present, along with a small increase in the uptake coefficient. Assuming all SO_2 adsorbed on the surface of hematite aerosols could eventually be converted to adsorbed sulfate through further heterogeneous reactions, an upper limit to the amount of sulfate formed can be estimated. From the saturation coverage of SO_2 on dry hematite aerosols, the maximum amount of $SO_4^{2-}{}_{(ads)}$ is determined to be 1.4 ± 0.1 mg SO_4 g^{-1} α-Fe_2O_3; using the BET surface area of the sample, this value can also be expressed in terms of sulfate formed per unit surface area, 0.29 ± 0.2 mg SO_4 m^{-2} α-Fe_2O_3. Note that in the XPS experiments of Balustratis et al. [37], the conversion of the adsorbed sulfur to sulfate was complete on hematite surfaces when oxygen was present, regardless of the RH.

Toledano and Henrich showed that the sticking coefficient of SO_2 on α-Fe_2O_3 under illumination by UV-irradiation effectively doubled, which the authors proposed to be due to the creation of transient Fe^{2+} sites [47]. This photochemistry might also be important for assessing the reactivity of hematite aerosols in the atmosphere, and it would

be beneficial to see how the presence of water vapor might affect this pathway for SO_2 uptake in future studies.

Notes

1. Tegen, I.; Harrison, S. P.; Kohfeld, K.; Prentice, I. C.; Coe, M.; Heimann, M., Impact of vegetation and preferential source areas on global dust aerosol: Results from a model study. *J. Geophys. Res.* **2002,** *107*, 4576, doi:10.1029/2001JD000963

2. Usher, C. R.; Michel, A. E.; Grassian, V. H., Reaction on Mineral Dust. *Chemical Reviews* **2003,** *103* (12), 4882-4939.

3. Hoffmann, P.; Dedik, A. N.; Ensling, J.; Weinbruch, S.; Weber, S.; Sinner, T.; Gütlich, P.; Ortner, H. M., Speciation of Iron in Atmospheric Aerosol Samples. *Journal of Aerosol Science* **1996,** *27* (2), 325-337.

4. Weber, S.; Hoffmann, P.; Ensling, J.; Dedik, A. N.; Weinbruch, S.; Miehe, G.; Gütlich, P.; Ortner, H. M., Characterization of Iron Compounds from Urban and Rural Aerosol Sources. *Journal of Aerosol Science* **2000,** *31* (8), 987-997.

5. Mogili, P. K.; Yang, K. H.; Young, M. A.; Kleiber, P. D.; Grassian, V. H., Environmental aerosol chamber studies of extinction spectra of mineral dust aerosol components: Broadband IR-UV extinction spectra. *J. Geophys. Res.* **2007,** *112*, D21204, doi:10.1029/2007JD008890.

6. Duce, R. A.; Tindale, N. W., Atmospheric Transport of Iron and its Deposition in the Ocean. *Limnology and Oceanography* **1991,** *36* (8), 1715-1726.

7. Fan, S.-M.; Moxim, W. J.; Levy II, H., Aeolian input of bioavailable iron to the ocean. *Geophysical Research Letters* **2006,** *33* (L07602), doi:10.1029/2005GL024852

8. Kraemer, S. M., Iron oxide dissolution and solubility in the presence of siderophores. *Aquatic Sciences* **2004,** *66* (1), 3-18.

9. Mawji, E.; Gledhill, M.; Milton, J. A.; Tarran, G. A.; Ussher, S.; Thompson, A.; Wolff, G. A.; Worsfold, P. J.; Achterberg, E. P., Hydroxamate Siderophores: Occurrence and Importance in the Atlantic Ocean. *Environmental Science & Technology* **2008,** *42* (23), 8675-8680.

10. Wagener, T.; Pulido-Villena, E.; Guieu, C., Dust iron dissolution in seawater: Results from a one-year time-series in the Mediterranean Sea. *Geophys. Res. Lett.* **2008,** *35*, L16601, doi:10.1029/2008GL034581..

11. Kuma, K.; Matsunaga, K., Availability of colloidal ferric oxides to coastal marine phytoplankton. *Marine Biology* **1995,** *122* (1), 1-11.

12. Meskhidze, N.; Nenes, A., Phytoplankton and Cloudiness in the Southern Ocean. *Science* **2006,** *314* (5804), 1419-1423.

13. Meskhidze, N.; Chameides, W. L.; Nenes, A., Dust and pollution: A recipe for enhanced ocean fertilization? *J. Geophys. Res.* **2005,** *110*, D03301, doi:10.1029/2004JD005082.

14. Blain, S.; Queguiner, B.; Armand, L.; Belviso, S.; Bombled, B.; Bopp, L.; Bowie, A.; Brunet, C.; Brussaard, C.; Carlotti, F.; Christaki, U.; Corbiere, A.; Durand, I.; Ebersbach, F.; Fuda, J.-L.; Garcia, N.; Gerringa, L.; Griffiths, B.; Guigue, C.; Guillerm, C.; Jacquet, S.; Jeandel, C.; Laan, P.; Lefevre, D.; Lo Monaco, C.; Malits, A.; Mosseri, J.; Obernosterer, I.; Park, Y.-H.; Picheral, M.; Pondaven, P.; Remenyi, T.; Sandroni, V.; Sarthou, G.; Savoye, N.; Scouarnec, L.; Souhaut, M.; Thuiller, D.; Timmermans, K.; Trull, T.; Uitz, J.; van Beek, P.; Veldhuis, M.; Vincent, D.; Viollier, E.; Vong, L.; Wagener, T., Effect of natural iron fertilization on carbon sequestration in the Southern Ocean. *Nature* **2007,** *446* (7139), 1070-1074.

15. Martin, J. H.; Fitzwater, S. E., Iron deficiency limits phytoplankton growth in the north-east Pacific subarctic. *Nature* **1988,** *331* (6154), 341-343.

16. Majestic, B. J.; Schauer, J. J.; Shafer, M. M.; Turner, J. R.; Fine, P. M.; Singh, M.; Sioutas, C., Development of a Wet-Chemical Method for the Speciation of Iron in Atmospheric Aerosols. *Environmental Science & Technology* **2006,** *40* (7), 2346-2351.

17. Baker, A. R.; French, M.; Linge, K. L., Trends in aerosol nutrient solubility along a west-east transect of the Saharan dust plume. *Geophys. Res. Lett.* **2006,** 33, L07805, doi:10.1029/2005GL024764.

18. Desboeufs, K. V.; Losno, R.; Vimeux, F.; Cholbi, S., The pH-dependent dissolution of wind-transported Saharan dust. *J. Geophys. Res.* **1999,** *104* (D17), 21,287-21,299.

19. Spokes, L. J.; Jickells, T. D., Factors controlling the solubility of aerosol trace metals in the atmosphere and on mixing into seawater. *Aquatic Geochemistry* **1995,** *1* (4), 355-374.

20. Meskhidze, N.; Chameides, W. L.; Nenes, A.; Chen, G., Iron mobilization in mineral dust: Can anthropogenic SO2 emissions affect ocean productivity? *Geophys. Res. Lett.* **2003,** *30*, 2085, doi:10.1029/2003GL018035.

21. Desboeufs, K. V.; Sofikitis, A.; Losno, R.; Colin, J. L.; Ausset, P., Dissolution and solubility of trace metals from natural and anthropogenic aerosol particulate matter. *Chemosphere* **2005,** *58* (2), 195-203.

22. Ooki, A.; Nishioka, J.; Ono, T.; Noriki, S., Size dependence of iron solubility of Asian mineral dust particles. *J. Geophys. Res.*, **2009,** *114*, D03202, doi:10.1029/2008JD010804.

23. Mahowald, N. M.; Baker, A. R.; Bergametti, G.; Brooks, N.; Duce, R. A.; Jickells, T. D.; Kubilay, N.; Prospero, J. M.; Tegen, I., Atmospheric global dust cycle and iron inputs to the ocean. *Global Biogeochem. Cycles* **2005,** *19*, GB4025, doi:10.1029/2004GB002402.

24. Journet, E.; Desboeufs, K. V.; Caquineau, S.; Colin, J.-L., Mineralogy as a critical factor of dust iron solubility. *Geophys. Res. Lett.*, **2007,** *35*, L07805, doi:10.1029/2007GL031589.

25. Baker, A. R.; Jickells, T. D., Mineral particle size as a control on aerosol iron solubility. *Geophys. Res. Lett.*, **2006,** *33*, L17608, doi:10.1029/2006GL026557.

26. Hand, J. L.; Mahowald, N. M.; Chen, Y.; Siefert, R. L.; Luo, C.; Subramaniam, A.; Fung, I., Estimates of atmospheric-processed soluble iron from observations and a global mineral aerosol model: Biogeochemical implications. *J. Geophys. Res.* **2004,** *109*, D17205, doi:10.1029/2004JD004574

27. Adams, J. W.; Rodriguez, D.; Cox, R. A., The uptake of SO_2 on Saharan dust: a flow tube study. *Atmospheric Chemistry and Physics* **2005,** *5* (10), 2679-2689.

28. Khoder, M. I., Atmospheric conversion of sulfur dioxide to particulate sulfate and nitrogen dioxide to particulate nitrate and gaseous nitric acid in an urban area. *Chemosphere* **2002,** *49*, 675-684.

29. Ullerstam, M.; Vogt, R.; Langer, S.; Ljungstrom, E., The kinetics and mechanism of SO2 oxidation by O3 on mineral dust. *Physical Chemistry Chemical Physics* **2002,** *4* (19), 4694-4699.

30. Usher, C. R.; Al-Hosney, H.; Carlos-Cuellar, S.; Grassian, V. H., A laboratory study of the heterogeneous uptake and oxidation of sulfur dioxide on mineral dust particles. *Journal of Geophysical Research* **2002,** *107*, 4713, doi:10.1029/2002JD002051

31. Worsnop, D. R.; Zahniser, M. S.; Kolb, C. E.; Gardner, J. A.; Watson, L. R.; Van Doren, J. M.; Jayne, J. T.; Davidovits, P., The temperature dependence of mass accommodation of sulfur dioxide and hydrogen peroxide on aqueous surfaces. *The Journal of Physical Chemistry* **1989,** *93* (3), 1159-1172.

32. Brimblecombe, P., *Air composition and chemistry*. 2nd ed.; Cambridge University Press: Cambridge, 1996.

33. Fu, H.; Wang, X.; Wu, H.; Yin, Y.; Chen, J., Heterogeneous Uptake and Oxidation of SO_2 on Iron Oxides. *Journal of Physical Chemistry C* **2007,** *111* (16), 6077-6085.

34. Seisel, S.; Keil, T.; Lian, Y.; Zellner, R., Kinetics of the uptake of SO_2 on mineral oxides: Improved initial uptake coefficients at 298 K from pulsed Knudsen cell experiments. *International Journal of Chemical Kinetics* **2006,** *38* (4), 242-249.

35. Kim, K. H.; Choi, J. S., Kinetics and Mechanism of the Oxidation of Sulfur Dioxide on α-Fe_2O_3. *Journal of Physical Chemistry* **1981,** *85* (17), 2447-2450.

36. Zhang, X.; Zhuang, G.; Chen, J.; Wang, Y.; Wang, X.; An, Z.; Zhang, P., Heterogeneous Reactions of Sulfur Dioxide on Typical Mineral Particles. *Journal of Physical Chemistry B* **2006,** *110* (25), 12588-12596.

37. Baltrusaitis, J.; Cwiertny, D. M.; Grassian, V. H., Adsorption of sulfur dioxide on hematite and goethite particle surfaces. *Physical Chemistry Chemical Physics* **2007,** *9* (41), 5542-5554.

38. Bauer, S. E.; Koch, D., Impact of heterogeneous sulfate formation at mineral dust surfaces on aerosol loads and radiative forcing in the Goddard Institute for Space Studies general circulation model. *J. Geophys. Res.* **2005,** *110*, D17202, doi:10.1029/2005JD005870.

39. Mogili, P. K.; Kleiber, P. D.; Young, M. A.; Grassian, V. H., Heterogeneous Uptake of Ozone on Reactive Components of Mineral Dust Aerosol: An Environmental Aerosol Reaction Chamber Study. *Journal of Physical Chemistry A* **2006,** *110* (51), 13799-13807.

40. Preszler Prince, A.; Wade, J. L.; Grassian, V. H.; Kleiber, P. D.; Young, M. A., Heterogeneous reactions of soot aerosols with nitrogen dioxide and nitric acid: atmospheric chamber and Knudsen cell studies. *Atmospheric Environment* **2002,** *36*, 5729-5740.

41. Preszler Prince, A. M. Investigations Into The Heterogeneous Atmospheric Interactions of Isolated Metal Oxide, Carbonate, and Soot Aerosols. University of Iowa, Iowa City, **2003**.

42. Pivovarov, S., Surface Structure and Site Density of the Oxide-Solution Interface. *Journal of Colloid and Interface Science* **1997,** *196* (2), 321-323.

43. Liang, L.; Morgan, J. J., Chemical aspects of iron oxide coagulation in water: Laboratory studies and implications for natural systems. *Aquatic Sciences - Research Across Boundaries* **1990,** *52* (1), 32-55.

44. Ullerstam, M.; Johnson, M. S.; Vogt, R.; Ljungstrom, E., DRIFTS and Knudsen cell study of the heterogeneous reactivity of SO_2 and NO_2 on mineral dust. *Atmospheric Chemistry and Physics* **2003,** *3* (6), 2043-2051.

45. Jang, J.-H.; Dempsey, B. A.; Burgos, W. D., Solubility of Hematite Revisited: Effects of Hydration. *Environmental Science & Technology* **2007,** *41* (21), 7303-7308.

46. Judeikis, H. S.; Stewart, T. B.; Wren, A. G., Laboratory Studies of Heterogeneous Reactions of SO_2. *Atmospheric Environment* **1978,** *12*, 1663-1641.

47. Toledano, D. S.; Henrich, V. E., Kinetics of SO_2 Adsorption on Photoexcited α-Fe_2O_3. *Journal of Physical Chemistry B* **2001,** *105* (18), 3872-3877.

CHAPTER 4
COMPETITIVE UPTAKE OF OZONE AND SULFUR DIOXIDE ON HEMATITE AEROSOL UNDER ATMOSPHERICALLY RELEVANT CONDITIONS

4.1 Abstract

We have investigated the uptake of SO_2 on hematite particles in the presence of a common atmospheric oxidant, O_3. The competitive, coadsorption of these two species was studied in an atmospheric reaction chamber using IR absorption spectroscopy to monitor the loss of gas phase reactants. In addition, the RH inside the reaction chamber was varied to present more atmospherically relevant conditions and to evaluate the impact of gas phase water on SO_2 uptake. The presence of ozone did not greatly enhance the uptake of SO_2 on dry hematite and no new loss channels, perhaps due to oxidation, were observed. The SO_2 uptake coefficient, γ_{SO2}, exhibited approximately the same, relatively insensitive, dependence on the experimental RH as in the analogous studies in the absence of ozone until elevated RH was reached. Experiments with 1% < RH < 40% displayed pseudo-first order uptake for SO_2 and O_3 and the surface became saturated as in dry experiments. However, at RH > 50%, the SO_2 uptake appeared to follow zero-order behavior and the surface did not become saturated with respect to SO_2. The total amount of O_3 uptake remained constant when water vapor pressure was varied, although the O_3 uptake coefficient, γ_{O3}, decreased significantly as a function of RH, as observed in previous studies without SO_2. Evidence of competitive coadsorption was seen in the ozone uptake, which appeared to saturate or be much reduced when SO_2 was coadsorbed. These results indicate that acidification of hematite aerosol through sulfate formation is not facilitated when O_3 is the oxidant.

4.2 Introduction

Mineral dust is a ubiquitous component of the total atmospheric aerosol load and can impact atmospheric chemistry and global climate in a variety of ways. A direct effect is from the large available surface area which can act as an effective sink for trace atmospheric gases at rates that can be competitive with more well understood homogenous gas phase pathways. In particular, species that have a large anthropogenic component, such as SO_2 and nitrogen oxides, NO_y, can readily partition to mineral dust aerosol surfaces. Removal of trace gases by heterogeneous reaction can impact global cycles. For example, modeling studies demonstrate that uptake of H_xO_y and N_xO_y, two reactive species in the photochemical oxidant cycle, by mineral dust was likely linked to observed decreases in tropospheric ozone concentrations [1, 2]. In addition, heterogeneous oxidation of SO_2 and NO_y can alter the optical properties of mineral dust by creating layers of sulfate and nitrate around particles, which in turn alters its impact on radiative forcing [3, 4].

Mineral dust particles also play an important role in biogeochemical processes. Iron is an essential nutrient for many marine microorganisms, and iron deficiency in remote areas of the ocean is often a major limiting factor in the growth of phytoplankton [5, 6]. While the deposition of mineral aerosol from continental landmasses acts as a major source of iron to the remote ocean, the iron content of the particulate matter is generally in a very insoluble oxide form (hematite, goethite), and only a small fraction is available for use by microorganisms [7-9]. It has been proposed that chemical processing of mineral aerosols by acidic gasses may lower the pH sufficiently to promote dissolution and enhance bioavailability [10, 11].

Nitric acid (HNO_3) and sulfur dioxide (SO_2) are common acidic gases in the atmosphere that originate primarily from anthropogenic sources and could be directly absorbed onto mineral dust surfaces. The presence of alkaline components (such as $CaCO_3$) internally mixed with the mineral dust may act as buffers and greatly reduce acidification through this pathway; particle acidification is expected to be most effective in areas containing high ratios of acid gas to dust loading [10]. A small amount of $CaCO_3$ in the aerosol may actually aid in acidification, as it reacts with atmospheric HNO_3 to produce the very hygroscopic product $Ca(NO_3)_2$ [12]. $Ca(NO_3)_2$ has a low deliquescence relative humidity of approximately 13 - 18% [13, 14], and could facilitate the formation of multiple water layers around the mineral dust core which would have a very high affinity for further HNO_3 uptake and acidification (again, provided the acid gas concentration is sufficient to overcome the buffering capacity of $CaCO_3$). Typically, the concentration of SO_2 is larger than HNO_3 by about a factor of 10 in urban air plumes [15, 16]. Particulate phase SO_2 may be oxidized to S(VI) through a variety of mechanisms involving gas phase oxidants or even catalytic processes mediated by metallic species in the aerosol itself. Surface coatings of hygroscopic sulfate could lead to the deliquescence that is one necessary condition for dissolution of particulate iron before reaching the ocean [11]. Sulfate formation and subsequent acidification of an iron oxide aerosol may be an important pathway for the production of bioavailable iron *via* atmospheric processing. Several studies have correlated various methods of atmospheric processing with changes in the solubility of minerals [17-20], although it has also been proposed that this observation is due primarily to the changes in the physical properties of aerosol plumes over the same transport period [21, 22]. Despite several laboratory investigations

and numerical simulations that suggest the potential importance of acid-processing, there are few field studies that attempt to directly observe this process [23]. Baker *et al.*, for example, did not observe increased iron solubility in Saharan dust after 5 - 10 days of processing over the Atlantic Ocean, although perhaps this particular dust event did not pass over an area of sufficiently high acid gas concentrations [24].

In our previous work, we observed a significant uptake of SO_2 onto hematite, α-Fe_2O_3 aerosol in a series of environmental chamber studies. We were only able to observe the loss of the gas phase SO_2 and could not directly determine the surface speciation or sulfur oxidation state. Related studies using XPS measured a large increase in sulfate formation relative to sulfite on the hematite surface when gas phase oxygen was present [25]; the addition of oxygen was also shown to increase the overall amount of oxidized sulfur species formed on hematite [25, 26]. In our work, however, the absence of oxygen in the buffer gas did not have a measureable effect on the magnitude of the SO_2 uptake, in terms of total surface coverage. The potential oxidation of surface adsorbed sulfur by oxygen apparently does not increase subsequent uptake of SO_2. However, in the actual troposphere, many more powerful oxidants, such as OH and O_3, may play a role in SO_2 uptake.

Sulfur dioxide is naturally emitted into the atmosphere through geochemical activity, such as volcanic eruptions, and biological processes. Sulfur dioxide is also released as a byproduct of anthropogenic activities, which is the dominant source of SO_2 in urban air plumes. In the troposphere, SO_2 is readily oxidized to SO_4^{2-} through a variety of processes. While homogeneous oxidation mechanisms play a role, most atmospheric SO_2 is oxidized in cloud and water droplets as well as on the surface of mineral dust and

sea salt aerosol. In the presence of water, SO_2 hydrolyzes via the following series of reactions.

$$SO_2(g) + H_2O(l) \xleftrightarrow{H_{SO_2}} H_2SO_3(aq) \quad 4.1$$

$$H_2SO_3(aq) \xleftrightarrow{K_{a1}} H^+ + HSO_3^-(aq) \quad 4.2$$

$$HSO_3^-(aq) \xleftrightarrow{K_{a2}} H^+ + SO_3^{2-}(aq) \quad 4.3$$

The sulfite species can then be oxidized by species such as dissolved ozone,

$$SO_3^{2-}(aq) + O_3(aq) \rightarrow SO_4^{2-}(aq) + O_2(aq) \quad 4.4$$

Similar reactions with SO_2 and bisulfite, HSO_3^- , are also possible but are slower. The rate of the ozone reaction increases at higher pH values. Dissolved metal ions, such as Fe(III) can also catalyze the oxidation of SO_2. Low vapor pressure H_2SO_4 or particulate sulfate can coat aerosol particles and alter their optical and physical properties, such as hygroscopicity and heterogeneous reactivity.

Ozone is also highly reactive towards certain mineral dust surfaces. A Knudsen reactor study by Hanisch and Crowley showed that ozone can be converted to oxygen on Saharan dust surfaces, which are representative of typical aerosol particulates [27]. This study also noted that the uptake coefficient γ_{O3} and the stoichiometry of the conversion of O_3 to O_2 was increased when the reactive dust samples were heated prior to reaction. The authors suggest this was due to removal of surface bound water, which may block reactive sites both on the surface and in pores.[27]. The reactive uptake of ozone on representative mineral dusts (α-Fe_2O_3 and α-Al_2O_3) and the impact of water vapor on the reaction were also examined with the environmental reaction chamber used in this study. Mogili et al. found that O_3 was quantitatively consumed by hematite aerosol in a catalytic process that was not observed on other oxides, such as alumina, α-Al_2O_3. At atmospherically relevant levels of relative humidity, the uptake coefficient, γ_{O3}, was

dramatically reduced by up to a factor of 50 [28]. Other studies have also noted that various mineral components of aerosols can facilitate catalytic ozone destruction. In particular, it is notable that the surfaces of α-Fe_2O_3, α-Al_2O_3, and Saharan dust did not become completely passivated to O_3 uptake on the time scale of several hours during Knudsen cell experiments[29].

Surface sensitive studies can aid in elucidating the fate of SO_2 once it becomes adsorbed on a mineral surface. Several investigators have utilized diffuse reflectance infrared Fourier transform spectroscopy (DRIFTS) to monitor the heterogeneous reaction of SO_2 on laboratory dust samples that are representative of mineral aerosol composition [26, 30, 31]. Fu et al. used X-ray photoelectron spectroscopy (XPS) to identify SO_3^{2-} and SO_4^{2-} formation on the surface of several metal oxides exposed to SO_2 and O_2 [26]. The simultaneous decrease in the DRIFTS signal for OH stretching modes during SO_2 absorption showed the likely involvement of surface hydroxyl groups. The degree of oxidation of $S(IV)_{(ads)}$ to $S(VI)_{(ads)}$ was found to depend strongly on the partial pressure of O_2, and reducing the mineral surface with H_2 before reaction also greatly reduced the formation of oxidized products. Another DRIFTS study, followed by ion chromatography of exposed surfaces to quantify sulfate formation, investigated ozone as an oxidant in the heterogeneous reaction of SO_2 with Saharan dust [31]. Although little SO_4^{2-} was formed in the absence of O_3, the addition of ozone caused almost complete conversion of $SO_{2(ads)}$ to $SO_4^{2-}{}_{(ads)}$. The uptake coefficient, γ_{SO2}, was on the order of 10^{-7} (based on BET surface area) in the absence of O_3 and was in the range $10^{-6} - 10^{-8}$ during coexposure of Saharan dust to SO_2 and O_3. Exposure to water vapor increased the total amount of sulfate formed in these studies by 47%. NO_2 was also found to be an appropriate oxidant of sulfur to

S(VI) on Saharan dust, although the rate of oxidation was too slow to be considered an important sink of SO_2 in the atmosphere [30]. Adsorbed water on the surface of metal oxides has also been shown to effect the relative amount of S(VI) formed through heterogeneous reaction [25, 32]. The goal of the studies presented in this chapter is to determine the effect of a common atmospheric oxidant, O_3, on the uptake of SO_2 by hematite. Hematite was chosen as a proxy mineral dust aerosol due to its demonstrated reactivity towards both O_3 and SO_2, and its potentially large biogeochemical impact, as discussed above. An environmental simulation chamber will allow investigation of the kinetics and total amount of uptake of both O_3 and SO_2, simultaneously. The relative humidity in the chamber will also be systematically varied to simulate the variations in water vapor concentration that are found in the troposphere.

4.3 Experimental

The environmental simulation chamber has been described in Chapter 5 and in several publications by other authors [13, 28, 33, 34]. The large volume (151 L), Teflon coated chamber operates at room temperature, stable to ± 1 ^{o}C throughout a 12 hour experiment. In a typical experiment, the chamber is evacuated to a base pressure of 20 - 30 mTorr with a trapped mechanical pump. The desired pressure of SO_2 (American Gas Group) is added to the evacuated chamber from a glass gas manifold. An electrical-arc based ozone generator (OREC, Model O3V5-O) produces ozone from a pure oxygen source (Air Products, USP grade). The output of the ozone generator, which consists of several thousand ppm O_3 and a large excess of oxygen gas, is sent directly into the chamber. Therefore, the introduction of O_3 into the chamber results in an elevated oxygen content compared to atmospheric levels. Typically 10 - 30 Torr of the $O_2 + O_3$ mixture

was needed to achieve a final ozone concentration in the range of 50 - 100 ppm. The ozone generator is operated at an oxygen pressure of 10 psi, an electrical current of 2 amperes, and a flow rate setting of "10" controlled by a rotameter. The O_3 and SO_2 gas phase concentrations were monitored in real time with either an FTIR spectrometer or a fiber optic UV-Vis (Ocean Optics SD2000) instrument. The probe beams were coupled into the chamber through side arms on the main chamber and were oriented perpendicular with respect to each other but sampling the same horizontal plane, with the same active path length (59 cm).

The chamber, containing the desired mixture of SO_2, O_3, and residual O_2 (which was introduced during the ozone generation process), was then pressurized to a total pressure near 760 Torr with purge air. The flow of purge air could be partially diverted through a bubbler containing high purity water (Fischer Scientific, Optima grade) to provide control of the relative humidity within the chamber. A solid state RH sensor monitored the flow of humidified air into the chamber but the final, reported, experimental RH was confirmed through a Beer's law calibration using the FTIR spectrometer. Similarly, the concentration of SO_2 was also quantified via a calibrated measurement of the IR absorption. The O_3 concentration was measured in either the IR or the UV using previously reported peak absorption cross-sections at appropriate wavelengths. The reagent gas concentration was monitored for at least two hours prior to aerosol introduction to quantify background reaction and wall losses, which are evident despite the inner surfaces of the chamber being coated with Teflon. Single beam FTIR spectra (average of 256 scans) are continuously acquired at 8 cm^{-1} resolution, providing quantification of gas phase species every 51 seconds. The time resolution of the UV-Vis

instrument was controlled by varying the integration time of the CCD detector and was adjusted to have a similar time resolution.

A sample of hematite powder with a specific BET surface area of 5.1 m^2 (previously determined using a Quantachrome BET apparatus) is placed in a cartridge sample holder and evacuated for at least three hours prior to the experiment to remove residual water. The cartridge is isolated from the main chamber by a slide valve. When the aerosol is to be introduced, the slide valve is retracted, and a one second burst of argon at 100 psi pressurizes the sample cartridge, forcing the powder through a nozzle and impactor assembly. The impactor efficiently deagglomerates the particles and the gas burst rapidly mixes the chamber contents, dispersing the mineral dust aerosol within the chamber. Weighing the residual powder on the impactor and in the sample holder provides a correction for the total mass (and surface area) of hematite introduced into the chamber. Care was taken to use approximately the same mass in each experiment, about 2.8 grams. Since the efficiency of aerosol introduction was generally constant, each experiment involved a hematite surface area of 14 ± 1 m^2. This allowed a direct comparison of the measured kinetics in different experiments although the final reported values for the coverage or the uptake coefficient were always calculated with respect to the actual mass of powder introduced into the chamber. The FTIR and UV-Vis spectroscopic probes could continuously record the gas phase concentration of reactant and product species for experiments that could last as long as 10 - 12 hours after dust introduction.

4.4 Results

4.4.1 FTIR Spectral Results

Typical FTIR spectral results for an experiment with SO_2, O_3 and hematite aerosol under dry, << 1% RH, conditions are shown in Figure 4.1. The spectral signatures of the chamber contents both before, and after, introduction of the hematite aerosol sample are represented. The asymmetric stretch of SO_2 is apparent in the absorption feature at 1365 cm^{-1}. Integration of the asymmetric stretch band was used, along with a previously determined Beer's law calibration, to quantify the SO_2 pressure in the chamber as a function of time. The ozone concentration can be measured either in the UV, via the peak absorptivity of the Hartley band (253.7nm) [35], or by using the O_3 v_3 vibrational band observed in the IR spectrum at 1054 cm^{-1} [36]. The peak absorptivity of the IR band has been previously measured to have a value 3.74 x 10^{-4} ppm^{-1} m^{-1} at a total pressure of one atmosphere [37]. In the experimental investigations described here, which entail relatively high pressures of O_3, the IR spectra were utilized to determine the ozone concentration in the chamber. Trace amounts of CO_2 either inside the chamber or in the long external FTIR probe beam path yielded an absorption band at 2349 cm^{-1} due to the strong asymmetric stretch mode. Immediately following aerosol injection, light scattering by the suspended particles causes a distinctive slope in the IR spectral baseline; a correction for the baseline slope is made prior to quantification of the gaseous species *via* integration or net absorbance measurements. As gravitational settling removes aerosols from the active IR path length, the baseline slope gradually returns towards its initial value. Uptake of either SO_2 or O_3 was detected as a loss in the gas phase concentration as

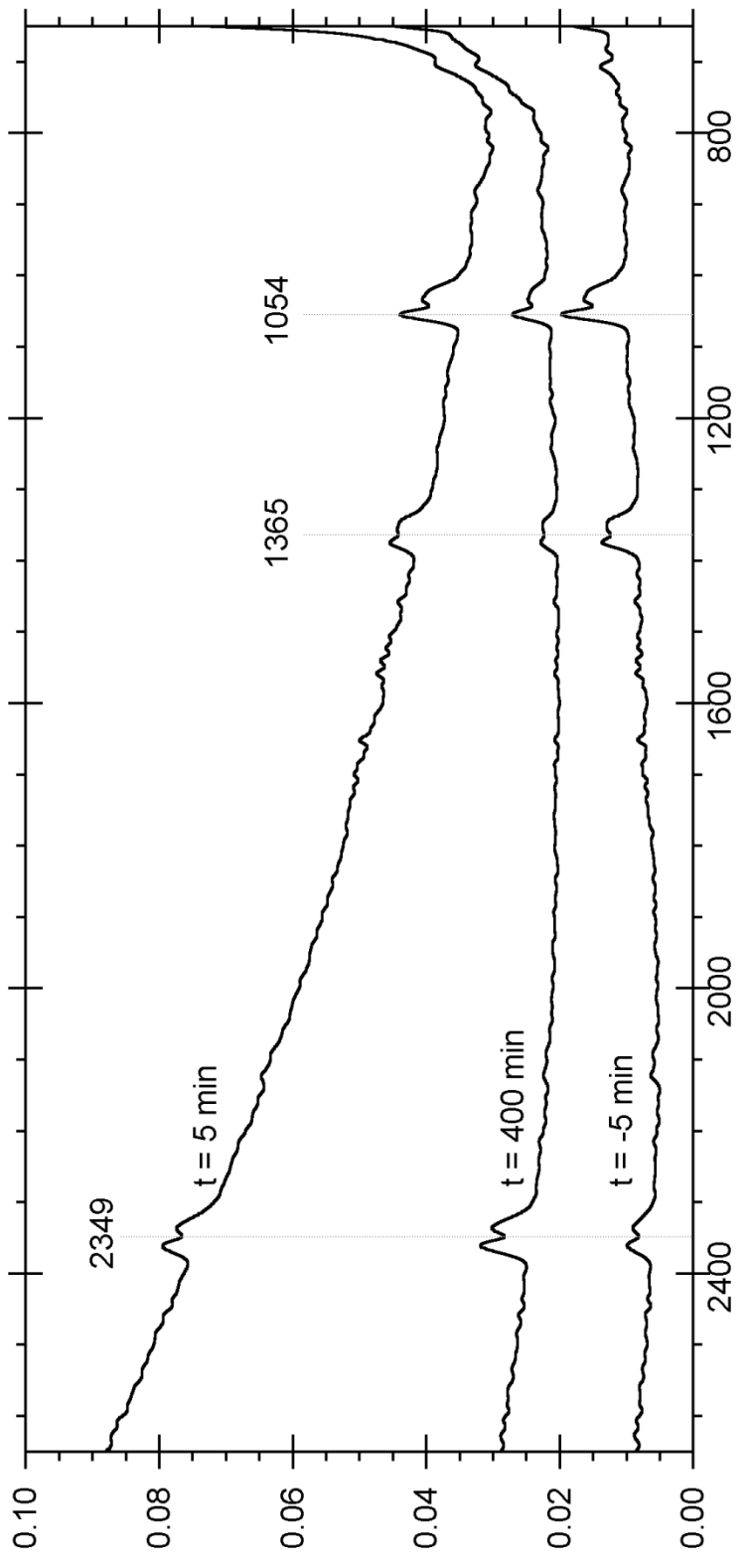

Figure 4.1. Representative FTIR spectra during an experiment performed under driest possible conditions (RH << 1%). Hematite aerosol with a total BET surface area of 13.3 m^2 is injected into the chamber containing 12 mTorr of SO_2, 36 mTorr of O_3 and 760 Torr of dry buffer gas at time t = 0 minutes. The increase in slope following aerosol introduction is due to Mie scattering. Trace water absorptions have been subtracted, and spectra are offset for clarity.

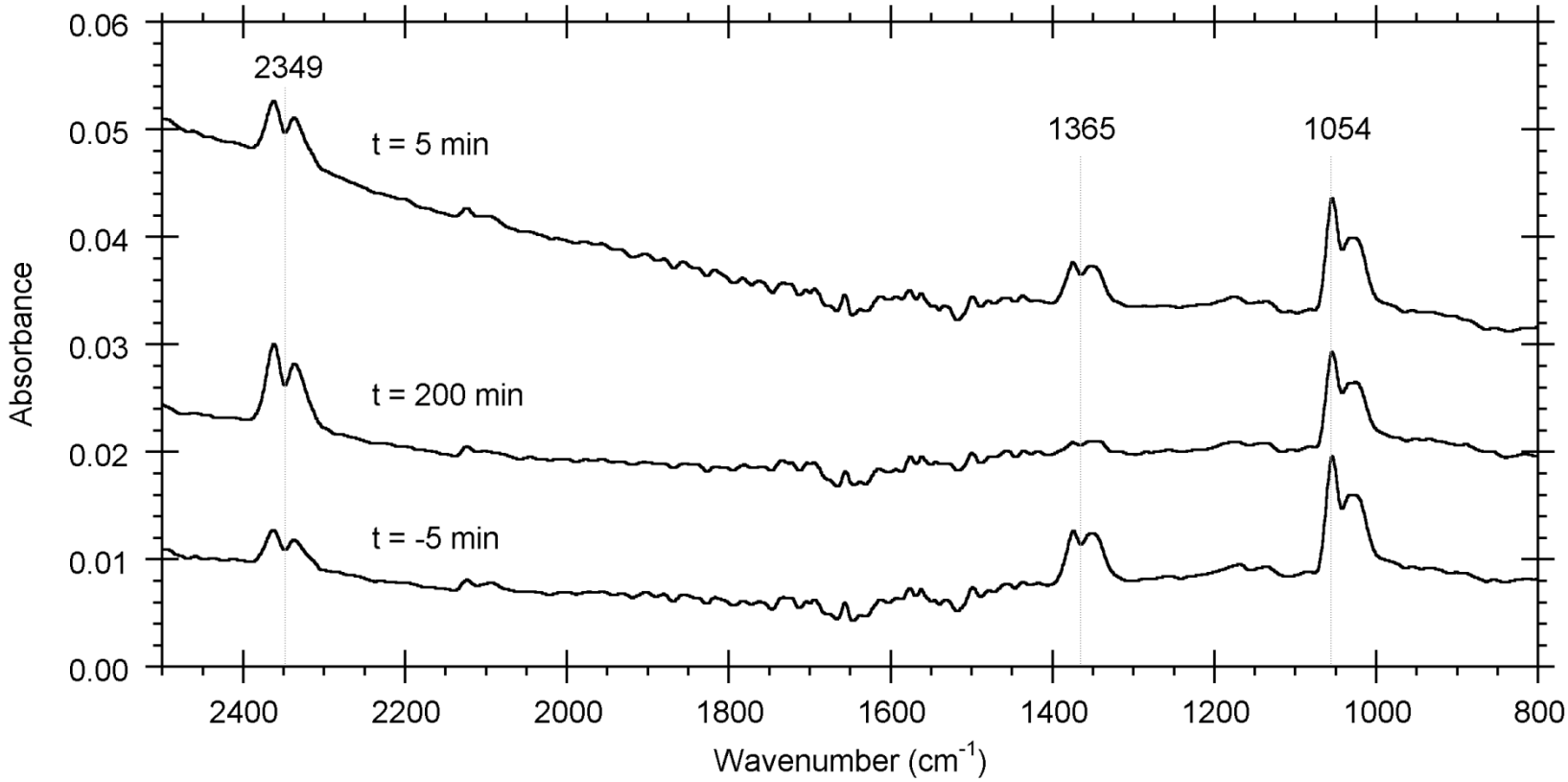

Figure 4.2. FTIR spectra of the interaction between SO_2, O_3, and hematite aerosol under moderately humid conditions (40% RH). Hematite is injected into the chamber containing 11 mTorr of SO_2, 35 mTorr of O_3 and 760 Torr of humid buffer gas at time t = 0 minutes, causing an increase in baseline slope towards higher wavenumbers due to Mie scattering. Water absorptions have been subtracted, leading to additional noise in the 1300 - 1900 cm^{-1} region. Spectra are offset for clarity.

a function of time, as observed in the IR spectral data. In the course of all dry experiments, no new, possible product, species were observed in the spectra.

A series of experiments were performed in which the coadsorption of SO_2 and O_3 on hematite was studied as the relative humidity was varied. Figure 4.2 is representative of results obtained when the humidity was in the range of 8 - 40%. After subtraction of water absorptions, the time resolved FTIR spectra for conditions of low humidity are qualitatively similar to the results obtained with a dry buffer gas (ex., Figure 4.1). The absorption bands due to water are many times more intense than the SO_2 peak which they overlap, and subtraction adds additional uncertainty to the quantification of P_{SO2}. No product species are observed *via* FTIR when the relative humidity is within this range.

When the humidity is increased further, to RH $\geq$ 50%, the formation of a possible product species is observed in the FTIR spectra when both O_3 and SO_2 are present. Figure 4.3 shows the results of such an experiment where a feature at 867 cm^{-1}, with a broad shoulder of less intense peaks that continue through the 867 – 1100 cm^{-1} region, is observed to appear. A broad, less intense absorption is also observed centered at 754 cm^{-1} after 200 minutes of reaction. A small amount (absorbance of 0.003 at 867 cm^{-1}) of the product is formed prior to the introduction of aerosol, during the approximately 90 minutes of reaction time with only gaseous species present in the chamber ($t<0$). However, the intensity increases at a much greater rate when hematite aerosol is injected. Two hundred minutes after aerosol introduction, the peak grew in intensity by two orders of magnitude in this experiment, and continued to increase until the broad shoulder interfered greatly with quantification of O_3 via the 1054 cm^{-1} peak. The growth of the product peak continued throughout the experiment (over 400 minutes), even though all

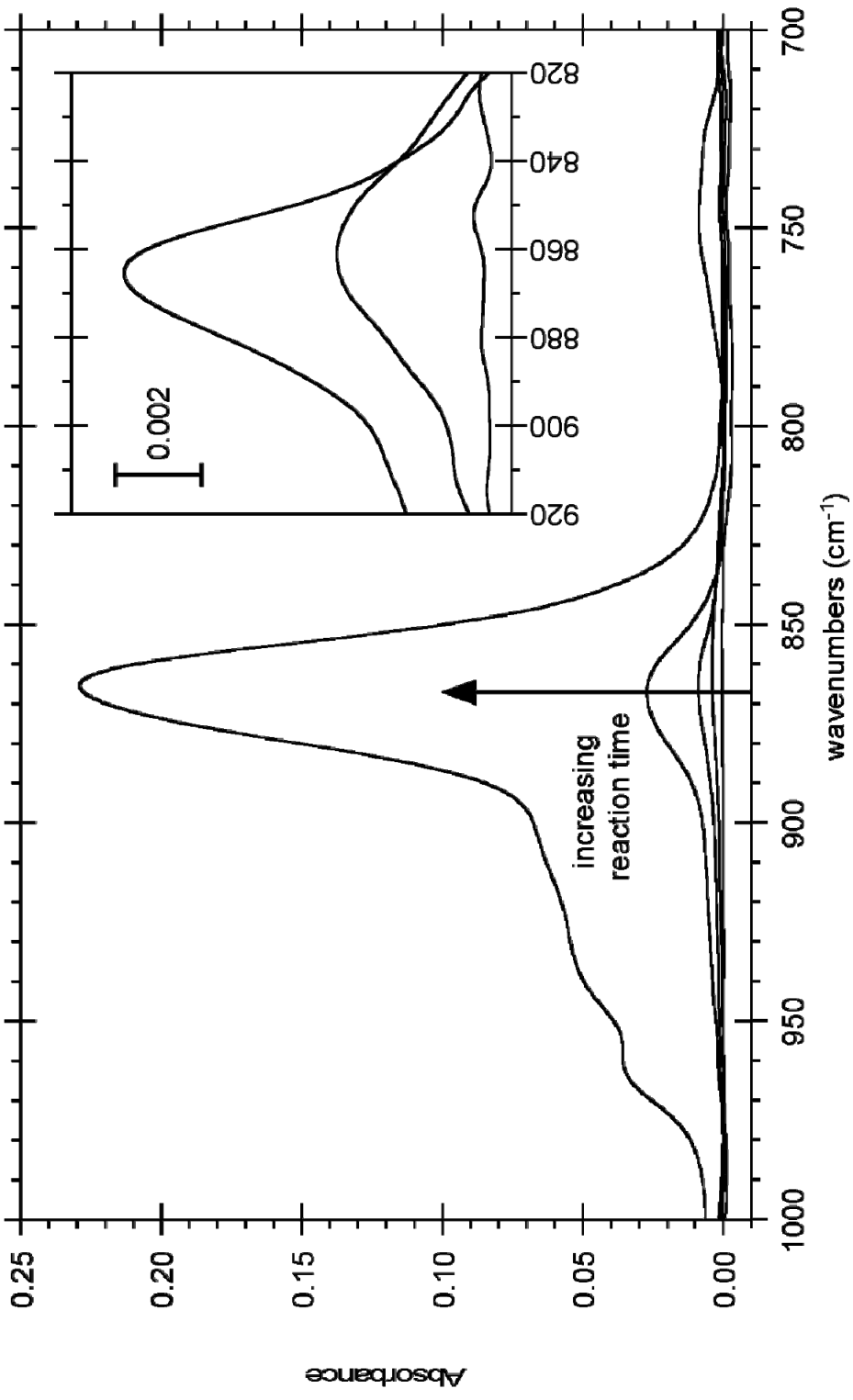

Figure 4.3. FTIR spectra acquired during the exposure of hematite aerosol to 11 mTorr of SO_2 and 33 mTorr of O_3 at 60% relative humidity (RH). The spectra were taken after reaction times of -90, -1, 10, 40, and 200 minutes. Aerosol is injected at t = 0 minutes. The inset shows a detail of the 820 – 920 cm^{-1} for reaction times of -90, -1, and 10 minutes.

gas phase SO_2 was consumed after about 120 minutes. The product was stable to vacuum pumping after the experiment, indicating that it was non-volatile and was associated with the germanium windows. The usual window cleaning procedure of rinsing and gently wiping with lens paper, first with methanol then with water (spectroscopic grade), left a light red stain on the Ge window. After placing the window back on the reaction chamber, the intense absorption peak at 867 cm^{-1} remained and was not greatly reduced in intensity by the cleaning procedure. The IR transmission of the Ge window was restored by cleaning with a liquid detergent and copious amounts of water. From a visual inspection, the quartz windows and Teflon coated surfaces of the chamber seemed to easily wipe clean, suggesting that the formation of this product was promoted by the surface of the germanium windows.

It was also found in a subsequent experiment that the product responsible for the 867 cm^{-1} peak can be observed when hematite is exposed to SO_2 in the *absence* of O_3, but only under very humid conditions ($\geq$ 80% RH), significantly higher than the 50% threshold above which the peak appears with O_3.. However, without O_3, the product is formed at a much lower rate. Peak intensities of 0.002 – 0.004 were observed only after 8 - 10 hours of reaction between hematite and SO_2 without O_3.

An expected product of the oxidation of SO_2 by ozone is sulfate. The aqueous phase absorptions for SO_4^{2-}(aq) (1104 cm^{-1}) or HSO_4^-(aq) (1194, 1051, and 891 cm^{-1}) were not observed in any of the chamber IR spectra and are not coincident with the spectral features of the Ge window product. Hug observed absorptions at 1128 and 1060 cm^{-1} for sulfate adsorbed on hematite using ATR-FTIR [38]. Product bands at these frequencies were also not apparent in our experiments. Strong, broad bands indicative of

common anhydrous and hydrated forms of Fe(II or III) sulfate ranging from approximately 900 – 1300 cm^{-1} were also not apparent here [39]. No other product species were identified in the chamber spectra in either the gas or the condensed phases.

4.4.2 Coadsorption of SO_2 and O_3 on dry hematite

A preliminary experiment was performed in which hematite aerosol was allowed to react with 44 mTorr of ozone in a dry chamber atmosphere. The results, displayed in Figure 4.4, indicate that all ozone is rapidly removed from the gas phase as it reacts with the aerosol. The results are consistent with previous work in our laboratory utilizing the chamber where we observed quantitative destruction of gaseous ozone on α-Fe_2O_3, presumably due to a catalytic decomposition pathway on the particle surface[28]. The measured uptake coefficient, γ_{O3}, $(7 \pm 3) \times 10^{-7}$, is somewhat higher than the value of $(1.0 \pm 0.3) \times 10^{-7}$ reported in the previous study[28]. As noted in that study and demonstrated here, hematite aerosol has the capacity to adsorb large amounts of ozone, corresponding to a coverage in excess of $1.6 \pm 0.2 \times 10^{15}$ molecules cm^{-2} in this particular experiment. No saturation of the surface is observed, at least in the absence of water vapor and SO_2.

In a series of experiments, hematite aerosol was exposed to mixtures of SO_2 and O_3 in various proportions in order to investigate the effects of coadsorption under dry conditions. The reaction kinetics and the uptake of both gas phase species were quantified as a function of time using IR spectroscopy. Typical time resolved data are shown in Figure 4.5 for both SO_2 and O_3. Both species exhibit qualitatively similar decay kinetics; an initial, rapid drop in pressure of a few mTorr upon aerosol introduction followed by a

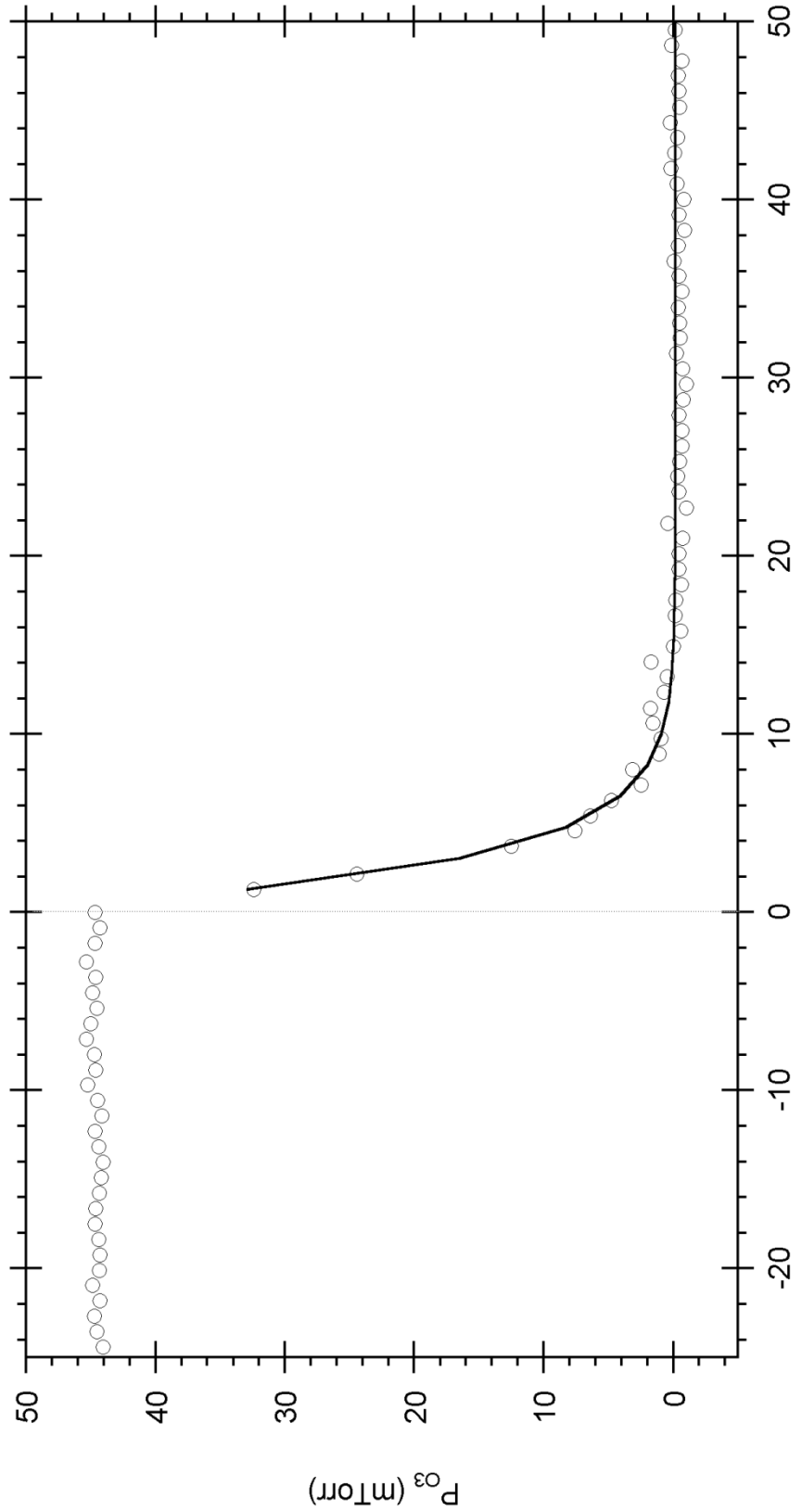

Figure 4.4. Uptake of ozone on hematite aerosol under driest possible conditions (RH<<1%). Hematite aerosol with a BET surface area of 13.5 m^2 was exposed to 44 mTorr of O_3 in the chamber. Aerosol is injected at t = 0 minutes. Solid line represents an least-squares fit to an exponential decay function for t > 0 minutes.

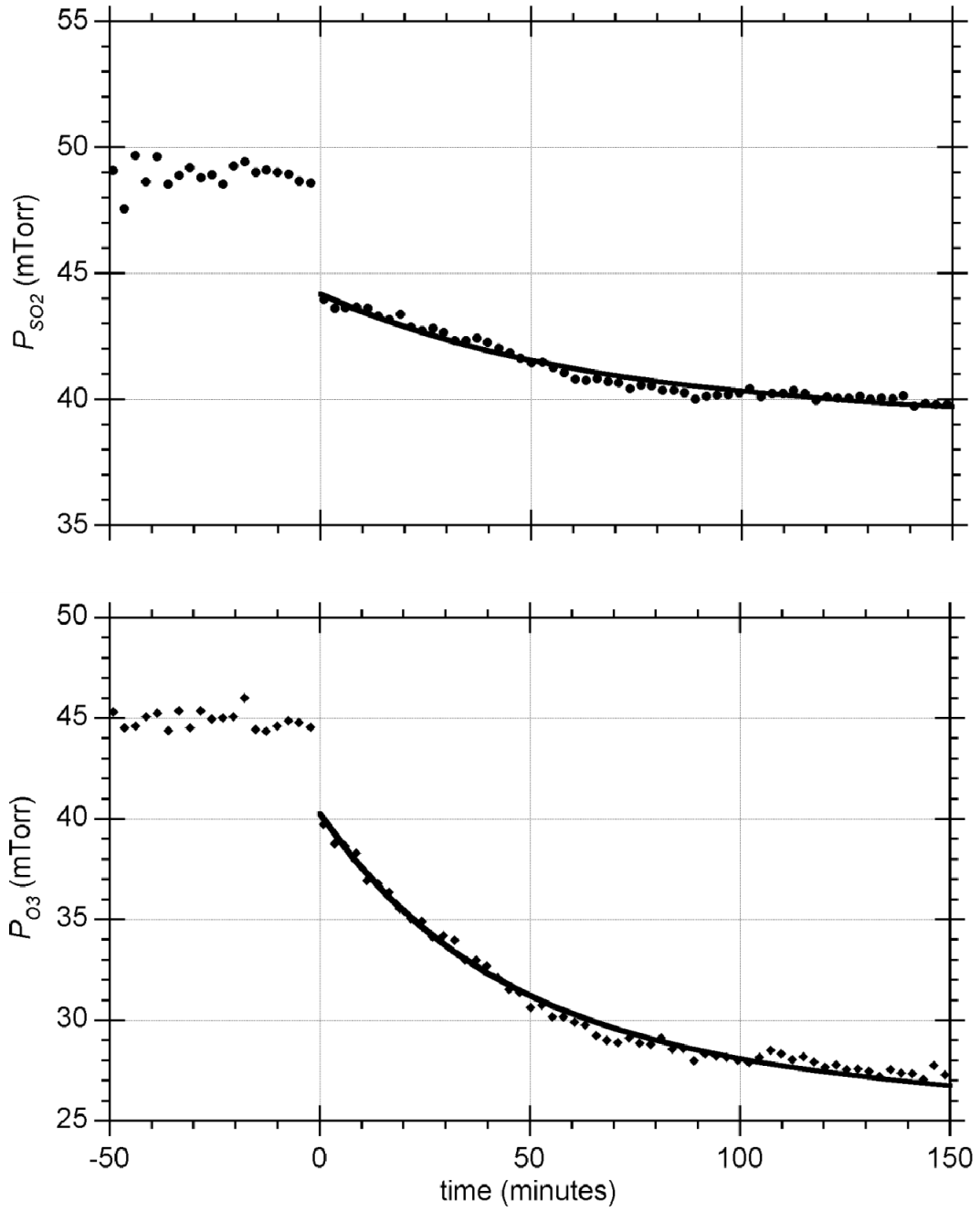

Figure 4.5 Simultaneous uptake of ozone and sulfur dioxide on hematite aerosol under driest possible conditions (RH << 1%). Hematite aerosol with a BET surface area of 13.7 m^2 was exposed to 45 mTorr of O_3 and 49 mTorr of SO_2 in the chamber. Aerosol is injected at t = 0 minutes. Solid lines represent a least-squares fit to an exponential decay function for t > 0 minutes. Only every third data point is plotted for clarity.

slower decay reaching an asymptotic value by the end of the experiment. In all of the dry experiments with more than a few mTorr of O_3 initially present in the chamber, we observe effective saturation of the ozone loss process with significant amounts of ozone remaining in the chamber at the end of the experiment. Similarly, the SO_2 time course data also shows evidence for saturation on the experimental time scales, similar to our previous observations in the absence of O_3. Unless < 5-10 mTorr of either reagent gas was used, significant amounts of gaseous O_3 and SO_2 remained in the chamber during the duration of the experiment, indicating the hematite surface had become saturated.

4.4.3 Time resolved uptake of O_3 and SO_2 in a humid atmosphere

A series of experiments were performed in which the relative humidity was systematically varied to explore the effect of water vapor on the coadsorption of O_3 and SO_2 on hematite aerosol. Figure 4.6 is representative of the time-resolved P_{O3} and P_{SO2} data for a relative humidity in the range of 8 – 40%. As in the dry experiments, both O_3 and SO_2 undergo qualitatively similar changes with time. Prior to aerosol introduction, the only loss mechanisms are due to either gas phase reactions, or reactions with the walls of the chamber (which are Teflon coated). The background loss rates vary with RH, but are typically < 20 μTorr minute^{-1}. Introduction of α-Fe_2O_3 at t = 0 minutes causes an immediate decrease of several mTorr in both O_3 and SO_2. The pressure of each species then decays slowly as uptake continues, until after several hundred minutes, the loss rate reaches the background loss rate.

Increasing the relative humidity above 50% revealed qualitatively different behavior in the uptake of SO_2 and O_3. Figure 4.7, acquired at a relative humidity of 53%, is representative of the time-resolved decay of SO_2 and O_3 observed under very humid

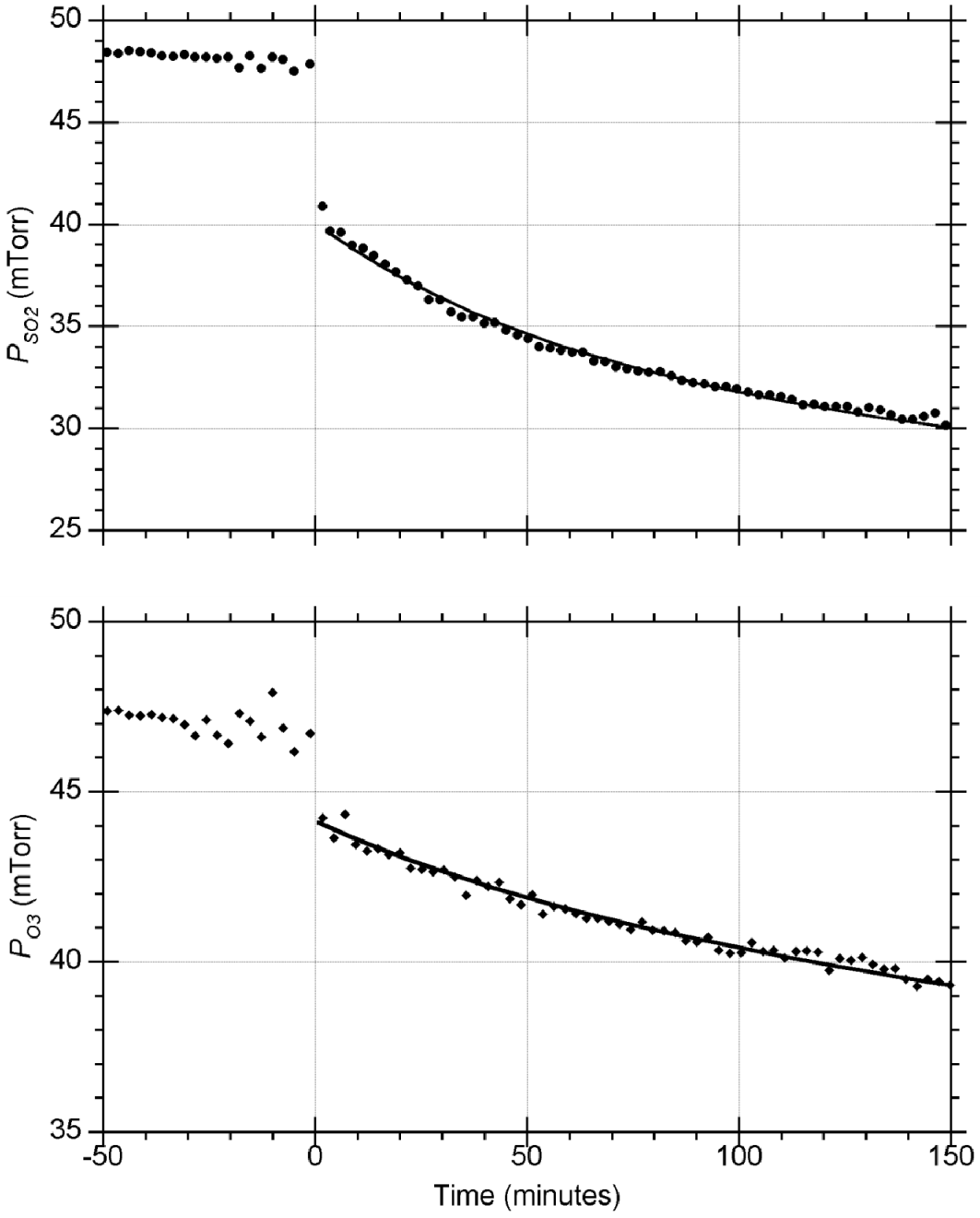

Figure 4.6. Simultaneous uptake of ozone and sulfur dioxide on hematite aerosol under humid conditions (22% RH). Hematite aerosol with a BET surface area of 14.2 m^2 was exposed to 48 mTorr of SO_2 and 47 mTorr of O_3 in the chamber. Aerosol is injected at t = 0 minutes. Solid lines represent a least-squares fit to a combination exponential-linear decay function for t > 0 minutes. Only every third data point is plotted for clarity.

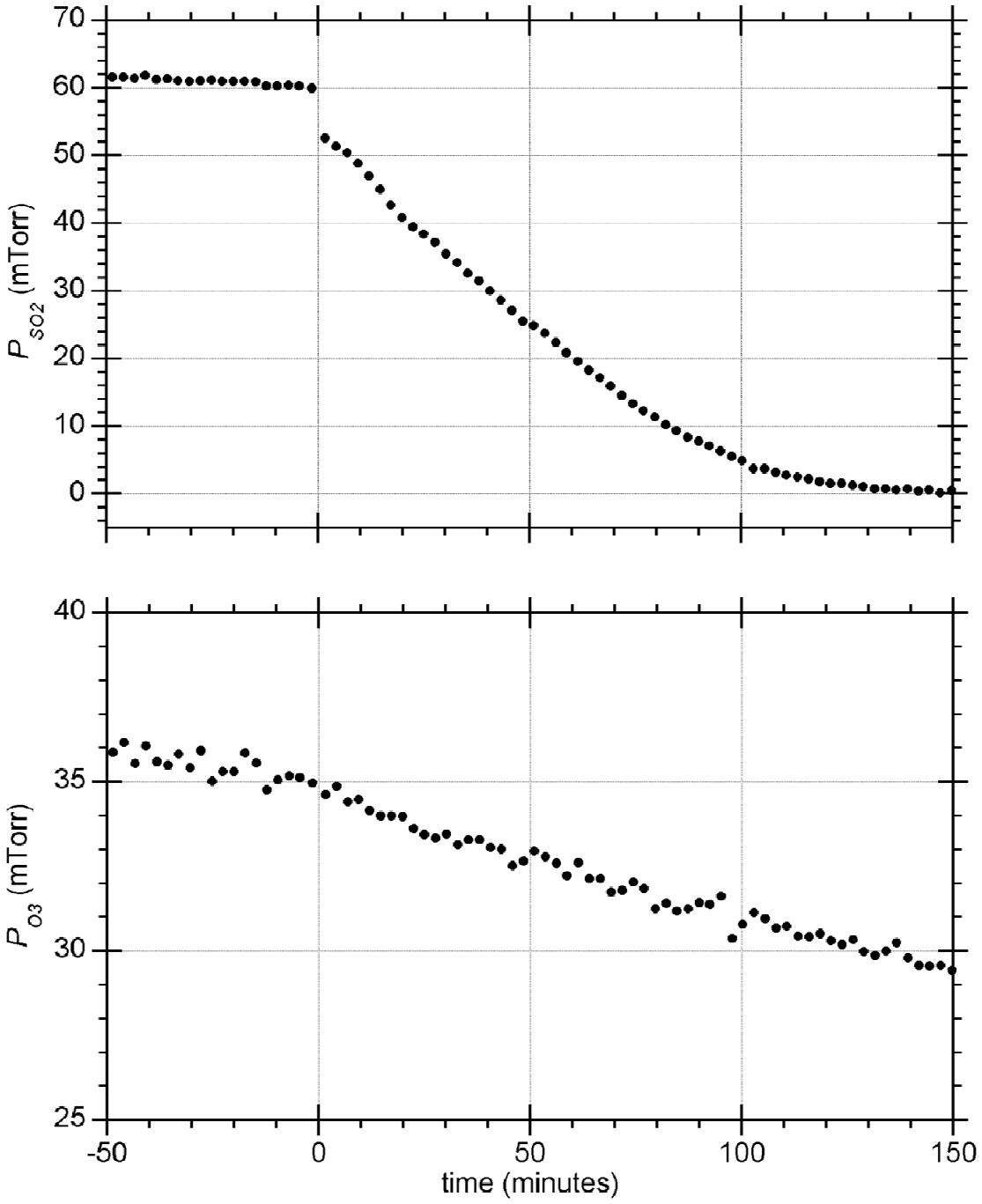

Figure 4.7. Simultaneous uptake of ozone and sulfur dioxide on hematite aerosol under humid conditions (53% RH). Hematite aerosol with a BET surface area of 13.6 m^2 was exposed to 60 mTorr of SO_2 and 35 mTorr of O_3 in the chamber. Aerosol is injected at t = 0 minutes. Only every third data point is plotted for clarity.

conditions. While P_{SO2} still undergoes a marked drop of several mTorr immediately upon aerosol introduction at 53% RH, there is no longer any significant O_3 uptake evident within the first 2 minutes of exposure. All gaseous SO_2 is rapidly consumed, indicating that the hematite surface does *not* become saturated with respect to SO_2 as it does in the absence of ozone, or in experiments performed at lower RH. The decay of SO_2 is no longer well fit to an exponential function, but appears to be nearly linear, indicating a 0^{th} order uptake process. The rate of ozone uptake may actually follow an exponential decay with a time constant longer than the duration of this experiment. Mogili *et al.* also observed a large reduction in γ_{O3} as the humidity was increased in the absence of SO_2; in particular, at RH > 58%, γ_{O3} became too low to reliably measure with our method[28].

4.4.4 Uptake on hematite as a function of RH

Since no gaseous products are observed *via* FTIR spectroscopy, it is assumed that every molecule of SO_2 and O_3 that is removed from the gas phase in the chamber becomes either physisorbed or chemisorbed on the surface of the hematite aerosols. In humid experiments, dissolution of the gaseous species in the water layer(s) surrounding the hematite is also possible. The total uptake of SO_2 and O_3 on hematite can be quantified by determining the reduction in the partial pressure of either species throughout the experiment. The initial pressure of each gas (P_I) in the chamber is determined by taking the average of 15 - 20 measurements immediately prior to aerosol introduction; background losses are negligible over this time period. The final pressure of each gas at the end of the experiment is determined by fitting the P vs. time data to an exponential-linear function of the following form:

$$P(t) = P_F + Ae^{-t/\tau} - Bt \quad (4.5)$$

Here, τ is the time decay constant (in minutes), and A and B are fitting parameters representing the amount of uptake and the background wall loss rate of the gas, respectively. The final pressure of the gas, P_F, can then be acquired from this fit. It is advantageous to find P_F in this manner for direct comparison of uptake reactions that may have rates differing by an order of magnitude, as well as different rates of background loss. If wall losses are negligible in a particular experiment, the linear term can be neglected (i.e., let B = 0). The data fitting was typically performed after truncating the first few minutes of data, $0 < t < 5$ minutes, in order to avoid the initial noise associated with the variations in background scattering due to rapid mixing of the aerosol in the chamber and the gravitational settling of large particles.

By using the ideal gas law to determine the number of moles of gas removed by hematite during the reaction, the surface coverage of species J (n_J) can be estimated by Equation 4.6.

$$n_J = \frac{(P_I - P_F)VN_A}{RTS_{BET}} \quad (4.6)$$

Here, V is the chamber volume (151 L), T is the temperature (K), S_{BET} is the surface area of the aerosol introduced to the chamber (cm^2), R is the ideal gas constant, and N_A is Avogadro's number. The uptake of gas J can also be described in terms of the dimensionless coverage θ_J, which is the coverage per surface site.

$$\theta_J = \frac{n_J}{n_0} \quad (4.7)$$

Here, a value of 4.8 x 10^{14} cm^{-2} is used as the surface site number density (n_0), based on literature values for the number density of surface hydroxyls on hematite [28, 40], although reported values do vary between 2 - 10 x 10^{14} cm^{-2} [41].

The uptake capacity of hematite for both SO_2 and O_3 under dry conditions is summarized in Table 4.1 The reported uncertainty in the measured n_J for each experiment is obtained by propagating estimated uncertainties e_i in each variable in Equation 4-2, where e_i is the uncertainty in variable i. The uncertainty in P_i is estimated by inspection of a plot of P_{SO2} vs. time for each experiment, and noting the variance in P_{SO2} for $-15 < t < 0$ minutes, and is typically in the range of ±0.10 - 0.25 mTorr. The value of e_{SBET} is estimated at 10% due to the mass of powder that remains in the dust impactor and does not become suspended in the chamber, but may participate in some rapid uptake during the < 10 seconds it is open to the chamber atmosphere. Although it was established in Chapter 3 that variations in the initial P_{SO2} in the range of 10 - 50 mTorr had no significant effect on the uptake capacity n_{SO2} under dry conditions, $P_{I,SO2}$ was also investigated as a variable in studies with ozone. From Table 4.1, it can be concluded that ozone has no measurable effect on n_{SO2} on hematite aerosol, even at a $P_{I,O3} / P_{I,SO2}$ ratio of nearly 20. The mean n_{SO2} for the five experiments with 10-13 mTorr $P_{I,SO2}$ and varying amounts of ozone is 1.9 ± 0.4 x 10^{14} cm^{-2}, comparable to that observed for dry experiments with no ozone present as reported in Chapter 3 of this thesis. For the experiments with higher P_{SO2} of 40.5 – 48.7 mTorr, there may be up to a 40% increase in n_{SO2} when approximately stoichiometric amounts of O_3 are present, but that increase is not much greater than the uncertainty in these experiments. It is important to establish that n_{SO2} is not sensitive to the initial P_{SO2} in the chamber, because as will be discussed

P_{SO2} (mTorr)	P_{O3} (mTorr)	n_{SO2} (10^{14} cm^{-2})	n_{O3} (10^{14} cm^{-2})	Total uptake (10^{14} cm^{-2})
0.0	44.0	N/A	16(±2)*	16(±2)
11.3	0.0	2.0(±0.2)	N/A	2.0(±0.2)
12.6	3.1	2.4(±0.3)	1.1(±0.3)*	3.5(±0.4)
10.8	33.1	2.0(±0.2)	1.3(±0.2)	3.3(±0.3)
11.9	36.0	1.7(±0.3)	1.9(±0.3)	3.7(±0.4)
10.8	215	1.6(±0.2)	12.1(±1.2)	13.7(±1.3)
40.5	0.0	2.2(±0.3)	N/A	2.2(±0.3)
43.6	11.3	2.5(±0.4)	2.2(±0.6)	4.6(±0.7)
48.7	44.6	3.1(±0.4)	5.9(±0.8)	9.0(±0.9)

∗ - All ozone in chamber was consumed. N/A – not applicable.

Table 4.1. Uptake capacity of hematite aerosol upon simultaneous exposure to SO_2 and O_3 under driest possible conditions (RH << 1%).

later, the background loss rates of SO_2 and O_3 vary with RH, making it difficult to control $P_{I,SO2}$ and $P_{I,O3}$ with an accuracy of better than 5 mTorr.

The capacity of hematite to remove O_3 from the gas phase is strongly reduced when simultaneously exposed to SO_2. The ozone uptake, n_{O3}, was also determined for each experiment using Equation 4-2 and the results can be found in Table 4-1. Without SO_2 present, hematite aerosol consumed all 44 mTorr of gaseous O_3 in the dry chamber within 10 minutes, corresponding to n_{O3} of $1.6 \pm 0.2 \times 10^{15}$ cm^{-2}. In all experiments with SO_2 present, less than 100% uptake of gas phase O_3 occurred, with the exception of one experiment with a very low $P_{I,O3}$ of 3.5 mTorr. For example, with a $P_{I,O3} / P_{I,SO2}$ ratio of approximately unity, only 51% of the O_3(g) is removed. Even with a large excess of P_{O3} relative to P_{SO2} (by a factor of 19.9), the total uptake of O_3 on hematite was inhibited by SO_2.

As can be seen in Figures 4.5, 4.6, and 4.7, a significant amount of uptake occurs immediately upon aerosol introduction, at a rate beyond the temporal resolution of our technique. This indicates that there may be multiple types of reactive sites on the hematite surface, with different uptake kinetics and capacity. The initial coverage for species J will be quantified as $\theta_{I,J}$, which will be defined as the uptake occurring in the first five minutes after aerosol introduction. For clarity, the final coverage of the sample at the end of the experiment will be denoted $\theta_{F,SO2}$ or $\theta_{F,O3}$.

Figure 4.8 displays both the initial and final coverage of SO_2 and O_3 on hematite as the humidity is varied. In every experiment, there is a discrete decrease in P_{SO2} when hematite is injected. In a dry chamber, $\theta_{I,SO2}$ on α-Fe_2O_3 was 0.38 ± 0.6. In two cases, $\theta_{I,SO2}$ was somewhat elevated by humidity, namely 0.61 ± 0.07 and 0.65 ± 0.07 at RH of

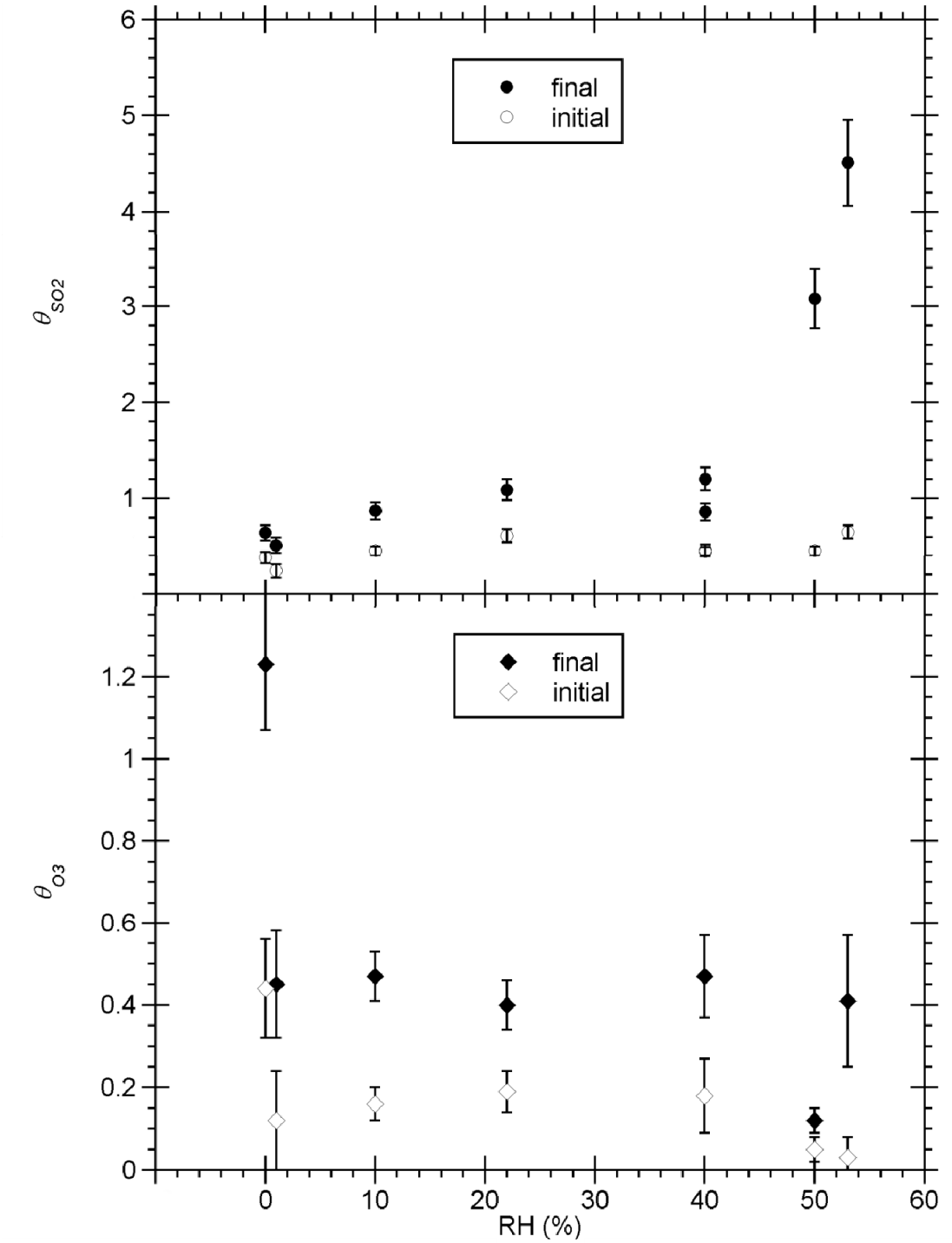

Figure 4.8. Coverage of hematite surface by SO_2 (top) and O_3 (bottom) at various levels of relative humidity (RH). The initial coverage, defined as the coverage after 5 minutes of exposure, is denoted by open symbols, and the final coverage is denoted by filled symbols.

22% and 53%, respectively. There was, however, no systematic trend as the humidity was varied, and the majority of trials gave the same $\theta_{I,SO2}$ as the dry experiment, within error. This indicates that SO_2 molecules adsorbed to the "fast" reactive sites on the surface more quickly than water vapor, even though the water was present at pressures several orders of magnitude greater than P_{SO2} in the chamber. Alternatively, it may be that the adsorbing SO_2 and H_2O molecules do not compete for the same sites for this reaction channel. The initial coverage of O_3 for a dry experiment was $\theta_{I,O3} = 0.44 \pm 0.12$. The value of $\theta_{I,O3}$ depended strongly on RH, being reduced by half for RH in the range of 1 – 40%, and by a factor of 10 for RH > 50%.

Along with the kinetics, the final coverage is an important parameter for determining the relative importance of hematite aerosol as a sink for SO_2 and O_3. For SO_2, $\theta_{F,SO2}$ was 0.64 ± 0.08 in a dry experiment. Increasing the RH up to 40% led to a steady increase in $\theta_{F,SO2}$, although it remained near monolayer coverage. However, when the RH was further increased above 50%, $\theta_{F,SO2}$ increased to multiple monolayers, and was in fact limited by the amount of SO_2 originally in the chamber. Conversely, ozone underwent a decrease in $\theta_{F,O3}$ as the humidity was increased. While $\theta_{F,O3}$ was near monolayer coverage for dry experiments, it was reduced to $\theta_{F,O3} = 0.4 \pm 0.1$ in a humid environment. There was no trend in $\theta_{F,O3}$ as the RH was varied in the range 1 - 53% RH; all studies with water vapor present showed a similar decrease in $\theta_{F,O3}$ relative to dry experiments.

4.4.5 Kinetics of SO_2 and O_3 uptake under humid conditions

The gas phase loss of either SO_2 or O_3 can be modeled as a simple one step uptake process with a rate constant, k,

$$R + S \xrightarrow{k} P \qquad 4.8$$

where R represents the reactant species, S is an available particle surface site, and P represents any reaction product species. The rate of this reaction could also be described by the characteristic time decay constant, τ, which is the reciprocal of the rate constant k.

$$\tau = \frac{1}{k} \qquad 4.9$$

Reaction 4.8 can be characterized in terms of the heterogeneous uptake coefficient, γ, which is the fraction of gas-surface collisions that lead to successful uptake. Assuming pseudo first-order reaction conditions (an excess of surface sites), γ can be determined as in Equation 4.10.

$$\gamma = \frac{4}{\tau S_{BET}[c_{mass}]\bar{c}} \qquad 4.10$$

S_{BET} is the specific surface area of the α-Fe_2O_3 sample (5.06 m^2 g^{-1}), $[c_{mass}]$ is the mass concentration of mineral dust in the chamber (g m^{-3}), and $\bar{c}$ is the meanspeed of the reagent gas at the experimental temperature (m s^{-1}). The decay constant τ is obtained by fitting the time resolved decay of P_{SO2} or P_J to an exponential decay with a linear component, as described in Equation 4.5.

A series of experiments were performed to determine whether atmospherically relevant levels of RH would cause a significant effect on the kinetics of coadsorption of SO_2 and O_3 on hematite. Table 4.2 summarizes the measured values of γ_{SO2} and γ_{O3} for

RH (%)	P_{SO2} (mTorr)	P_{O3} (mTorr)	γ_{SO2} (10^8)	γ_{O3} (10^8)
<1	13	3	9.7(±2.0)	3.0(±0.4)
1	12	3	8.5(±1.5)	*
<1	11	33	14(±3)	13(±4)
8	13	38	2.4(±0.3)	2.8(±0.3)
30	11	36	2.4(±0.3)	3.5(±0.4)
40	11	35	2.2(±0.2)	1.6(±0.2)
64	10	33	5.9(±0.9)	**
<1	12	214	18(±6)	13(±4)
40	36	98	3.4(±0.4)	3.1(±0.5)
<1	49	45	5.1(±0.7)	5.5(±0.8)
22	48	47	4.7(±0.6)	2.8(±0.3)
50	49	45	1.2(±0.1)	8.5(±1.8)

* - Low signal to noise ratio prevented kinetic analysis. ** - Appearance of intense "product peak" caused spectral interference with O_3 peak at 1054 cm^{-1}.

Table 4.2. The effect of relative humidity (RH) on the uptake coefficients of SO_2 and O_3 on hematite aerosol.

various conditions of RH, P_{SO2}, and P_{O3}.

The effect of RH on the uptake coefficients is detailed in Figure 4.9. One convenient way to describe the effects of humidity is to report the γ_{wet} / γ_{dry} ratio at a given RH, where γ_{wet} is the uptake coefficient in the humid chamber, and γ_{dry} is the uptake coefficient in the dry chamber (with similar $P_{I,SO2}$ and $P_{I,O3}$). Values of γ_{wet} / γ_{dry} less than one indicate that the uptake coefficient is reduced by the presence of water vapor.

Figure 4.9 includes points at 0% RH for comparison; in a dry chamber with P_{SO2} = 11 mTorr and P_{O3} = 33 mTorr, both γ_{SO2} and γ_{O3} are approximately 1.3×10^{-7}. The uptake coefficients for both SO_2 and O_3 are reduced by humidity in the range of 8 - 64%. There is no direct correlation between the actual percentage of relative humidity and γ_{SO2}; the presence of any water vapor at 8-40% RH is sufficient to lower γ_{wet} / $\gamma_{dry,SO2}$ to 0.17. At RH of 64%, γ_{SO2} seems to be increasing towards its dry value, possibly due to the creation of a new reactive pathway at elevated RH. Mogili *et al.* performed humidity studies of the ozone reaction on hematite (without SO_2 present) with the same experimental apparatus, and noted that increasing humidity steadily decreases the observed γ_{O3}[28]. For example, at 41% RH and with P_{O3} = 34 ppm, Mogili found that γ_{O3} was reduced to only 4.4($\pm$1.1)% of its dry value. With SO_2 present in this study, γ_{O3} did not systematically decline with increasing RH, but was lowered to γ_{wet} / $\gamma_{dry,O3}$ = 0.20 for RH in the range of 8-40%. The effect of humidity on γ_{SO2} and γ_{O3} was less pronounced when the absolute pressure of each reactant gas was increased to 47 $\pm$ 2 mTorr. The value of γ_{wet} / $\gamma_{dry,SO2}$ at 22% RH was within error of unity, while increasing the RH to 50% reduced γ_{wet} / $\gamma_{dry,SO2}$ to 0.23, similar to the case when lower P_{SO2} and P_{O3} were utilized.

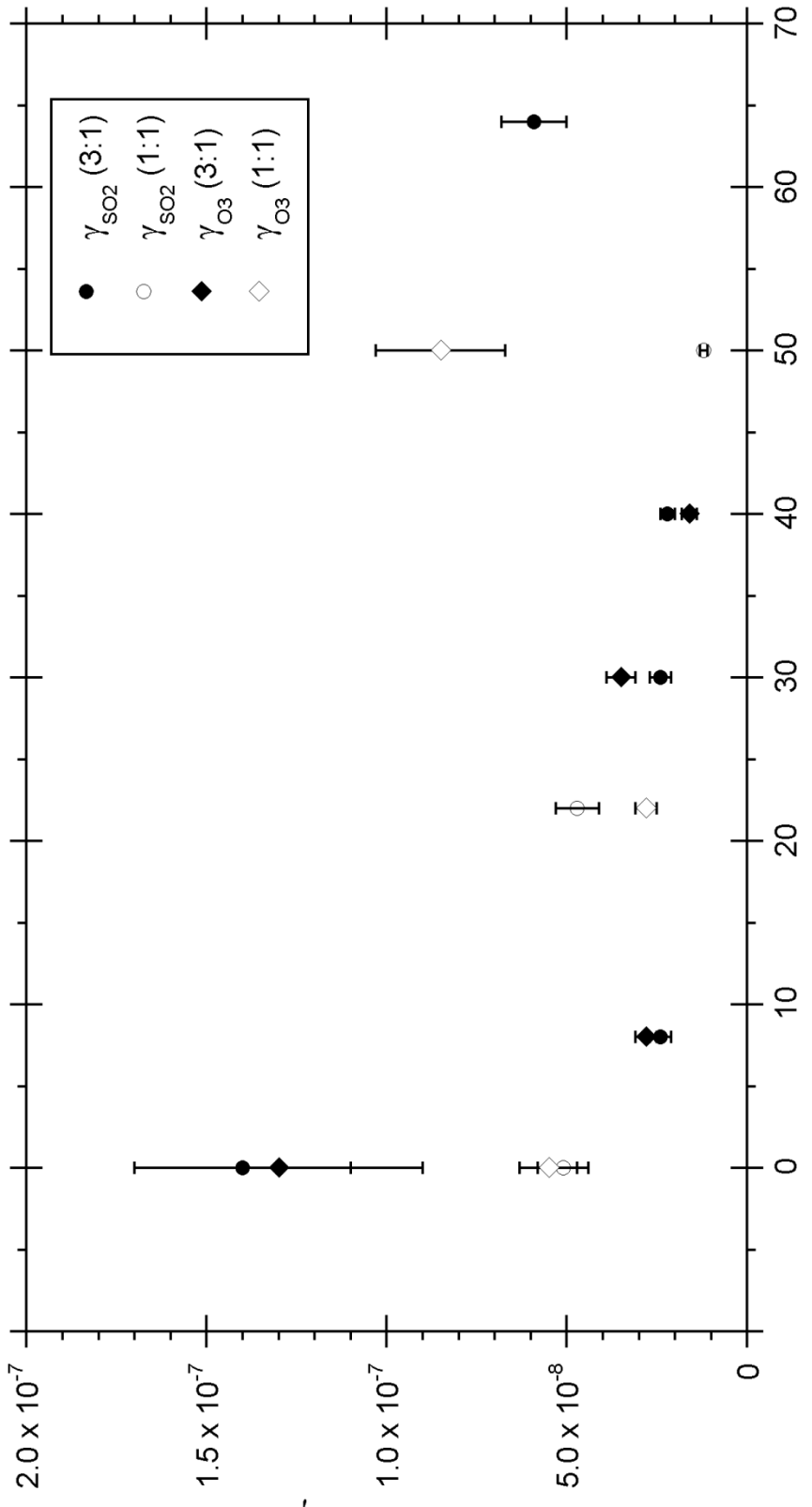

Figure 4.9. The effect of RH on the uptake coefficient of SO_2 and O_3 on hematite aerosol. For a 3:1 ratio of O_3:SO_2 (36±3 mTorr O_3, 12±2 mTorr SO_2), γ_{SO2} and γ_{O3} are denoted by the filled circles and diamonds, respectively. For a 1:1 ratio of O_3:SO_2 (48±1 mTorr O_3, 47±1 mTorr SO_2), γ_{SO2} and γ_{O3} are denoted by the open circles and diamonds, respectively.

The addition of 22% RH reduced $\gamma_{wet} / \gamma_{dry,O3}$ to 0.51(±0.09). In general, the series of experiments predicts that for the reaction of hematite exposed simultaneously to SO_2 and O_3 in all but the driest atmospheric conditions, γ_{SO2} and γ_{O3} will each be on the order of 2 - 4 x 10^{-8}. The heterogeneous reactions thus occur with rates over an order of magnitude slower than the reaction of either SO_2 or O_3 alone on dry hematite, which has been measured here and in other studies [28].

4.5 Discussion

4.5.1 Uptake on dry hematite

In previous chamber experiments, ozone was observed to catalytically decompose on hematite surfaces, resulting in quantitative destruction of all of the gaseous O_3 in the chamber on the time scale of the experiment, even at pressures up to 39 ppm, well above those likely to be found in the environment [28]. A proposed mechanism for the decomposition of ozone on metal oxide surfaces involves the formation of surface oxide and peroxide species [28, 42-47].

$$S + O_3 \rightarrow S\text{-}O + O_2 \qquad 4.11$$
$$S\text{-}O + O_3 \rightarrow S\text{-}O_2 + O_2 \qquad 4.12$$
$$S\text{-}O_2 \rightarrow S + O_2 \qquad 4.13$$
$$2(S\text{-}O) \rightarrow 2S + O_2 \qquad 4.14$$

The active surface species, *S*, is presumably a Lewis acid site and *S-O* and $S\text{-}O_2$ represent the product surface oxide and peroxide, respectively. As the reactive site *S* is regenerated through Reaction 4.13 or 4.14, this reaction scheme is consistent with the observed catalytic decomposition of ozone. There is also some spectroscopic evidence of the formation of the *S-O* [42] and $S\text{-}O_2$ [43, 44] intermediates in this mechanism,

although they were observed on different metal oxides (alumina and manganese oxide, respectively). The release of oxygen gas *via* Reaction 4.13 is thought to be relatively slow so that the recombination reaction, 4.14, is likely the main route to regeneration of the catalytic surface site [45]. A study by Fu et al. demonstrated that sulfate was not formed on an α-Fe_2O_3 surface that had been pretreated at high temperatures with H_2 to removed adsorbed oxygen [26]. This result also lends weight to the argument that *S-O* plays a role in the oxidation process; these authors also had spectral evidence which indicated that surface hydroxyl groups may act as the site for SO_2 adsorption.

The surface oxide species formed as a consequence of ozone decomposition on metal oxides may participate in heterogeneous oxidation reactions with other species. For example, in our previous work on cyclic volatile methylsiloxanes (cVMS) reactions with hematite aerosol, we found evidence for a catalytic loss pathway for siloxane when O_3 was present in the chamber [47]. The new channel was manifest in the observation of a linear, zero-order decay of the cVMS and O_3 at longer reaction times that was not apparent when hematite reacted with cVMS alone. The decay did not saturate on the time scale of the experiment, suggesting that it was catalytic in nature, perhaps producing polymerized siloxane product species on the dust particle surface. In a study of the reaction of dimethyl methylphosphonate (DMMP), a chemical warfare simulant, on alumina-supported iron oxide surfaces, the addition of ozone was found to greatly enhance the oxidation of the DMMP [48]. The proposed mechanism involves a reaction between DMMP (or a decomposition fragment) adsorbed at a Lewis acid site, with an ozone-produced surface oxide species in a Langmuir-Hinshelwood (LH) type surface reaction. The oxidation of SO_2 to S(VI) may be facilitated by such surface oxides in a

similar LH mechanism. Alternatively, the gas phase SO_2 could also be oxidized in a direct reaction with surface oxides in an Eley-Rideal (ER) type mechanism.

The spectral data shows no evidence for any new gas phase absorption features that might be due to volatile reaction products. The sensitivity of our instrumental setup is approximately 1 ppm for absorbers with typical IR oscillator strengths. For comparison, the measured SO_2 loss in these experiments is on the order of 10 ppm. The absence of any product bands in the spectra may be due to a low reaction yield for volatile products or any such products might have relatively small IR cross-sections. Alternatively, the product might be IR inactive, such as would be the case for the O_2 produced from the ozone decomposition process.

The FTIR spectral data for the reaction under dry conditions shows no evidence for oxidized SO_2, specifically sulfate species. Any such sulfate products would have negligible vapor pressure and would remain almost totally in the particle phase. We are also unable to directly confirm the formation of reactive surface oxides or peroxides resulting from ozone decomposition as in Reactions 4.11 – 4.14. We have previously observed particle phase product species in some systems where the surface has undergone considerable processing. Very weak sulfite features were observed on calcite ($CaCO_3$) aerosol after reaction with SO_2 under humid conditions, but only at a SO_2 coverage equivalent to 5-10 monolayers, well above the θ_{SO2} observed for hematite [13]. It may be that in the experiments detailed here, that adsorbed SO_2 is indeed oxidized to S(VI) but that we lack sufficient sensitivity to detect such conversion. Several published studies have examined the role of common atmospheric oxidants on the heterogeneous uptake of SO_2 by mineral dust. In studies of hematite surfaces, a nearly complete conversion of

surface adsorbed S(IV) species to S(VI) was observed in the presence of typical atmospheric concentrations of gas phase oxygen [25, 26]. The uptake of SO_2 onto authentic Saharan dust samples, consisting mainly of quartz and potassium feldspars, was studied using DRIFTS by Ullerstam *et al.* in two studies [30, 31]. The addition of either gaseous NO_2 or O_3 was found to almost totally convert the initially adsorbed sulfite species into sulfate. DRIFTS has also been utilized to show that the presence of ozone increases sulfate formation when other common aerosol components, such as $CaCO_3$ [49] and NaCl [50], are exposed to SO_2.

A common feature of the aforementioned studies is that the reaction was characterized by monitoring the appearance surface sulfite and sulfate species. Fu et al. performed in situ FTIR experiments to monitor loss of gas phase SO_2 on hematite, but it is possible that their measurements were on an already completely saturated surface, as the sample was allowed to equilibrate with SO_2 for 20 minutes prior to kinetic studies [26]. The work of Ullerstam et al. clearly emphasizes that the difference in approach greatly effects interpretation. They noted that the observed γ_{SO2} of the reaction between SO_2, NO_2, and Saharan dust varied by 4 orders of magnitude depending on whether it was determined by gas phase SO_2 loss or the appearance of sulfate products [30]. This indicates that oxidation of SO_2 on the mineral surface may be the rate limiting step. In the current work, we have directly measured the uptake of gas phase SO_2 while varying the concentration of the ozone oxidant and the RH of the experiment. Also, all of the previous results were with bulk powder samples rather than dispersed aerosols, as in the atmospheric reaction chamber, where the isolated particle conditions avoid complications arising due to bulk effects, such as diffusion in the powder.

From the series of dry experiments in Table 4.2, which each have γ_{SO2} of 1.2 ± 0.6 x 10^{-7}, it is apparent that increasing the pressure of ozone does not strongly affect the uptake rate of SO_2. Ozone also has no affect on the total SO_2 uptake, θ_{SO2} (see Table 4.1). This is similar to the conclusions of Adams et al., who noted that ozone did not affect the uptake coefficient of gas phase SO_2 on authentic Saharan dust [51]. Although ozone may facilitate the heterogeneous conversion of adsorbed SO_2 to sulfate species, it does not accelerate the separate mechanistic process of initial SO_2 absorption. If sulfur dioxide and ozone compete for the same surface sites, it appears that SO_2 is able to easily displace O_3 on the hematite surface and maintain a high uptake rate.

The uptake coefficient for SO_2 averaged over all of the dry ozone experiments is γ_{SO2} = 1.2 ± 0.6 x 10^{-7}. The reactive uptake coefficient for sulfate formation on Saharan dust in the presence of O_3 was measured to be $\gamma(SO_4^{2-}) \approx$ 4-5 x 10^{-7} by Ullerstam et al. using DRIFTS[31].While these values are not so different given the large amount of error in our determination, it is somewhat surprising that the Saharan dust has a higher uptake coefficient given its large proportion of SiO_2, which is less reactive towards SO_2 and O_3 than other metal oxides [29, 52, 53]. Differences in the experimental methodology could also account for any substantive differences as the DRIFTS approach measures the reactive uptake coefficient for a specific product channel. In addition, we used gas concentrations on the order of 10^{15} cm^{-3}, which are one hundred times greater than the DRIFTS experiments. The initial uptake on a surface is often much faster than after long exposures, when the surface coverage increases [54]. It is possible that all oxidation was occurring during the fast initial uptake period in the first several minutes of our experiments with an estimated γ_{SO2} of at least 10^{-6}, which would be more consistent with

the DRIFTS result. Ullerstam also observed the oxidation of SO_2 on Saharan dust had a zero-order dependence on O_3, suggesting SO_2 uptake may be the rate limiting step for that system [31].

The overall reaction extent, quantified by the surface coverage of SO_2 calculated from the gas phase loss, is not enhanced as the O_3 pressure is increased, as illustrated by Table 4.1. If the number or reactivity of active surface sites (such as *S-O* or *S-O*$_2$ from Reactions 4.11 – 4.14) is increased by the coadsorption of ozone, then θ_{SO2} might be expected to increase with the O_3 concentration. However, we observe no such effect. The average value of the total SO_2 coverage with ozone present is $2.2 \pm 0.6 \times 10^{14}$ cm^{-2}, or $\theta_{SO2} = 0.5 \pm 0.1$, about half of a monolayer. The previous work on sulfate formation noted that adding a strong oxidant led to large increases in surface sulfate species relative to the reduced sulfite and in most cases, an overall enhancement in surface product formation [25, 26, 51]. Adams et al. was able to use a flow tube reactor to determine that ozone does not lead to an observed increase in SO_2 uptake from the gas phase, but *only* the amount of irreversible uptake, as is likely the case in our experiment [51]. Ullerstam et al. used ion chromatography to determine a value of $\approx 4 \times 10^{13}$ ions cm^{-2} for the saturation coverage of SO_4^{2-} formed on their authentic Saharan dust samples [31]. Our measured SO_2 coverage corresponds to an average value of approximately 2.2×10^{14} molecules cm^{-2}. The larger value for saturation coverage that we measure is consistent with the reactive nature of hematite surfaces compared to the dominant components typical of Saharan sand, consisting of relatively unreactive silicates. This coverage is also similar to that observed by Goodman *et al.* on α-Al_2O_3 (1.4×10^{14} cm^{-2}) and MgO ($2.5 \times$

10^{14} cm^{-2} for 25 mTorr SO_2) using FTIR and volumetric measurements, without any added oxidants [32].

The uptake of ozone by the hematite aerosol is also, correspondingly, affected by the coadsorption of SO_2. All dry experiments with SO_2 present showed significantly lower ozone uptake coefficients than the $7 \pm 3 \times 10^{-7}$ exhibited in the ozone only experiment (Figure 4.4). We did not extensively evaluate the role of SO_2 gas pressure, evaluating only a "low" and a "high" SO_2 pressure regime, as our focus was on the sulfur dioxide uptake process. There is considerable scatter in the existing O_3 kinetic data as well. However, the overall reaction yield is clearly affected as we do not observe the catalytic decomposition of the gas phase ozone which results in quantitative loss of all of the initial O_3, as we have observed previously in the ozone-hematite system. It can be seen from Table 4.1 that the presence of SO_2 reduces n_{O3} nearly 10-fold relative to the value of $1.6 \pm 0.2 \times 10^{15}$ cm^{-2} observed for O_3 alone. The measured ozone coverages at the end of the experiments were generally less than a monolayer, with the exception of an experiment with very high P_{O3} = 215 mTorr. In the previous chamber study, the ozone coverages on hematite under similar conditions were greater than two (expressed in terms of "turnover" numbers) and indicative of a catalytic process [28]. The coadsorbing SO_2 may be preferentially partitioning to reactive sites on the surface that facilitate the ozone catalytic decomposition process, as detailed in Reactions 4.11 – 4.14. However, given that the uptake coefficient and coverage for SO_2 and O_3 are similar, it is more likely that the adsorbed sulfur species is interfering with the catalytic mechanism. For example, there may be sufficient adsorbed SO_2 in our experiments to prevent the recombination reactions, Reactions 4.13 and 4.14, which regenerate the active catalytic site on the

hematite surface. The creation of bidentate sulfate on the surface may consume reactive surface oxides (*S**-*O*) and block recombination as well.

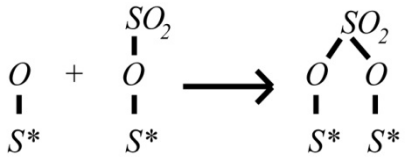

4.15

Here, *S** represents a surface site in order to avoid confusion with the sulfur atom. Fu *et al.* did observe spectral evidence for the formation of bidentate sulfate on α-Fe_2O_3 and several other iron oxides [26]. There is some evidence for a competitive adsorption process between O_3 and SO_2 from the data presented in Table 4.1, although the trend is not obvious in the limited data set.

It is unclear why the time resolved data appears to exhibit two distinct regimes of kinetic behavior – the "fast" initial uptake within 5 minutes of aerosol introduction, and the following "slow" uptake from which our reported γ_{SO2} and γ_O are derived. Adsorptions studies using pyridine and carbon monoxide have demonstrated the existence of multiple non-equivalent Lewis acid sites on hematite, which may explain the observation of the distinct "fast" and "slow" uptake behavior for SO_2 and O_3 [55]. Density functional theory results indicate that the hydrated hematite (0 0 0 1) surface consists of two different hydroxyl terminations, either singly or doubly coordinated to iron atoms. Each may offer a reactive uptake site with differing reactivity [56]. It may simply be the observation of a saturation phenomenon, with the high pressures of reagent gases quickly saturating the surface in the first few minutes of exposure, followed by uptake to a largely saturated surface [54].

4.5.2 Uptake on hematite at elevated RH

The amount of gas phase water, as characterized by the RH at a given temperature, is a critical determinant for heterogeneous processes in the atmosphere. Particles injected into the atmospheric reaction chamber are expected to rapidly come into equilibrium with the specific RH of the gas phase reaction mixture. The resultant surface adsorbed water can greatly influence the subsequent uptake and reaction of other trace gas species. Our own work has revealed that water vapor can either increase or decrease the rates and reaction yields of heterogeneous reactions between trace gasses and aerosol surfaces [28, 34, 47].

In experiments with variable RH in the chamber, we did not observe any new gas phase products using the IR probe, as was the case for the dry experiments with sulfur dioxide and ozone. We did note some product spectral features that were attributed to a reaction occurring on the surface of the Ge windows in the IR probe beam path. We could not identify this product feature and it was not associated with surface adsorptions on the suspended hematite aerosol. We were unable to identify any other spectral features that might be ascribed to particle phase, nonvolatile products, such as surface sulfate species. Again, the lack of information regarding product species could be due to a lack of sensitivity for surface adsorbed products, and/or a low yield, weak oscillator strengths or lack of IR activity for any possible gas phase products. We are limited to monitoring the gas phase loss of SO_2 and O_3 in these experiments.

The decay of the gaseous SO_2 could be described by simple pseudo-first order kinetics at moderate RH, below 50% (Figure 4.6). When the RH was increased above 50%, we observed that the order of the reaction appears altered (Figure 4.7). The data is

no longer well fit to an exponential decay, but appears to follow zero-order kinetics with a rate constant k_0 of 3 x 10^{-8} M s^{-1}. As discussed in Section 4.5.1, our research and that of others have highlighted the role of such ozone mediated decay channels in other systems [28, 42-48]. Overall, the uptake coefficient for SO_2 appears to be relatively independent of the RH value, over the range of ≈ 5 – 50%, as illustrated by the plot in Fig. 4.9. The average value of the uptake coefficient for all of the variable RH experiments which exhibited pseudo-first order decay kinetics (n = 8) is γ_{SO2} =3.8 ± 2.4 x 10^{-8}. We can compare this average value from the RH experiments to the average value in the dry experiments with O_3 present in the gas mixture, which is γ_{SO2} = 1.2 ± 0.6 x 10^{-7}. While the measured coefficient is smaller in the elevated RH experiments, there is quite a bit of scatter in the data and the values are near the experimental error. We can also compare to the average uptake coefficient for SO_2 from RH studies in the absence of any ozone, which we have previously determined to be γ_{SO2} = 5.8 ± 1.3 x 10^{-8} (See Chapter 3). It appears that while water vapor and ozone both reduce γ_{SO2} by a similar degree when present individually, there is no additional effect on γ_{SO2} when SO_2 , O_3, and H_2O are all coadsorbed. The DRIFTS experiments of Li *et al.* on $CaCO_3$ aerosol recorded a reactive uptake coefficient of $\gamma(SO_4^{2-})$ ≈ 1-2 x 10^{-8} over a RH range of 40 – 60% and with O_3 present[49]. While calcium carbonate is generally a highly reactive component of mineral dust aerosol towards acidic gasses, the uptake rate of SO_2 appears to be even less than in our experiments. However, as we have noted, the DRIFTS measurement is for reactive uptake only, not the total loss of gas phase SO_2 which is likely to include significant reversible uptake as in our experiment. In a flow tube reactor study the gas phase loss rate of SO_2 to authentic Saharan dust did not change in the presence of O_3 or for a RH of ≈

25%, contrary to our observations [51]. It is possible that another reactive component of the Saharan dust sample that was not sensitive to RH was responsible for the uptake of SO_2 in the flow cell study.

The fractional SO_2 coverages, as summarized in Fig. 4.8, manifest an obvious dependence on the experimental RH conditions. The coverage increases moderately relative to the dry value of $\theta_{SO2} = 0.64 \pm 0.08$ as the RH is varied between 1 and 50%, but the coverage remains near one monolayer. The RH dependence on θ_{SO2} for this range is similar to that observed without ozone in this work, as θ_{SO2} increases by a factor of ≈1.3 when water vapor is present. Above 50% RH, as the kinetics of SO_2 uptake were observed to resemble zero-order decay, the coverage of SO_2 also increases sharply; the observed θ_{SO2} for the high RH experiments may actually underestimate hematite's reactive capacity, as all SO_2 in the chamber was consumed in these experiments. This large increase in capacity was not observed in high RH conditions without ozone, nor with similar pressures of ozone at RH ranging from 0 - 40%. There is more error in the experiments with gas phase water due to issues associated with our spectral subtraction procedure, as detailed above (*vide supra*) but this coverage is significantly larger than the value of $\theta_{SO2} = 0.64 \pm 0.08$ that we measure under dry, (≤ 1% RH) conditions, of 0.64 ± 0.8. It may be that there is some synergistic effect of O_3 and RH that leads to higher SO_2 coverages in our experiment. The total coverages we measure, up to 2.2×10^{15} molecules cm^{-2}, are considerably larger than the saturation coverages determined by Ullerstam *et al.* of approximately 4×10^{13} SO_4^{2-} cm^{-2} on dry Saharan dust [31]. These values were determined from bulk measurements for the sulfate ion component only while our surface coverages are calculated from the total gas phase SO_2 loss.

The ozone coverage in the humid experiments has an average value of θ_{O3} = 0.39 ± 0.13. Despite the relatively large error, the average value is lower than that determined in the dry experiments of θ_{O3} = 1.2 ± 0.2, , and is considerably less than the multilayer coverages observed in previous work with the ozone-hematite system [28]. Clearly there is no catalytic pathway accessible when there is surface adsorbed water and coadsorption of SO_2. The previous chamber studies observed that increasing the RH lowered the uptake coefficient for the adsorbing ozone but did not necessarily reduce the final (total) coverage. The adsorbed SO_2 appears to block the catalytic ozone decomposition occurring on hematite and the addition of water only exacerbates the decreased reactivity and certainly does not enhance the O_3 uptake in the hematite system. Similar to what we observed in the dry experiments, there appears to be a competitive uptake between SO_2 and O_3.

4.5.3 Implications for Atmospheric Chemistry

A model by Ammann *et al.* can be used to describe Langmuir-Hinshelwood surface reactions on atmospheric particles [54]. Numerical integration of this model demonstrates that γ_X can vary by several orders of magnitude with time, as the surface becomes saturated. Depending on the fundamental kinetic parameters relating to adsorption, desorption, and heterogeneous reaction, and the initial pressures of the reactant gasses, the measured γ_X could vary greatly. Therefore, it would be beneficial to study a reaction system such as O_3, SO_2, and hematite surface using several techniques that measure γ_X over a large range of time scales and gas concentrations, in order to assess the relative contributions of the sticking coefficient and surface reaction rates.

Previous product resolved studies have indicated that common atmospheric oxidants, such as O_2, O_3, and NO_2, can efficiently oxidize adsorbed S(IV) to S(VI) species. However, our data suggests that even if such processes are active the overall uptake of SO_2 to hematite surfaces is not enhanced. Experiments at tropospherically relevant RH conditions show that surface adsorbed water may lead to catalytic uptake of SO_2 at high RH. At lower RH, there is a competition between ozone and sulfur dioxide for adsorption sites on the hematite surface. The uptake coefficients we measure are small, even for a relatively reactive mineral dust aerosol component, hematite. The uptake coefficient is further reduced by the presence of water vapor and/or ozone, but in general, will be within a factor of 2 of γ_{SO2} measured under dry conditions. Our results indicate that heterogeneous loss of SO_2 to mineral dust aerosol will not be competitive with more typical homogeneous pathways or other heterogeneous reactions, for example partitioning to liquid phase aerosol, except possibly at very high RH. While we measure a higher SO_2 coverage than experiments that only quantify the amount of surface sulfate present, the hematite surface eventually becomes saturated, with the exception of the rather specific case in which O_3 and SO_2 coadsorb on hematite at RH > 50 %. Thus, even if all of the adsorbed sulfur is oxidized to sulfate, direct acidification of hematite aerosol due to SO_2 adsorption does not seem a likely pathway to rationalize the bioavailability of iron in aerosol deposited in remote marine environments. The atmospheric processing of internally mixed hematite and calcite aerosol may provide a more likely route to the formation of a sufficiently acidified particle phase. The factors controlling dissolution and biological uptake of iron in hematite aerosol may be dominated by reactions in the marine environment itself rather than atmospheric processing of mineral aerosol.

Notes

1. Phadnis, M. J.; Carmichael, G. R., Numerical Investigation of the Influence of Mineral Dust on the Tropospheric Chemistry of East Asia. *Journal of Atmospheric Chemistry* **2000,** *36* (3), 285-323.

2. Jacob, D. J., Heterogeneous chemistry and tropospheric ozone. *Atmospheric Environment* **2000,** *34* (12-14), 2131-2159.

3. Bauer, S. E.; Koch, D., Impact of heterogeneous sulfate formation at mineral dust surfaces on aerosol loads and radiative forcing in the Goddard Institute for Space Studies general circulation model. *J. Geophys. Res.* **2005,** *110*, D17202, doi:10.1029/2005JD005870.

4. Bauer, S. E.; Mishchenko, M. I.; Lacis, A. A.; Zhang, S.; Perlwitz, J.; Metzger, S. M., Do sulfate and nitrate coatings on mineral dust have important effects on radiative properties and climate modeling? **2007,** *112*, D06307, doi:10.1029/2005JD006977.

5. Martin, J. H.; Fitzwater, S. E., Iron deficiency limits phytoplankton growth in the north-east Pacific subarctic. *Nature* **1988,** *331* (6154), 341-343.

6. Johnson, K. S.; Gordon, R. M.; Coale, K. H., What controls dissolved iron concentrations in the world ocean? *Marine Chemistry* **1997,** *57* (3-4), 137-161.

7. Duce, R. A.; Tindale, N. W., Atmospheric Transport of Iron and its Deposition in the Ocean. *Limnology and Oceanography* **1991,** *36* (8), 1715-1726.

8. Fan, S.-M.; Moxim, W. J.; Levy II, H., Aeolian input of bioavailable iron to the ocean. *Geophysical Research Letters* **2006,** *33* (L07602), doi:10.1029/2005GL024852

9. Kraemer, S. M., Iron oxide dissolution and solubility in the presence of siderophores. *Aquatic Sciences* **2004,** *66* (1), 3-18.

10. Meskhidze, N.; Chameides, W. L.; Nenes, A., Dust and pollution: A recipe for enhanced ocean fertilization? *J. Geophys. Res.* **2005,** *110*, D03301, doi:10.1029/2004JD005082.

11. Meskhidze, N.; Chameides, W. L.; Nenes, A.; Chen, G., Iron mobilization in mineral dust: Can anthropogenic SO2 emissions affect ocean productivity? *Geophys. Res. Lett.* **2003,** *30*, 2085, doi:10.1029/2003GL018035.

12. Krueger, B. J.; Grassian, V. H.; Laskin, A.; Cowin, J. P., The transformation of solid atmospheric particles into liquid droplets through heterogeneous chemistry: Laboratory insights into the processing of calcium containing mineral dust aerosol in the troposphere. *Geophys. Res. Lett.* **2003,** *30* (3), 1148.

13. Preszler Prince, A.; Kleiber, P.; Grassian, V. H.; Young, M. A., Heterogeneous interactions of calcite aerosol with sulfur dioxide and sulfur dioxide-nitric acid mixtures. *Physical Chemistry Chemical Physics* **2007,** *9*, 3432-3439.

14. Tang, I. N.; Fung, K. H., Hydration and Raman scattering studies of levitated microparticles: $Ba(NO_3)_2$, $Sr(NO_3)_2$, and $Ca(NO_3)_2$. *The Journal of Chemical Physics* **1997,** *106* (5), 1653-1660.

15. Khoder, M. I., Atmospheric conversion of sulfur dioxide to particulate sulfate and nitrogen dioxide to particulate nitrate and gaseous nitric acid in an urban area. *Chemosphere* **2002,** *49*, 675-684.

16. Bari, A.; Ferraro, V.; Wilson, L. R.; Luttinger, D.; Husain, L., Measurements of gaseous HONO, HNO_3, SO_2, HCl, NH_3, particulate sulfate and $PM_{2.5}$ in New York, NY. *Atmospheric Environment* **2003,** *37* (20), 2825-2835.

17. Desboeufs, K. V.; Losno, R.; Colin, J. L., Factors influencing aerosol solubility during cloud processes. *Atmospheric Environment* **2001,** *35* (20), 3529-3537.

18. Desboeufs, K. V.; Losno, R.; Vimeux, F.; Cholbi, S., The pH-dependent dissolution of wind-transported Saharan dust. *J. Geophys. Res.* **1999,** *104* (D17), 21,287-21,299.

19. Solmon, F.; Chuang, P. Y.; Meskhidze, N.; Chen, Y., Acidic processing of mineral dust iron by anthropogenic compounds over the north Pacific Ocean. *J. Geophys. Res.* **2009,** *114*, D02305, doi:10.1029/2008JD010417.

20. Spokes, L. J.; Jickells, T. D., Factors controlling the solubility of aerosol trace metals in the atmosphere and on mixing into seawater. *Aquatic Geochemistry* **1995,** *1* (4), 355-374.

21. Baker, A. R.; Jickells, T. D., Mineral particle size as a control on aerosol iron solubility. *Geophys. Res. Lett.* **2006,** *33*, L17608, doi:10.1029/2006GL026557.

22. Ooki, A.; Nishioka, J.; Ono, T.; Noriki, S., Size dependence of iron solubility of Asian mineral dust particles. *J. Geophys. Res.* **2009,** *114*, D03202, doi:10.1029/2008JD010804.

23. Johansen, A. M.; Siefert, R. L.; Hoffmann, M. R., Chemical composition of aerosols collected over the tropical North Atlantic Ocean. *J. Geophys. Res.* **2000,** *105* (D12), 15277-15312.

24. Baker, A. R.; French, M.; Linge, K. L., Trends in aerosol nutrient solubility along a west-east transect of the Saharan dust plume. *Geophys. Res. Lett.* **2006,** 33, L07805, doi:10.1029/2005GL024764.

25. Baltrusaitis, J.; Cwiertny, D. M.; Grassian, V. H., Adsorption of sulfur dioxide on hematite and goethite particle surfaces. *Physical Chemistry Chemical Physics* **2007,** *9* (41), 5542-5554.

26. Fu, H.; Wang, X.; Wu, H.; Yin, Y.; Chen, J., Heterogeneous Uptake and Oxidation of SO_2 on Iron Oxides. *Journal of Physical Chemistry C* **2007,** *111* (16), 6077-6085.

27. Hanisch, F.; Crowley, J. N., Ozone decomposition on Saharan dust: an experimental investigation. *Atmospheric Chemistry Physics* **2003,** *3* (1), 119-130.

28. Mogili, P. K.; Kleiber, P. D.; Young, M. A.; Grassian, V. H., Heterogeneous Uptake of Ozone on Reactive Components of Mineral Dust Aerosol: An Environmental Aerosol Reaction Chamber Study. *Journal of Physical Chemistry A* **2006,** *110* (51), 13799-13807.

29. Michel, A. E.; Usher, C. R.; Grassian, V. H., Reactive uptake of ozone on mineral oxides and mineral dusts. *Atmospheric Environment* **2003,** *37* (23), 3201-3211.

30. Ullerstam, M.; Johnson, M. S.; Vogt, R.; Ljungstrom, E., DRIFTS and Knudsen cell study of the heterogeneous reactivity of SO_2 and NO_2 on mineral dust. *Atmospheric Chemistry and Physics* **2003,** *3* (6), 2043-2051.

31. Ullerstam, M.; Vogt, R.; Langer, S.; Ljungstrom, E., The kinetics and mechanism of SO2 oxidation by O3 on mineral dust. *Physical Chemistry Chemical Physics* **2002,** *4* (19), 4694-4699.

32. Goodman, A. L.; Li, P.; Usher, C. R.; Grassian, V. H., Heterogeneous Uptake of Sulfur Dioxide On Aluminum and Magnesium Oxide Particles. *The Journal of Physical Chemistry A* **2001,** *105* (25), 6109-6120.

33. Mogili, P. K.; Kleiber, P. D.; Young, M. A.; Grassian, V. H., N_2O_5 hydrolysis on the components of mineral dust and sea salt aerosol: Comparison study in an environmental aerosol reaction chamber. *Atmospheric Environment* **2006,** *40*, 7401-7408.

34. Preszler Prince, A. M. Investigations Into The Heterogeneous Atmospheric Interactions of Isolated Metal Oxide, Carbonate, and Soot Aerosols. University of Iowa, Iowa City, **2003**.

35. Orphal, J., A critical review of the absorption cross-sections of O3 and NO2 in the ultraviolet and visible. *Journal of Photochemistry and Photobiology A: Chemistry* **2003,** *157* (2-3), 185-209.

36. McCaa, D. J.; Shaw, J. H., The infrared spectrum of ozone. *Journal of Molecular Spectroscopy* **1968,** *25* (3), 374-397.

37. Hanst, P. L.; Stephens, E. R.; Scott, W. E.; Doerr, R. C., Absorptivities for the Infrared Determination of Trace Amounts of Ozone. *Analytical Chemistry* **1961,** *33* (8), 1113-1115.

38. Hug, S. J., In SituFourier Transform Infrared Measurements of Sulfate Adsorption on Hematite in Aqueous Solutions. *Journal of Colloid and Interface Science* **1997,** *188* (2), 415-422.

39. Dunn, J. G.; Gong, W.; Shi, D., A Fourier transform infrared study of the oxidation of pyrite. *Thermochimica Acta* **1992,** *208*, 293-303.

40. Liang, L.; Morgan, J. J., Chemical aspects of iron oxide coagulation in water: Laboratory studies and implications for natural systems. *Aquatic Sciences - Research Across Boundaries* **1990,** *52* (1), 32-55.

41. Pivovarov, S., Surface Structure and Site Density of the Oxide-Solution Interface. *Journal of Colloid and Interface Science* **1997,** *196* (2), 321-323.

42. Roscoe, J.; Abbatt, J., Diffuse reflectance FTIR study of the interaction of alumina surfaces with ozone and water vapor. *Journal of Physical Chemistry A* **2005,** *109* (40), 9028-9034.

43. Li, W.; Oyama, S., Mechanism of ozone decomposition on a manganese oxide catalyst. 2. Steady-state and transient kinetic studies. *Journal of the American Chemical Society* **1998,** *120* (35), 9047-9052.

44. Li, W.; Gibbs, G.; Oyama, S., Mechanism of ozone decomposition on a manganese oxide catalyst. I. In situ Raman spectroscopy and ab initio molecular orbital calculations. *Journal of the American Chemical Society* **1998,** *120* (35), 9041-9046.

45. Xi, Y.; Reed, C.; Lee, Y.; Oyama, S., Acetone oxidation using ozone on manganese oxide catalysts. *Journal of Physical Chemistry B* **2005,** *109* (37), 17587-17596.

46. Reed, C.; Lee, Y.; Oyama, S., Structure and oxidation state of silica-supported manganese oxide catalysts and reactivity for acetone oxidation with ozone. *Journal of Physical Chemistry B* **2006,** *110* (9), 4207-4216.

47. Navea, J. G.; Xu, S.; Stanier, C. O.; Young, M. A.; Grassian, V. H., Effect of Ozone and Relative Humidity on the Heterogeneous Uptake of Octamethylcyclotetrasiloxane and Decamethylcyclopentasiloxane on Model Mineral Dust Aerosol Components. *The Journal of Physical Chemistry A* **2009,** *113* (25), 7030-7038.

48. Mitchell, M. B.; Sheinker, V. N.; Cox, W. W., Room Temperature Reaction of Ozone and Dimethyl Methylphosphonate (DMMP) on Alumina-Supported Iron Oxide. *The Journal of Physical Chemistry C* **2007,** *111* (26), 9417-9426.

49. Li, L.; Chen, Z. M.; Zhang, Y. H.; Zhu, T.; Li, J. L.; Ding, J., Kinetics and mechanism of heterogeneous oxidation of sulfur dioxide by ozone on surface of calcium carbonate. *Atmos. Chem. Phys.* **2006,** *6* (9), 2453-2464.

50. Li, L.; Chen, Z. M.; Zhang, Y. H.; Zhu, T.; Li, S.; Li, H. J.; Zhu, L. H.; Xu, B. Y., Heterogeneous oxidation of sulfur dioxide by ozone on the surface of sodium chloride and its mixtures with other components. *J. Geophys. Res.* **2007,** *112,* D18301, doi:10.1029/2006JD008207.

51. Adams, J. W.; Rodriguez, D.; Cox, R. A., The uptake of SO_2 on Saharan dust: a flow tube study. *Atmospheric Chemistry and Physics* **2005,** *5* (10), 2679-2689.

52. Usher, C. R.; Al-Hosney, H.; Carlos-Cuellar, S.; Grassian, V. H., A laboratory study of the heterogeneous uptake and oxidation of sulfur dioxide on mineral dust particles. *Journal of Geophysical Research* **2002,** *107*, 4713, doi:10.1029/2002JD002051

53. Usher, C. R.; Michel, A. E.; Stec, D.; Grassian, V. H., Laboratory studies of ozone uptake on processed mineral dust. *Atmospheric Environment* **2003,** *37* (38), 5337-5347.

54. Ammann, M.; Poschl, U.; Rudich, Y., Effects of reversible adsorption and Langmuir-Hinshelwood surface reactions on gas uptake by atmospheric particles. *Physical Chemistry Chemical Physics* **2003,** *5* (2), 351-356.

55. Ferretto, L.; Glisenti, A., Study of the surface acidity of an hematite powder. *Journal of Molecular Catalysis A: Chemical* **2002,** *187* (1), 119-128.

56. Trainor, T. P.; Chaka, A. M.; Eng, P. J.; Newville, M.; Waychunas, G. A.; Catalano, J. G.; Brown, J. G. E., Structure and reactivity of the hydrated hematite (0 0 0 1) surface. *Surface Science* **2004,** *573* (2), 204-224.

BIBLIOGRAPHY

Adams, J. W.; Rodriguez, D.; Cox, R. A., The uptake of SO_2 on Saharan dust: a flow tube study. *Atmospheric Chemistry and Physics* **2005,** *5* (10), 2679-2689.

Ammann, M.; Poschl, U.; Rudich, Y., Effects of reversible adsorption and Langmuir-Hinshelwood surface reactions on gas uptake by atmospheric particles. *Physical Chemistry Chemical Physics* **2003,** *5* (2), 351-356.

Baker, A. R.; French, M.; Linge, K. L., Trends in aerosol nutrient solubility along a west-east transect of the Saharan dust plume. *Geophys. Res. Lett.* **2006,** *33*, L07805

Baker, A. R.; Jickells, T. D., Mineral particle size as a control on aerosol iron solubility. *Geophys. Res. Lett.* **2006,** *33*, L17608, doi:10.1029/2006GL026557.

Baltrusaitis, J.; Cwiertny, D. M.; Grassian, V. H., Adsorption of sulfur dioxide on hematite and goethite particle surfaces. *Physical Chemistry Chemical Physics* **2007,** *9* (41), 5542-5554.

Bari, A.; Ferraro, V.; Wilson, L. R.; Luttinger, D.; Husain, L., Measurements of gaseous HONO, HNO_3, SO_2, HCl, NH_3, particulate sulfate and $PM_{2.5}$ in New York, NY. *Atmospheric Environment* **2003,** *37* (20), 2825-2835.

Bauer, S. E.; Koch, D., Impact of heterogeneous sulfate formation at mineral dust surfaces on aerosol loads and radiative forcing in the Goddard Institute for Space Studies general circulation model. *J. Geophys. Res.* **2005,** *110*, D17202, doi:10.1029/2005JD005870.

Bauer, S. E.; Mishchenko, M. I.; Lacis, A. A.; Zhang, S.; Perlwitz, J.; Metzger, S. M., Do sulfate and nitrate coatings on mineral dust have important effects on radiative properties and climate modeling? *J. Geophys. Res.* **2007,** *112*, D06307, doi:10.1029/2005JD006977.

Bernstein, J. A.; Alexis, N.; Barnes, C.; Bernstein, I. L.; Nel, A.; Peden, D.; Diaz-Sanchez, D.; Tarlo, S. M.; Williams, P. B., Health effects of air pollution. *Journal of Allergy and Clinical Immunology* **2004,** *114* (5), 1116-1123.

Blain, S.; Queguiner, B.; Armand, L.; Belviso, S.; Bombled, B.; Bopp, L.; Bowie, A.; Brunet, C.; Brussaard, C.; Carlotti, F.; Christaki, U.; Corbiere, A.; Durand, I.; Ebersbach, F.; Fuda, J.-L.; Garcia, N.; Gerringa, L.; Griffiths, B.; Guigue, C.; Guillerm, C.; Jacquet, S.; Jeandel, C.; Laan, P.; Lefevre, D.; Lo Monaco, C.; Malits, A.; Mosseri, J.; Obernosterer, I.; Park, Y.-H.; Picheral, M.; Pondaven, P.; Remenyi, T.; Sandroni, V.; Sarthou, G.; Savoye, N.; Scouarnec, L.; Souhaut, M.; Thuiller, D.; Timmermans, K.; Trull, T.; Uitz, J.; van Beek, P.; Veldhuis, M.; Vincent, D.; Viollier, E.; Vong, L.; Wagener, T., Effect of natural iron

fertilization on carbon sequestration in the Southern Ocean. *Nature* **2007,** *446* (7139), 1070-1074.

Brimblecombe, P., *Air composition and chemistry*. 2nd ed.; Cambridge University Press: Cambridge, 1996.

Caffrey, P.; Hoppel, W.; Frick, G.; Pasternack, L.; Fitzgerald, J.; Hegg, D.; Gao, S.; Leaitch, R.; Shantz, N.; Albrechcinski, T.; Ambrusko, J., In-cloud oxidation of SO_2 by O_3 and H_2O_2: Cloud chamber measurements and modeling of particle growth. *J. Geophys. Res.* **2001,** *106* (D21), 27587-27601.

Ciencewicki, J.; Trivedi, S.; Kleeberger, S. R., Oxidants and the pathogenesis of lung diseases. *Journal of Allergy and Clinical Immunology* **2008,** *122* (3), 456-468.

Connick, R. E.; Zhang, Y.-X., Kinetics and Mechanism of the Oxidation of HSO_3^- by O_2. 2. The Manganese(II)-Catalyzed Reaction. *Inorganic Chemistry* **1996,** *35* (16), 4613-4621.

Connick, R. E.; Zhang, Y.-X.; Lee, S.; Adamic, R.; Chieng, P., Kinetics and Mechanism of the Oxidation of HSO_3^- by O_2. 1. The Uncatalyzed Reaction. *Inorganic Chemistry* **1995,** *34* (18), 4543-4553.

Cox, R. A., Chemical Kinetics and Atmospheric Chemistry: Role of Data Evaluation. *Chemical Reviews* **2003,** *103* (12), 4533-4548.

Curtis, L.; Rea, W.; Smith-Willis, P.; Fenyves, E.; Pan, Y., Adverse health effects of outdoor air pollutants. *Environment International* **2006,** *32*, 815-830.

Desboeufs, K. V.; Losno, R.; Colin, J. L., Factors influencing aerosol solubility during cloud processes. *Atmospheric Environment* **2001,** *35* (20), 3529-3537.

Desboeufs, K. V.; Losno, R.; Vimeux, F.; Cholbi, S., The pH-dependent dissolution of wind-transported Saharan dust. *J. Geophys. Res.* **1999,** *104* (D17), 21,287-21,299.

Desboeufs, K. V.; Sofikitis, A.; Losno, R.; Colin, J. L.; Ausset, P., Dissolution and solubility of trace metals from natural and anthropogenic aerosol particulate matter. *Chemosphere* **2005,** *58* (2), 195-203.

Donaldson, K.; Brown, D. M.; Mitchell, C.; Dineva, M.; Beswick, P. H.; Gilmour, P.; MacNee, W., Free Radical Activity of PM_{10}: Iron-mediated Generation of Hydroxyl Radicals. *Environmental Health Perspectives* **1997,** *105* (Suppl 5), 1285-1289.

Duce, R. A.; Tindale, N. W., Atmospheric Transport of Iron and its Deposition in the Ocean. *Limnology and Oceanography* **1991,** *36* (8), 1715-1726.

Dunn, J. G.; Gong, W.; Shi, D., A Fourier transform infrared study of the oxidation of pyrite. *Thermochimica Acta* **1992,** *208*, 293-303.

Fan, S.-M.; Moxim, W. J.; Levy II, H., Aeolian input of bioavailable iron to the ocean. *Geophysical Research Letters* **2006,** *33* (L07602), doi:10.1029/2005GL024852.

Ferretto, L.; Glisenti, A., Study of the surface acidity of an hematite powder. *Journal of Molecular Catalysis A: Chemical* **2002,** *187* (1), 119-128.

Forster, P.; Ramaswarmy, V.; Artaxo, P.; Berntsen, T.; Betts, R.; Fahey, D. W.; Haywood, J.; Lean, J.; Lowe, D. C.; Myrhe, G.; Nganga, J.; Prinn, R.; Raga, G.; Schulz, M.; Van Dorland, R., Changes in Atmospheric Constituents and in Radiative Forcing. In *Climate Change 2007: The Physical Science Basis. Contribution of Working Group I to the Fourth Assessment Report of the Intergovernmental Panel on Climate Change*, Solomon, S.; Qin, D.; Manning, M.; Chen, Z.; Marquis, M.; Averyt, K. B.; Tignor, M.; Miller, H. L., Eds. Cambridge University Press, Cambridge, United Kingdom and New York, NY, USA: 2007.

Fu, H.; Wang, X.; Wu, H.; Yin, Y.; Chen, J., Heterogeneous Uptake and Oxidation of SO_2 on Iron Oxides. *Journal of Physical Chemistry C* **2007,** *111* (16), 6077-6085.

Fu, H.; Xu, T.; Yang, S.; Zhang, S.; Chen, J., Photoinduced Formation of Fe(III)-Sulfato Complexes on the Surface of α-Fe2O3 and Their Photochemical Performance. *The Journal of Physical Chemistry C* **2009,** *113* (26), 11316-11322.

Gaffney Jeffrey, S.; Marley Nancy, A., The Importance of the Chemical and Physical Properties of Aerosols in Determining Their Transport and Residence Times in the Troposphere. In *Urban Aerosols and Their Impacts*, American Chemical Society: Washington, DC, 2005; pp 286-299.

Gebel, M. E.; Finlayson; Pitts, B. J.; Ganske, J. A., The uptake of SO_2 on synthetic sea salt and some of its components. *Geophys. Res. Lett.* **2000,** *27* (6), 887-890.

Gilmour, P. S.; Brown, D. M.; Lindsay, T. G.; Beswick, P. H.; MacNee, W.; Donaldson, K., Adverse health effects of PM10 particles: involvement of iron in generation of hydroxyl radical. *Occupational and Environmental Medicine* **1996,** *53* (12), 817-822.

Goodman, A. L.; Li, P.; Usher, C. R.; Grassian, V. H., Heterogeneous Uptake of Sulfur Dioxide On Aluminum and Magnesium Oxide Particles. *The Journal of Physical Chemistry A* **2001,** *105* (25), 6109-6120.

Hand, J. L.; Mahowald, N. M.; Chen, Y.; Siefert, R. L.; Luo, C.; Subramaniam, A.; Fung, I., Estimates of atmospheric-processed soluble iron from observations and a global mineral aerosol model: Biogeochemical implications. *J. Geophys. Res.* **2004,** *109*, D17205, doi:10.1029/2004JD004574.

Hanisch, F.; Crowley, J. N., Ozone decomposition on Saharan dust: an experimental investigation. *Atmos. Chem. Phys.* **2003,** *3* (1), 119-130.

Hanst, P. L.; Stephens, E. R.; Scott, W. E.; Doerr, R. C., Absorptivities for the Infrared Determination of Trace Amounts of Ozone. *Analytical Chemistry* **1961,** *33* (8), 1113-1115.

Hoffmann, P.; Dedik, A. N.; Ensling, J.; Weinbruch, S.; Weber, S.; Sinner, T.; Gütlich, P.; Ortner, H. M., Speciation of Iron in Atmospheric Aerosol Samples. *Journal of Aerosol Science* **1996,** *27* (2), 325-337.

Hug, S. J., In SituFourier Transform Infrared Measurements of Sulfate Adsorption on Hematite in Aqueous Solutions. *Journal of Colloid and Interface Science* **1997,** *188* (2), 415-422.

Jacob, D. J., Heterogeneous chemistry and tropospheric ozone. *Atmospheric Environment* **2000,** *34* (12-14), 2131-2159.

Jang, J.-H.; Dempsey, B. A.; Burgos, W. D., Solubility of Hematite Revisited: Effects of Hydration. *Environmental Science & Technology* **2007,** *41* (21), 7303-7308.

Johansen, A. M.; Siefert, R. L.; Hoffmann, M. R., Chemical composition of aerosols collected over the tropical North Atlantic Ocean. *J. Geophys. Res.* **2000,** *105* (D12), 15277-15312.

Johnson, K. S.; Gordon, R. M.; Coale, K. H., What controls dissolved iron concentrations in the world ocean? *Marine Chemistry* **1997,** *57* (3-4), 137-161.

Journet, E.; Desboeufs, K. V.; Caquineau, S.; Colin, J.-L., Mineralogy as a critical factor of dust iron solubility. *Geophys. Res. Lett.*, **2007,** *35*, L07805, doi:10.1029/2007GL031589.

Judeikis, H. S.; Stewart, T. B.; Wren, A. G., Laboratory Studies of Heterogeneous Reactions of SO_2. *Atmospheric Environment* **1978,** *12*, 1663-1641.

Khoder, M. I., Atmospheric conversion of sulfur dioxide to particulate sulfate and nitrogen dioxide to particulate nitrate and gaseous nitric acid in an urban area. *Chemosphere* **2002,** *49*, 675-684.

Kim, K. H.; Choi, J. S., Kinetics and Mechanism of the Oxidation of Sulfur Dioxide on α-Fe_2O_3. *Journal of Physical Chemistry* **1981,** *85* (17), 2447-2450.

Kraemer, S. M., Iron oxide dissolution and solubility in the presence of siderophores. *Aquatic Sciences* **2004,** *66* (1), 3-18.

Krueger, B. J.; Grassian, V. H.; Laskin, A.; Cowin, J. P., The transformation of solid atmospheric particles into liquid droplets through heterogeneous chemistry: Laboratory insights into the processing of calcium containing mineral dust aerosol in the troposphere. *Geophys. Res. Lett.* **2003,** *30* (3), 1148, doi:10.1029/2002GL016563.

Kuma, K.; Matsunaga, K., Availability of colloidal ferric oxides to coastal marine phytoplankton. *Marine Biology* **1995,** *122* (1), 1-11.

Li, L.; Chen, Z. M.; Zhang, Y. H.; Zhu, T.; Li, J. L.; Ding, J., Kinetics and mechanism of heterogeneous oxidation of sulfur dioxide by ozone on surface of calcium carbonate. *Atmos. Chem. Phys.* **2006,** *6* (9), 2453-2464.

Li, L.; Chen, Z. M.; Zhang, Y. H.; Zhu, T.; Li, S.; Li, H. J.; Zhu, L. H.; Xu, B. Y., Heterogeneous oxidation of sulfur dioxide by ozone on the surface of sodium chloride and its mixtures with other components. *J. Geophys. Res.* **2007,** *112,* D18301, doi:10.1029/2006JD008207.

Li, W.; Gibbs, G.; Oyama, S., Mechanism of ozone decomposition on a manganese oxide catalyst. I. In situ Raman spectroscopy and ab initio molecular orbital calculations. *Journal of the American Chemical Society* **1998,** *120* (35), 9041-9046.

Li, W.; Oyama, S., Mechanism of ozone decomposition on a manganese oxide catalyst. 2. Steady-state and transient kinetic studies. *Journal of the American Chemical Society* **1998,** *120* (35), 9047-9052.

Liang, L.; Morgan, J. J., Chemical aspects of iron oxide coagulation in water: Laboratory studies and implications for natural systems. *Aquatic Sciences - Research Across Boundaries* **1990,** *52* (1), 32-55.

Lind, J.; Lazrus, A.; Kok, G., Aqueous Phase Oxidation of Sulfur(IV) by Hydrogen Peroxide, Methylhydroperoxide, and Peroxyacetic Acid. *Journal of Geophysical Research* **1995,** *92* (D4), 4171-4177.

Lovejoy, E. R.; Hanson, D. R., Measurement of the Kinetics of Reactive Uptake by Submicron Sulfuric Acid Particles. *The Journal of Physical Chemistry* **1995,** *99* (7), 2080-2087.

Maahs, H., Kinetics and Mechanism of the Oxidation of S(IV) by Ozone in Aqueous Solution with Particular Reference to SO_2 Conversion in Nonurban Tropospheric Clouds. *Journal of Geophysical Research* **1983,** *88* (C15), 10721 - 10732.

Mahowald, N. M.; Baker, A. R.; Bergametti, G.; Brooks, N.; Duce, R. A.; Jickells, T. D.; Kubilay, N.; Prospero, J. M.; Tegen, I., Atmospheric global dust cycle and iron inputs to the ocean. *Global Biogeochem. Cycles* **2005,** *19* (4), GB4025.

Majestic, B. J.; Schauer, J. J.; Shafer, M. M.; Turner, J. R.; Fine, P. M.; Singh, M.; Sioutas, C., Development of a Wet-Chemical Method for the Speciation of Iron in Atmospheric Aerosols. *Environmental Science & Technology* **2006,** *40* (7), 2346-2351.

Martin, J. H.; Fitzwater, S. E., Iron deficiency limits phytoplankton growth in the north-east Pacific subarctic. *Nature* **1988,** *331* (6154), 341-343.

Mawji, E.; Gledhill, M.; Milton, J. A.; Tarran, G. A.; Ussher, S.; Thompson, A.; Wolff, G. A.; Worsfold, P. J.; Achterberg, E. P., Hydroxamate Siderophores: Occurrence and Importance in the Atlantic Ocean. *Environmental Science & Technology* **2008,** *42* (23), 8675-8680.

McCaa, D. J.; Shaw, J. H., The infrared spectrum of ozone. *Journal of Molecular Spectroscopy* **1968,** *25* (3), 374-397.

Meskhidze, N.; Chameides, W. L.; Nenes, A., Dust and pollution: A recipe for enhanced ocean fertilization? *J. Geophys. Res.* **2005,** *110*, D03301, doi:10.1029/2004JD005082.

Meskhidze, N.; Chameides, W. L.; Nenes, A.; Chen, G., Iron mobilization in mineral dust: Can anthropogenic SO2 emissions affect ocean productivity? *Geophys. Res. Lett.* **2003,** *30*, 2085, doi:10.1029/2003GL018035.

Meskhidze, N.; Nenes, A., Phytoplankton and Cloudiness in the Southern Ocean. *Science* **2006,** *314* (5804), 1419-1423.

Michel, A. E.; Usher, C. R.; Grassian, V. H., Reactive uptake of ozone on mineral oxides and mineral dusts. *Atmospheric Environment* **2003,** *37* (23), 3201-3211.

Mitchell, M. B.; Sheinker, V. N.; Cox, W. W., Room Temperature Reaction of Ozone and Dimethyl Methylphosphonate (DMMP) on Alumina-Supported Iron Oxide. *The Journal of Physical Chemistry C* **2007,** *111* (26), 9417-9426.

Mogili, P. K.; Kleiber, P. D.; Young, M. A.; Grassian, V. H., Heterogeneous Uptake of Ozone on Reactive Components of Mineral Dust Aerosol: An Environmental Aerosol Reaction Chamber Study. *Journal of Physical Chemistry A* **2006,** *110* (51), 13799-13807.

Mogili, P. K.; Kleiber, P. D.; Young, M. A.; Grassian, V. H., N_2O_5 hydrolysis on the components of mineral dust and sea salt aerosol: Comparison study in an environmental aerosol reaction chamber. *Atmospheric Environment* **2006,** *40*, 7401-7408.

Mogili, P. K.; Yang, K. H.; Young, M. A.; Kleiber, P. D.; Grassian, V. H., Environmental aerosol chamber studies of extinction spectra of mineral dust aerosol components: Broadband IR-UV extinction spectra. *J. Geophys. Res.* **2007,** *112*, D21204, doi:10.1029/2007JD008890.

Mogili, P. K.; Yang, K. H.; Young, M. A.; Kleiber, P. D.; Grassian, V. H., Extinction spectra of mineral dust aerosol components in an environmental aerosol chamber: IR resonance studies. *Atmospheric Environment* **2008,** *42* (8), 1752-1761.

Nash, D. G.; Baer, T.; Johnston, M. V., Aerosol mass spectrometry: An introductory review. *Int. J. Mass Spectrom.* **2006,** *258* (1-3), 2-12.

Navea, J. G.; Xu, S.; Stanier, C. O.; Young, M. A.; Grassian, V. H., Effect of Ozone and Relative Humidity on the Heterogeneous Uptake of Octamethylcyclotetrasiloxane and Decamethylcyclopentasiloxane on Model Mineral Dust Aerosol Components. *The Journal of Physical Chemistry A* **2009,** *113* (25), 7030-7038.

Nel, A., ATMOSPHERE: Enhanced: Air Pollution-Related Illness: Effects of Particles. *Science* **2005,** *308* (5723), 804-806.

Noble, C. A.; Prather, K. A., Real-time single particle mass spectrometry: A historical review of a quarter century of the chemical analysis of aerosols. *Mass Spectrometry Reviews* **2000,** *19* (4), 248-274.

Ooki, A.; Nishioka, J.; Ono, T.; Noriki, S., Size dependence of iron solubility of Asian mineral dust particles. *J. Geophys. Res.* **2009,** *114*, D03202, doi:10.1029/2008JD010804.

Orphal, J., A critical review of the absorption cross-sections of O3 and NO2 in the ultraviolet and visible. *Journal of Photochemistry and Photobiology A: Chemistry* **2003,** *157* (2-3), 185-209.

Phadnis, M. J.; Carmichael, G. R., Numerical Investigation of the Influence of Mineral Dust on the Tropospheric Chemistry of East Asia. *Journal of Atmospheric Chemistry* **2000,** *36* (3), 285-323.

Pivovarov, S., Surface Structure and Site Density of the Oxide-Solution Interface. *Journal of Colloid and Interface Science* **1997,** *196* (2), 321-323.

Poeschl, U., Atmospheric aerosols: Composition, transformation, climate and health effects. *Angew. Chem., Int. Ed.* **2005,** *44* (46), 7520-7540.

Preszler Prince, A.; Kleiber, P.; Grassian, V. H.; Young, M. A., Heterogeneous interactions of calcite aerosol with sulfur dioxide and sulfur dioxide-nitric acid mixtures. *Physical Chemistry Chemical Physics* **2007,** *9*, 3432-3439.

Preszler Prince, A.; Wade, J. L.; Grassian, V. H.; Kleiber, P. D.; Young, M. A., Heterogeneous reactions of soot aerosols with nitrogen dioxide and nitric acid: atmospheric chamber and Knudsen cell studies. *Atmospheric Environment* **2002,** *36*, 5729-5740.

Preszler Prince, A. M. Investigations Into The Heterogeneous Atmospheric Interactions of Isolated Metal Oxide, Carbonate, and Soot Aerosols. University of Iowa, Iowa City, 2003.

Prospero, J. M.; Uematsu, M.; Savoie, D. L., Mineral aerosol transport to the Pacific Ocean. In *Chemical Oceanography*, Riley, J. P., Ed. Academic Press: New York, 1989; Vol. 10, pp 187 - 218.

Ravishankara, A. R., Heterogeneous and Multiphase Chemistry in the Troposphere. *Science* **1997,** *276* (5315), 1058-1065.

Reed, C.; Lee, Y.; Oyama, S., Structure and oxidation state of silica-supported manganese oxide catalysts and reactivity for acetone oxidation with ozone. *Journal of Physical Chemistry B* **2006,** *110* (9), 4207-4216.

Roscoe, J.; Abbatt, J., Diffuse reflectance FTIR study of the interaction of alumina surfaces with ozone and water vapor. *Journal of Physical Chemistry A* **2005,** *109* (40), 9028-9034.

Sedlak, D. L.; Hoigne, J., Oxidation of S(IV) in Atmospheric Water by Photooxidants and Iron in the Presence of Copper. *Environmental Science & Technology* **1994,** *28* (11), 1898-1906.

Seisel, S.; Keil, T.; Lian, Y.; Zellner, R., Kinetics of the uptake of SO_2 on mineral oxides: Improved initial uptake coefficients at 298 K from pulsed Knudsen cell experiments. *International Journal of Chemical Kinetics* **2006,** *38* (4), 242-249.

Shea, K. M.; Truckner, R. T.; Weber, R. W.; Peden, D. B., Climate change and allergic disease. *Journal of Allergy and Clinical Immunology* **2008,** *122* (3), 443-453.

Sipin, M. F.; Guazzotti, S. A.; Prather, K. A., Recent Advances and Some Remaining Challenges in Analytical Chemistry of the Atmosphere. *Analytical Chemistry* **2003,** *75* (12), 2929-2940.

Smith, K. R.; Aust, A. E., Mobilization of Iron from Urban Particulates Leads to Generation of Reaction Oxygen Species *in Vitro* and Induction of Ferritin Synthesis in Human Lung Epithelial Cells. *Chemical Research in Toxicology* **1997,** *10* (7), 828-834.

Solmon, F.; Chuang, P. Y.; Meskhidze, N.; Chen, Y., Acidic processing of mineral dust iron by anthropogenic compounds over the north Pacific Ocean. *J. Geophys. Res.* **2009,** *114*, D02305, doi:10.1029/2008JD010417.

Spokes, L. J.; Jickells, T. D., Factors controlling the solubility of aerosol trace metals in the atmosphere and on mixing into seawater. *Aquatic Geochemistry* **1995,** *1* (4), 355-374.

Suess, D. T.; Prather, K. A., Mass Spectrometry of Aerosols. *Chemical Reviews* **1999,** *99* (10), 3007-3035.

Sullivan, R. C.; Prather, K. A., Recent Advances in Our Understanding of Atmospheric Chemistry and Climate Made Possible by On-Line Aerosol Analysis Instrumentation. *Analytical Chemistry* **2005,** *77* (12), 3861-3886.

Tang, I. N.; Fung, K. H., Hydration and Raman scattering studies of levitated microparticles: $Ba(NO_3)_2$, $Sr(NO_3)_2$, and $Ca(NO_3)_2$. *The Journal of Chemical Physics* **1997,** *106* (5), 1653-1660.

Tegen, I.; Harrison, S. P.; Kohfeld, K.; Prentice, I. C.; Coe, M.; Heimann, M., Impact of vegetation and preferential source areas on global dust aerosol: Results from a model study. *J. Geophys. Res.* **2002,** *107* (D21), 4576, doi:10.1029/2001JD000963

Toledano, D. S.; Henrich, V. E., Kinetics of SO_2 Adsorption on Photoexcited α-Fe_2O_3. *Journal of Physical Chemistry B* **2001,** *105* (18), 3872-3877.

Trainor, T. P.; Chaka, A. M.; Eng, P. J.; Newville, M.; Waychunas, G. A.; Catalano, J. G.; Brown, J. G. E., Structure and reactivity of the hydrated hematite (0 0 0 1) surface. *Surface Science* **2004,** *573* (2), 204-224.

Ullerstam, M.; Johnson, M. S.; Vogt, R.; Ljungstrom, E., DRIFTS and Knudsen cell study of the heterogeneous reactivity of SO_2 and NO_2 on mineral dust. *Atmospheric Chemistry and Physics* **2003,** *3* (6), 2043-2051.

Ullerstam, M.; Vogt, R.; Langer, S.; Ljungstrom, E., The kinetics and mechanism of SO_2 oxidation by O_3 on mineral dust. *Physical Chemistry Chemical Physics* **2002,** *4* (19), 4694-4699.

Usher, C. R.; Al-Hosney, H.; Carlos-Cuellar, S.; Grassian, V. H., A laboratory study of the heterogeneous uptake and oxidation of sulfur dioxide on mineral dust particles. *Journal of Geophysical Research* **2002,** *107*, 4713, doi:10.1029/2002JD002051.

Usher, C. R.; Michel, A. E.; Grassian, V. H., Reactions on Mineral Dust. *Chemical Reviews* **2003,** *103* (12), 4882-4939.

Usher, C. R.; Michel, A. E.; Stec, D.; Grassian, V. H., Laboratory studies of ozone uptake on processed mineral dust. *Atmospheric Environment* **2003,** *37* (38), 5337-5347.

Wagener, T.; Pulido-Villena, E.; Guieu, C., Dust iron dissolution in seawater: Results from a one-year time-series in the Mediterranean Sea. *Geophys. Res. Lett.* **2008,** *35*, L16601, doi:10.1029/2008GL034581.

Waqif, M.; Saad, A. M.; Bensitel, M.; Bachelier, J.; Saur, O.; Lavalley, J.-C., Comparative Study of SO_2 Adsorption on Metal Oxides. *Journal of the Chemical Society, Faraday Transactions* **1992,** *88* (19), 2931-2936.

Weber, S.; Hoffmann, P.; Ensling, J.; Dedik, A. N.; Weinbruch, S.; Miehe, G.; Gütlich, P.; Ortner, H. M., Characterization of Iron Compounds from Urban and Rural Aerosol Sources. *Journal of Aerosol Science* **2000,** *31* (8), 987-997.

Worsnop, D. R.; Zahniser, M. S.; Kolb, C. E.; Gardner, J. A.; Watson, L. R.; Van Doren, J. M.; Jayne, J. T.; Davidovits, P., The temperature dependence of mass accommodation of sulfur dioxide and hydrogen peroxide on aqueous surfaces. *The Journal of Physical Chemistry* **1989,** *93* (3), 1159-1172.

Xi, Y.; Reed, C.; Lee, Y.; Oyama, S., Acetone oxidation using ozone on manganese oxide catalysts. *Journal of Physical Chemistry B* **2005,** *109* (37), 17587-17596.

Zhang, X.; Zhuang, G.; Chen, J.; Wang, Y.; Wang, X.; An, Z.; Zhang, P., Heterogeneous Reactions of Sulfur Dioxide on Typical Mineral Particles. *Journal of Physical Chemistry B* **2006,** *110* (25), 12588-12596.